Energy Regulation by the Skeleton: Exploring the Role of Bone-Derived Lipocalin-2

Steven Shikhel

Columbia University
2019

Abstract

Energy Regulation by the Skeleton: Exploring the Role of Bone-Derived Lipocalin-2

Steven Shikhel

Life relies on the integration of external environmental stimuli and internal signals to balance fluctuations in nutrient availability to achieve homeostasis. Bone has recently emerged as a pleiotropic endocrine organ that secretes at least two hormones, FGF23 and osteocalcin, which regulate kidney function and glucose homeostasis, respectively. These findings have raised the question of whether other bone-derived hormones exist and what their potential functions are. Here we identify, through molecular and genetic analyses in mice, lipocalin 2 (LCN2) as an osteoblast-enriched, secreted protein. Loss- and gain-of-function experiments in mice demonstrate that osteoblast-derived LCN2 maintains glucose homeostasis by inducing insulin secretion and improves glucose tolerance and insulin sensitivity. In addition, osteoblast-derived LCN2 inhibits food intake. LCN2 crosses the blood–brain barrier, binds to the melanocortin 4 receptor (MC4R) in the paraventricular and ventromedial neurons of the hypothalamus and activates an MC4R-dependent anorexigenic (appetite-suppressing) pathway. These results identify LCN2 as a bone-derived hormone with metabolic regulatory effects, which suppresses appetite in a MC4R-dependent manner, and show that the control of appetite is an endocrine function of bone. Furthermore, we show that serum LCN2 levels correlate with insulin levels and β-cell function, indices of healthy glucose metabolism, in genetic and diet-induced mouse models of obesity and in obese, healthy or pre-diabetic patients. However, LCN2 serum levels also correlate with body mass index (BMI) and insulin resistance in the same patients; and are increased in obese mice. To dissect this apparent discrepancy, we examined LCN2 effects in hyperphagia and β-cell function mouse models of obesity or β-cell destruction. Silencing *Lcn2* expression increases hyperphagia, fat and body weight and worsens β-

cell function and general metabolic dysfunction in obese, leptin receptor-deficient mice. Conversely, LCN2 increases β-cell numbers and promotes β-cell function after streptozotocin-induced β -cell failure by (STZ) and acts as a growth factor necessary for β -cell adaptation to higher metabolic load in mice. These results support a protective role for LCN2 in obesity-induced glucose intolerance and insulin resistance that stem from its ability to decrease food intake and promote adaptive β-cell proliferation.

Table of Contents

Acknowledgements

As I look back on the years during my time as a PhD student, I must first thank my thesis advisor and mentor, Dr. Stravroula Kousteni. Thank you for giving me the opportunity to learn and work in your laboratory, for giving me the opportunity to be surrounded by talented, awesome people. I am beyond grateful for the knowledge and skill sets I have received herein. My work in the Kousteni Lab has allowed me to work at the forefront of physiology research and has led to marked improvement as a creative thinker, multi-disciplinary scientist and effective communicator. She has taught and shown me what steadfast determination it takes to become successful. This lesson is not one I will easily forget as I plan to continue engage as a student of the universe More than ever, I am confident and excited in my ability to undertake my career goals.

I would also like to extend my gratitude to my qualifying and thesis research advisory committee members – Drs. Gerard Karsenty, Lori Zeltser, Jonathan Barasch, and Liza Pon. I thank them for their comments and advice throughout the progression of my thesis projects. Even more importantly, I thank them for guiding me to make the transition from being a student to a scientist. Thanks to their training, I am more confident now to present my research.

In addition, I want to take this opportunity to express my gratitude to all the members and faculty of the Institute of human Nutrition at CUMC. Especially Drs. Richard Decklebaum and Debra Wolgemuth for their training to allow me grow as a scientist. Thanks to the effort of the department, I was able to focus on doing good science while feeling at home at CUMC. The department and people within are truly supportive and I'm beyond fortunate to have been part of such a wonderful community.

It would not have been the experience it was without all the current and past members of the Kousteni lab. The diverse strengths and personalities of the lab made every day a pleasure to work in. I must give an incredible amount of special thanks to Dr. Ioanna Mosialou whom I had the pleasure of working very

closely with through the entirety of the graduate school process. From day one of my rotation Ioanna had allowed me to work alongside her. She has no reservations in sharing her technical know-how, her experiences, and her profound knowledge of the world. Ioanna has been such a huge source of inspiration and I owe so much to everything Ioanna has given me.

Finally, I must express my profound gratitude to my parents, Lina and Igor Shikhel, and my brother and sister-in-law, David and Michelle. Thank you for your patience, your belief in me and your unwavering love. These years have been a journey for all of us. It was a big decision to come to graduate school. I would not have gotten through the difficult parts of the journey without knowing you guys always had my back. In the process we have all learned a lot about ourselves and our family and for that I am beyond grateful. Thank you for your encouragement, support and love.

Dedication

This thesis is dedicated to my beloved family for their endless love, and encouragement. My grandparents Lara, Michael and Sofa. My parents Lina and Igor. My brother David and sister-in-law Michelle.

In memory of my great-grandparents Michael and Anna and my grandfather Alexander.

Chapter I: General Introduction

Nutrition and Metabolic Biology

Metabolism is broadly defined as the sum of chemical processes needed to maintain life. Its regulation relies on the integration of external environmental stimuli and internal signals to balance fluctuations in nutrient availability and achieve homeostasis. Generally, anabolic pathways are active when nutrient supply exceeds demand to promote storage and growth while catabolic pathways become active in breakdown to meet the caloric and nutrients demands of the organism[1].   The ability to store nutrients from the diet for later times has supported the development of animal life for nearly 600 million years. However, in the last 50 years, it has gone awry for a large population of humans[2].

In a remarkably short time, we have gone through gastronomic and technological revolutions. We have shaped our environment to one of caloric surplus through the creation and accessibility of highly palatable calorie dense foods while decreasing the need to expend energy[3]. Diet-induced obesity (DIO) has existed throughout human history. It was a relatively rare condition associated with affluence. The association between obesity and high mortality rates was recognized even in biblical times. In the sixth century CE., the increase in mortality was explained due to divine retribution for violating two of the seven cardinal sins, "gluttony" and "sloth," namely overnutrition and under-exertion. Supplanting divine retribution, the scientific community has offered new explanations on the cardinal causes of obesity-induced mortality. However, there is a current lack of consensus regarding obesity pathogenesis[5]. This lack of agreement results in poorly justified claims both from within and outside the scientific community, leaving individuals and patients weary, confused, and dissatisfied with the scientific process as it pertains to obesity treatment. To break this cycle, and to identify effective treatment modalities, we need to better understand obesity's underlying causes[4].

Colloquially, obesity is defined as an excess of body fat mass. Quantifying fat-mass requires sophisticated tools not widely available. Therefore, body mass index (BMI), which expresses body weight (kg) as a function of body height squared (m^2) is used as a surrogate measure of body fat accumulation. Population-based actuarial studies place the upper limit of normal BMI in adults at 25 kg/m^2, and define obesity as BMI > 30 kg/m^2, and designate a BMI between 25 and 30 as "overweight"[4]. Though BMI is an imprecise measure of adiposity, the CDC was able to track marked increases in the obesity rate among people living in developed and developing nations. This is especially true for children and adolescence and therefore a legitimate public health concern.

Metabolic Syndrome (MeS) is characterized by a collection of metabolic abnormalities which include obesity, dyslipidemia, hypertension, hyperglycemia, hyperinsulinemia, and insulin resistance. Obesity has reached endemic proportions and has been deemed the leading cause of preventable death. The burden of obesity on health extends across multiple organ systems and increases the risk of chronic diseases, like nonalcoholic fatty liver disease (NAFLD), type 2 diabetes (T2D), atherosclerotic cardiovascular disease, cancer, pulmonary disease, chronic kidney disease, sleep apnea and rheumatoid arthritis[5].

These diseases exert tremendous strain on society through contributing to increased morbidity and mortality rates which stress limited health system resources. In the United States, obesity and its associated co-morbidities cost $1.42 trillion/year (8% of GDP), and this number is only expected to increase[6]. To develop therapies to combat obesity's growing burden on population health, we must define the sources, causes and mechanisms underlying the pathogenesis of obesity. It is, therefore, necessary to integrate molecular, genetic, developmental, behavioral and environmental factors[4].

Metabolic syndrome pathogenesis involves chronic caloric surplus resulting from small cumulative imbalances of energy intake and expenditure. In most mammals, including humans, the meal is the functional behavioral unit of food intake. The size and frequency of the meals ultimately determine the total daily energy intake which can vary greatly. For example, predatory hunters like lions and wolves may only eat once every couple of days, provided they can eat the entirety of their kill in what amounts to a single meal. In contrast, grazing animals will spend the majority of their waking hours on feeding. Humans eat multiple meals a day, and each meal constitutes a modest fraction of total daily caloric intake[7]. The identification of the molecular mechanisms which control short- and long-term feeding behaviors will better enable preventative and therapeutic approaches to obesity.

Feeding behavior is largely due to two motivational aspects; to fulfill metabolic and hedonic needs. When body-fuel and nutrient sources are sensed to be low, metabolic feeding aims to alleviate its associated discomfort. Hedonic feeding results from the anticipation of a rewarding experience included with eating. Energy balance neurocircuitry has identified neuronal substrates implicated in these distinct but complementary sources of motivation. To date, neuronal populations in the hypothalamus and brainstem have been ascribed as the main central regulators' areas of energy homeostasis.

The arcuate nucleus (ARC) of the hypothalamus contains two populations of neurons with opposing effects on food intake[8]. The activity of both populations of neurons can be influenced by the periphery due to the ARC's proximity to the median eminence, a breach in the blood-brain barrier due to fenestrated capillaries[9]. Peripheral hormones have been described to signal short-term availability clues, such as those emanating from the gut. Others, like leptin, have been regarded as hormones which relay information regarding long-term energy stores[10]. Gut hormones like PYY and GLP1 can signal directly to the arcuate nucleus and to the brainstem. They can also act through vagal afferents which converge in the nucleus of

the tractus solitarius of the brainstem. Neuronal projections from the brainstem can then carry signals to the hypothalamus[10].

Cholecystokinin (CCK) is a peptide secreted from enteroendocrine cells of the gut in response to intestinal nutrient intake. CCK acts by modulating vagal inputs and by directly effecting central brainstem/hypothalamic feeding circuits. CCK-expressing gut enteroendocine cells are located adjacent to CCKA-receptor positive vagal affect nerves making it possible for local paracrine effects to occur. When the vagal nerve signals below the diaphragm are surgically or chemically interrupted, the effects of CCK are blocked. CCKR positive neurons can be stimulated by mechanosensory mechanisms like gastric distention or stroking of the intestinal mucosa[7]. Plasma CCK levels rise within minutes of meal onset and is rapidly degraded following its release. The increase in CCK can activate cFOS in gut-recipient regions of the caudomedial NTS which is also mediated by vagal afferents. Combinations of gastric loads, duodenal nutrients infusion or gastric loads and peripheral CCK generate greater cFOS expression than any stimuli alone indicating both paracrine and endocrine roles of CCK [6]. Ghrelin is an orexigenic hormone secreted by gastric X/A cells. In contrast to CCK, ghrelin is increased during fasting and decreases after refeeding. Peripheral and central ghrelin administration rapidly promote appetitive and consummatory ingestive behaviors.

The adipokine leptin, which is secreted in proportion to body fat provides information about long-term energy stores. Peripheral and central administration of leptin suppresses fasting-induced increases in feeding which modulates meal size without affecting meal frequency[4]. Leptin receptor signaling in neurons which express peptide neurotransmitter pro-opiomelanocortin (POMC) and cocaine-amphetamine-regulated transcript (CART) cause a suppression of feeding while increasing metabolic rate. These anorexigenic neurons are located in the lateral ARC and express alpha-melanocyte stimulating

hormone (α-MSH) [11]. POMC is a prohormone that produces Υ-melanocyte-stimulating hormone (MSH), adrenocorticotropic hormone (ACTH) and β-lipotrophin. ACTH and β-lipotrophin produce several more substances including α-MSH and β-MSH which act as ligands to bind and activate the Melanocrtin-4 receptor (MC4R) in the paraventricular hypothalamus (PVH)[12]. A second group of neurons, the neuropeptide Y (NPY) and agouti-related peptide (AgRP), are inhibited by leptin receptor causing appetite to be stimulated [13–15]AGRP signals through PC1 as a natural antagonist of MC4R. These orexigenic neurons rapidly initiates food seeking behavior.

Genome wide association studies (GWAS) have consistently identified genetic variants within the *MC4R* coding region as important regulators of obesity and adiposity. However, other melanocortin receptor (MCRs) exist [16]. The melanocortin system consists of five 7-transmembrane G-protein coupled receptors, MC1R, MC2R, MC3R, MC4R and MC5R. Historically, the primary function of the melanocortin system was believed to be in pigmentation due to the function of MC1R which is primarily found in the periphery, especially in the skin. After cloning of the other receptors, it was found that many key physiological functions necessary for animal survival and reproduction can be attributed to the MCR system. The MCRs have varied tissue expression profiles. While MC1R is primarily expressed in the melanocytes of the skin, MC2R is expressed in the adrenal cortex of the adrenal gland, MC3R in the CNS, GI tract and kidney, MC4R in the CNS, and MC5R in exocrine cells throughout the body. The MCR system is involved in many critical functions including feeding behavior, energy homeostasis, response to stress, response to UV radiation, sexual function and behavior, pain response, fear flight, cardiovascular function, kidney function, immune response, sebaceous gland secretion and others[17].

Both MC3R and MC4R have effects on energy homeostasis but their roles are different. The MC4R-KO are obese, hyperphagic and hyperinsulinemic. The MC3R-KO are different and rather unusual. The increase in

weight is primarily observed in females but increase adipose mass in both sexes. The MC3R-KO mice are not hyperphagic suggesting the obesity phenotype results from increased energy efficiency. Though increase in adiposity is similar in both models, the MC3R mice are less insulin resistance and less steatotic. Whereas, other MCR's are more selective on their ligand binding preferences, MC3R does not discriminate. MC3R responds to physiological doses of α-, β-, ɣ-MSH, ACTH or AGRP.

Receptor	Site of expression	Major Functions
MC1R	Periphery i.e. skin	Pigmentation
MC2R	Adrenal cortex of adrenal gland	Adrenocortical steroidogenesis
MC3R	CNS, GI tract, kidney	Energy homeostasis - energy Expenditure/Efficiency
MC4R	CNS	Energy homeostasis – food intake, erectile dysfunction
MC5R	Exocrine cells	Synthesis and secretion of exocrine gland products

Evolution of Bone

Typically, the skeleton has been viewed as an assemblage of calcified tubes which provides the framework of the body, protects vital organs and creates points of attachment for skeletal muscle to allow for movement and ultimately life on land. However, that's not the entirety of the skeleton's biological role;the bone marrow is the predominant site of hematopoiesis[18] , and is essential for homeostatic control of minerals like calcium, phosphorus, and sodium. The skeleton contains more than 99% of the body's calcium, 80-90% of the body's phosphate and two-thirds of the body's sodium[19].

One of the most dramatic episodes of evolution occurred late in the Devonian period which started 419.2 million years ago and spanned 60 million years. Vertebrate organisms began to transition from aquatic to terrestrial living which allowed animals to escape competitive pressures from the water and explore niche opportunities on land. However, these first terrestrial animals experienced significant barriers which necessitated changes in the morphological and physiological mechanisms that underlie most life

processes such as movement, feeding, respiration, and reproduction. Minerals could no longer be freely absorbed from the surrounding aqueous environment, gas exchange and water balance require vastly different mechanisms between water and air, and gravity on land is far stronger than in water[20,21].

Osteichthyes evolved approximately 420 million years ago and were the first organism to have a fully mineralized endoskeleton[22]. The skeleton is comprised of two distinctive tissues, bone, and cartilage. Bone contains osteoblasts, osteocytes, and osteoclasts while chondrocytes reside within cartilage. The osteoblasts and chondrocytes are derived from mesenchymal origins[23] whereas osteoclasts are derived from multinucleated cells of hematopoietic origins in the bone marrow[24].

To survive on land, terrestrial animals developed a much larger, energy-expensive appendicular skeleton for seemingly opposing purposes: a stable structure to facilitate ambulation, and mechanisms to maintain mineral homeostasis. Endochondral ossification is the process by which mineralized bone is formed from an intermediate cartilaginous template which provides a substantially stronger and mineral filled skeleton. The process starts when cartilage is invaded by blood vessels that deliver osteoblasts into what becomes the marrow space. Osteoblasts use the cartilage template to form lattice-like spicules of trabecular or 'spongy' bone which is remodeled by osteoclasts, specialized bone cells that resorb bone matrix. Also, osteoblasts differentiate in the fibrous tissue that surrounds the developing bone and forms a dense cortical shell. Endochondral ossification provides a clear evolutionary advantage for life on land. The trabeculae provide a large surface area:bone volume ratio, and allow for osteoclastic resorption and the rapid release of calcium into circulation, while a dense cortical shell bears most of the mechanical force by bones.

The structural integrity of the skeleton is critical for vertebrate survival. For the skeleton to fulfill its many functions throughout adulthood, the skeleton constantly renews itself through a process called bone remodeling. Bone modeling is a process which occurs during development. Bone (re)modeling is characterized by resorption of pre-existing mineralized bone extra-cellular matrix (ECM) by osteoclasts followed by de novo bone formation by osteoblasts[25]. Bone resorption and bone formation occur sequentially and in a balanced manner to maintain bone mass during adulthood[26]. Any imbalance between these two processes would cause skeletal disorders characterized by either a low or a high bone mass phenotype[25]. The most common bone remodeling disease, osteoporosis, is characterized by either increased osteoclastic activity, decreased osteoblastic activity or a combination of both, leading to low bone mass and increased risk of fracture.

Endocrine networks have enjoyed tremendous evolutionary success because they provide the means to sense internal and external changes in the environment, and the ability to integrate this information into coordinated, tissue-specific responses in the organism. Endocrine systems arose to regulate extracellular mineral ion concentrations using dietary sources and dissolution from skeletal stores via osteoclastic resorption. Mineralization of the skeleton meant being in constant danger of extracellular calcium loss which would be detrimental to muscle and nerve function. The emergence of the parathyroid-calcium axis works to resolve this issue. The parathyroid gland detects a decrease in calcium in the blood by using calcium-sensing receptors, which mediates the secretion of PTH, which then works in a rapid, pleiotropic fashion to increase calcium levels. PTH works by stimulating osteoclasts to access internal calcium stores through bone resorption and acts in the kidney to increase calcium reabsorption in the distal convoluted tubule and production of active Vitamin D, which, in turn, increases intestinal calcium absorption[27].

Bone as an Endocrine Organ

The first discovery that implicated bone as an endocrine organ concerns the role of bone in regulating phosphate homeostasis through FGF23. Phosphate is ingested through the diet, absorbed by the small intestine through either a sodium-phosphate co-transporter or by diffusion. However, the major control point for phosphate homeostasis is the kidney, which expresses hormone-regulated proteins to modulate phosphate filtration. FGF23 signals to promote phosphate excretion by downregulating NPT2a, a hormone-regulated protein in the kidney, and inhibits Vitamin-D production as a counter-regulatory phosphaturic hormone to remove excess phosphate that accompanies PTH-stimulated bone resorption during calcium mobilization. Interestingly, FGF23 is produced almost exclusively by the osteocytes, an ideal situation to negatively feed into the PTH-vitamin D endocrine loop[27].

Considering the skeleton's sheer size, its many functions, and the continuous nature of bone remodeling, it is easy to postulate the skeleton requires a large amount of energy[28]. Using 18F-fluorodeoxyglucose and PET imaging, it was shown that total glucose uptake in bone exceeds that of traditional glucose-utilizing organs, including muscle, WAT and liver. The accumulation of glucose in bone was located predominantly in osteoblast-enriched regions, and the amount of glucose uptake decreases with age[29].

Simple clinical observations add credence the possibility that a relationship between energy metabolism and bone exists. Insufficient food intake during childhood results in arrested growth. Patients with anorexia nervosa, a psychiatric disease characterized by voluntary food restriction leading to weight loss, display decreased or arrested bone growth and bone loss[30]. Conversely, type 2 diabetes patients who are overweight or obese with visceral fat accumulation, have an adequate or increased bone mineral density[31]. However, fracture risk is increased with diabetes. Higher body weight exerts a great mechanical load on the skeleton which explains the absence of bone loss, but adipose tissue produces cytokines which

have a deleterious effect on bone[32]. In addition, menopause is associated with a decrease in skeletal integrity, called postmenopausal osteoporosis. Decreasing sex-steroid hormones like estrogen have powerful effects on energy metabolism and bone remodeling[33,34]. Estrogen deficiency causes a decrease in energy expenditure and induces activation of receptor activator of nuclear factor kappa-B ligand (RANKL) by osteoblasts which recruit osteoclasts and favors bone resorption causing bone loss[35].

It has been difficult to tease apart the pathophysiology of complex metabolic diseases. However, with advances in genetic techniques, scientists can systematically decipher the function a gene of interest in vivo to reveal hidden crosstalk between organs that influence in each other. The first supportive molecular evidence that energy and bone metabolism are linked originated from the realization that leptin, an adipocyte-derived protein, inhibits appetite, gonadal function and bone mass[36]. Leptin inhibits bone mass accrual by signaling brainstem neurons to prevent synthesis of serotonin [37]. Thereafter, other adipokines (adiponectin) and gut-derived (GLP1, GLP2, and serotonin) proteins were observed to regulate energy homeostasis and bone mass[30].

Analysis of clinical and murine observations lead to the hypothesis that regulation of bone mass and energy metabolism is coordinated and a bone-energy endocrine loop exists[36]. The revelation that bone itself can regulate energy metabolism in a reciprocal manner via a secreted hormone was uncovered to be osteocalcin[38].

Osteocalcin is secreted exclusively by osteoblasts and is a multifunctional hormone. Osteocalcin is most abundant non-collagenous protein the bone ECM. It contains 46-50 amino acid residues that undergo post-translational modifications of three glutamic acid residues (GLA)[39]. This post-translational modification of osteocalcin is essential for calcium and hydroxyapatite binding which allows deposition of

osteocalcin in the bone ECM. Uncarboxylated osteocalcin has a low affinity to hydroxyapatite and is easily released into the circulation (Patti et al., 2013). Circulating undercarboxylated osteocalcin is the active form which signals peripherally. When the gene is deleted in mice bone mineralization is normal, but *Ocn-/-* mice are abnormally docile, fat and breed poorly.

Genetic studies in mice and humans have shown that activated, under-carboxylated osteocalcin influences glucose metabolism, male fertility and brain development and functions[38,40–42]. Osteocalcin promotes glucose homeostasis by increasing pancreatic β-cell proliferation and insulin secretion, improving insulin sensitivity in muscle and adipose tissue[38,43]. These results showed that bone is a true endocrine organ and can influence whole-body glucose metabolism.

The integration of bone and energy metabolism via osteocalcin is modulated through insulin signaling. Osteocalcin secreted by osteoblasts regulate insulin secretion, but insulin signaling in osteoblasts in return regulates activation of osteocalcin. First insight into the regulation of osteocalcin came from the observation that another osteoblast-derived gene, *Esp*, encoding for osteoblast testis-specific protein tyrosine phosphatase (OST-PTP), also regulates glucose homeostasis. *Esp-/-* mice display a mirror image of what is observed in the *Ocn-/-* mice[38]. *Esp-/-* mice are hypoglycemic, hyperinsulinemic and the serum fraction of undercarboxylated osteocalcin was significantly higher than in control mice[38]. Since OST-PTP is a tyrosine phosphatase, the insulin receptor (INSR) in osteoblasts was hypothesized to be the target of OST-PTP since INSR activity is often inhibited by protein tyrosine phosphatases[44].

Furthermore, studies in mice where InsR was removed in osteoblasts had a similar phenotype to that of the *Ocn-/-*. A more relevant and stronger phenotype was observed in *InsR$_{osb}$-/-* than in two classical insulin target organs, skeletal muscle and white adipose tissue (Bruning et al., 1998; Bluher et al., 2002). Double

heterozygous compounds for *InsR* and *Ocn* (*InsR$_{osb}$+/-; Ocn+/-*) display metabolic abnormalities similar to the *Ocn-/-* mice, whereas, removing one allele of *InsR* in the *Esp-/-* (*InsR$_{osb}$+/-; Esp-/-*) normalizes the metabolic abnormalities seen in the Esp -/-. These genetic studies verify that insulin signaling in osteoblasts is a determinant of osteocalcin activity in osteoblasts to whole-body glucose homeostasis [38,43].

The above studies which illustrate the contribution of *InsR* in the osteoblast in mice fed a normal diet raised an important follow-up question; does bone contribute to insulin resistance in mice fed a high-fat diet (HFD)? Indeed, genetic and biochemical observations suggest that insulin resistance in bone develops as a result of a loss of *InsR* mediated Smurf1 upon increases in the circulating level of free saturated fatty acids[45–48].

Additionally, the coordinated connection between bone and energy metabolism implicates that a decrease in osteoblast number would compromise glucose metabolism in an osteocalcin-dependent manner. To test this hypothesis, an inducible global ablation of osteoblasts model was used. By cross-breeding transgenic mice expressing a tamoxifen-regulated Cre under the control of the osteocalcin promoter with mice expressing an inactive form of Diptheria Toxin A (DTA) chain introduced into a ubiquitously expressed locus one can address such hypothesis. When tamoxifen was injected in these mice for ten days, the result was a loss of 50% of their osteoblasts, increased blood glucose levels, glucose intolerance, and insulin insensitivity. There was also a decrease in osteocalcin levels which could explain the changes in glucose metabolism. To examine whether changes were solely dependent on osteocalcin, 30ng/g of recombinant osteocalcin was administered for four weeks, causing restoration of osteocalcin levels. Administering osteocalcin rescued glucose intolerance and improved decreases in beta-cell area, beta cell mass, and islet number[49].

However, differential effects were still observed. Insulin sensitivity, gonadal fat weight, energy expenditure, and food intake persisted following osteocalcin treatment indicating the skeleton acts through osteoblasts to regulate aspects of energy metabolism in osteocalcin-dependent and -independent manners. Additionally, these results indicate a novel function of the skeleton on energy regulation since osteocalcin is not implicated in the regulation of appetite[49].

Furthermore, FOXO1, one of the four FOXO isoforms of Forkhead transcription factors, play a significant role in regulating whole-body energy metabolism. *FoxO1* is highly expressed in insulin-responsive tissues including pancreas, liver, skeletal muscle, adipose tissue, and bone. In these tissues, FOXO1 orchestrates a transcriptional cascade to maintain glucose homeostasis. In the fasted state, FOXO1 promotes the expression of gluconeogenic enzymes in the liver to increase endogenous glucose production. Following feeding, pancreatic beta cells secrete insulin which promotes the uptake of glucose by peripheral tissues and suppresses the activity of FOXO1 thus suppressing gluconeogenesis and glycogenolysis. FOXO1 inhibits insulin secretion and sensitivity in its peripheral target organs through its expression in osteoblasts[50]. Mice lacking *FoxO1* in osteoblasts (*FoxO1$_{osb}$-/-*) have improved glucose disposal load and glucose tolerance which was also related to the favorable glucose metabolism by the liver, muscle and white adipose tissue. At the molecular level, part of the metabolic actions of FoxO1 is through regulation of osteocalcin activity[51–53].

In search of other osteoblast-derived molecules involved in the regulation of energy metabolism, a microarray was performed on primary osteoblasts derived from the *FoxO1$_{osb}$-/-* mice. Amongst the most highly secreted proteins was Lipocalin-2 (LCN2), a glycoprotein implicated in the pathogenesis of obesity but not previously described in bone[54].

Lipocalin-2

Lipocalin-2 is a secreted protein which belongs to the Lipocalins, a group of transporters of small lipophilic molecules such as steroids, lipopolysaccharides, iron and fatty acids in circulation[55]. Typically, despite sequence diversity, lipocalins are distinguished by a characteristic cup-shape calyx formed by an eight-stranded, anti-parallel, symmetrical β-barrel fold with a cylindrical shape[56]. The hydrophobic residues which line the calyx provide a binding site for lipophilic molecules through hydrophobic interaction[57]. Lipocalins are typically named after the ligands they bind and their proposed function. It's therefore not surprising the LCN2 goes by many names including neutrophil gelatinase-associated lipocalin (NGAL), 24p3, oncogenic lipocalin, siderocalin, 25kDa-α2-microglobulin-related protein, and uterocalin.

Human LCN2 was initially isolated in purified by Kjeldsen and coworkers as a 25-kDa neutrophil protein which can be associated with gelatinase B (matrix metalloproteinase 9, MMP9) from human neutrophils[58]. LCN2 was then cloned one year later by the same group[59]. By examining the three-dimensional folds of LCN2, it was proposed that LCN2 is most closely related to epididymal retinoic acid-binding proteins and the major urinary protein[60]. Interestingly, LCN2 is unique in that it can bind macromolecules and hydrophobic molecules due to the much larger and shallower mouth of the calyx compared to the proteins previously mentioned[61]. Human and murine LCN2 share 85% homology in amino acid composition and exhibit 70% similarity in nucleotide composition[56].

The first ligand of LCN2 was discovered by while producing recombinant LCN2 (rLCN2). When expressed in bacteria, rLCN2 appeared either colorless or a light rosé depending on the particular strain used. The color was determined to be related to the presence of iron, and a small iron-binding molecule called enterobactin (enterochelin, Ent) (Goetz et al., 2000). Ent is a key siderophore of many gram-negative bacteria which are used to sequester iron from host cells[62–64]. The LCN2:siderophore:Fe complex can

15

inhibit iron acquisition which results in inhibition of their growth. This causes a "tug-of-war" for iron between the host and bacteria[65].

The initial finding that LCN2 plays a role in iron delivery linked LCN2 to immunity[63,66–68]. During bacterial infection, the expression of LCN2 is upregulated whereby it acts as an acute phase protein[58,69–71]. For example, the expression of LCN2 rises 1000-fold in humans and rodents in response to tubular injury[72,73].

Expression of LCN2 can be induced both in vitro and in vivo by a variety of factors such as lipopolysaccharide, pro-inflammatory cytokines like TNF-α, IL-1β, IL-3, IL-6 and IL-17, retinoic acid, growth factors and nutrients like glucose palmitate, oleate, and insulin. Transcriptional activity of the nuclear factor-κB (NF-κB) seems to be the main pathway involved in LCN2 stimulation[74] (Bu et al., 2006) but C/EBP has also been shown to play a critical role in *Lcn2* expression[75] (Larsen et al., 2014). Activation of *Lcn2* gene transcription is followed by synthesis and secretion where it thereby interacts with its receptors in the periphery.

LCN2 binds two cell-surface receptors: brain type organic cation transporter (24p3R) and megalin (LDL-related protein 2 or LRP2)[73,76,77]. Megalin, a multiligand endocytic receptor, was the first receptor of LCN2 to be characterized. It was found to be expressed in the kidney epithelia to facilitate the renal absorption of LCN2[78]. Through 24p3R, LCN2 has been shown to play a role in apoptosis and the inflammatory response[56,76,79]. In addition, LCN2 has been implicated in a variety of cellular processes such as cell death, cell migration, cell differentiation, cell proliferation, iron delivery, inflammation, insulin resistance and the innate immune response to bacterial infection[80].

In addition to the link observed between iron, bacterial immunity, and LCN2; LCN2 has been reported to play a role in numerous pathological conditions Recent studies have shown an increased expression and an important role of LCN2 in cancerous conditions like breast cancer, leukemias, pancreatic ductal adenocarcinoma, oral cancer, colorectal cancer, brain tumors, gastric cancer, endometrial cancer, hepatocellular carcinoma, multifaceted cancer; kidney diseases like acute kidney injury, chronic kidney disease/proteinuria, congenital obstructive nephropathy, kidney ischemia and reperfusion injury, virus-associated nephropathy, lupus nephritis; liver dysfunctions like acute liver injury, acute hepatic failure, fatty liver disease; cardiovascular disease like acute heart failure, chronic heart failure, autoimmune myocarditis, atherosclerosis, coronary artery disease, endothelial dysfunction and hypertension; pancreatic abnormalities like pancreatitis and pancreatic cancer; sepsis-induced acute respiratory distress syndrome; diabetes and obesity; psoriasis, rheumatoid arthritis and other diverse inflammatory conditions. Also, LCN2 plays a pivotal role in the CNS anomalies including neuroinflammatory and neurodegeneration conditions like mild-cognitive impairment and Alzheimer's disease, multiple sclerosis, gliomas, autoimmune disorders, brain injury, encephalitis, intracerebral hemorrhage, schizophrenia, and spinal cord injury. LCN2 is also involved in several behavioral responses including pair hypersensitivity, cognitive functions, emotional behaviors, depression, neuronal excitability, and anxiety[80,81].

Studies on the molecular mechanism of Metabolic syndrome (MeS) have revealed a tight association with low-grade chronic inflammation which may substantially contribute to its associated complications. This is illustrated by the fact some cytokines like IL-1 IL-6, and TNF-α are involved in modulating metabolic homeostasis and show immunomodulatory properties. Metabolic inflammation is characterized by the dysregulation of these cytokines which become highly expressed in inflamed tissues like liver and adipose and contribute substantially to increased circulating concentrations in obesity. LCN2 is no different in this regard and since it's expressed in adipose tissue has been considered an adipokine. The first evidence that

LCN2 is changed with obesity came from the observation that LCN2 expression is increased in the white adipose tissue (WAT) of *Lepr*[ob/ob] mice. Expression and serum levels are increased in genetic (*Lepr*[ob/ob], *Lepr*[db/db]), dietary (HFD) and microbiota-dependent (*Tlr5*) murine models of obesity[82–84]. The function and role of LCN2 in metabolic disease are controversial.

Experiments in Lcn2-deficient mice fed with a HFD significantly potentiated diet-induced obesity, dyslipidemia, fatty liver disease, and insulin resistance (IR) (Guo et al., 2010). However, this is disputed by the results of another study whereby no difference was observed in insulin sensitivity between WT and LCN2-deficient mice on a HFD[85]. These two studies were further contradicted by a third study which showed LCN2-knockout mice were protected from aging and HFD induced IR, and genetic deletion of LCN2 protected leptin receptor (*Lepr*[db/db]) deficient mice from IR[86]. The paradoxical roles of LCN2 are far from being resolved, but some possible explanation for the discordant phenotypes exist. First Guo et al. and Jun et al. used the same mice where exons 2 through 5 were deleted. Law et al. used a different *Lcn2-/-* mice where exons 1 through 6 were deleted. The targeting strategy and generation of mice could explain the phenotypic differences through giving rise to truncation products or differentially spliced protein with residual functions not detectable with anti-LCN2 antibodies since LCN2 was not detected in either model. In addition, diet and environment could play as a confounder. Different HFD formulations were used in all three studies which could elicit varying phenotypes. Differences in housing conditions such as temperature and cleanliness of the mouse facility can produce variations in microbiota and as a result weight gain.

In a subsequent study is was demonstrated LCN2 is a critical modulator of PPAR-ɣ activation at levels of the recruitment of coactivators/corepressors thereby impacting adipogenesis and lipogenesis in adipose tissues and liver[8787]. Impact on the formation of obesity, inflammation, and obesity-associated metabolic

dysfunction was also shown in rat models after feeding with a high-fructose diet for 4-8 weeks. Expression of Lcn2 correlated with hepatic inflammation, mitochondrial malfunction and oxidative stress[88]. In mouse models of NAFLD and in primary culture LCN2 was linked to the formation of intracellular accumulation of lipid droplet partly regulated by Perilipin 5[89]. Comparative analysis of wild-type and *Lcn2* deficient mice revealed that mice lacking LCN2 accumulated more lipids in the liver when fed on methionine and choline-deficient diets [89] . Furthermore, LCN2 was directly linked to the pathogenesis of NASH in Fatty Liver Shionogi (FLS) mice strain which are genetically programmed to develop NASH. These findings indicate LCN2 has an essential function in lipid metabolism[90].

Importantly, serum LCN2 is increased in obese humans and correlated with measures of insulin resistance. In 229 subjects a positive correlation was observed between serum LCN2 and adiposity, hypertriglyceridemia, hyperglycemia and CRP levels. Obese individuals with a BMI > 30 kg/m2 had 60% higher levels of serum LCN2 when compared to individuals with a BMI < 23 kg/m^2 [91]. A study investigating adult patients with type 1 diabetes, latent autoimmune diabetes, and type 2 diabetes, found LCN2 to be increased in all diabetes groups and correlated with increases in IL-6 levels[92]. In addition, plasma LCN2 and subcutaneous adipose tissue levels were increased in patients with gestational diabetes[93]. In yet another study, LCN2 levels were again increased in patients with T2DM and correlated positively with serum TNF-α levels and LDL concentration[94].

Interestingly, plasma levels of LCN2 were reduced in patients with long-term diabetes (T2D) [95] . Recently, a study aimed to investigate the role of LCN2 expression and serum levels of obese and non-obese Egyptian Women. 188 obese woman who were subdivided into three groups according to fasting blood glucose, normal glucose (NG), impaired glucose (IG) or diabetes (T2D). LCN2 expression and serum were

higher in obese woman compared to lean controls. They were also higher in the IG and T2DM compared to NG obese women[96].

A study investigating the development of NAFLD revealed a close correlation between serum LCN2 and the progression of insulin resistance[97]. Similarly, LCN2 was shown to be significantly higher in women with NAFLD than in women with severe obesity without liver disease. In the same study, TNF-α, IL-6, resistin, and adiponectin stimulated LCN2 expression in HepG2 cells,[98] confirming that expression of LCN2 is moderated by pro-inflammatory triggers[99]. Moreover, in another study analyzing adult patients with NAFLD, urinary LCN2 levels correlated with BMI, insulin resistance and lipid profiles[100]. Increased serum LCN2 levels were observed in Chinese men with coronary artery disease, especially in association with components of the metabolic syndrome[101]. However, another study did not observe differences in serum LCN2 levels but did detect an increase in serum LCN2-MMP9 complex and significant upregulation of LCN2 in visceral adipose tissue of obese individuals[102]. Furthermore, a study of 272 participants found no correlation between LCN2 serum levels and HOMA-IR and cardiovascular risk factors[103]. It remains likely that in obesity and related disorders, the increased expression of various pro-inflammatory cytokines like TNFα, IL-1β, IL-6, and IFN-ϒ, is involved in the upregulation and induction of LCN2[104].

The mechanism and the factors which contribute to the increased concentrations in patients with diabetes is unclear, but dietary factors such as saturated fat, has been shown to lead to an acute increase in circulating LCN2 levels in mice and humans[105,106]. Interestingly, insulin can upregulate circulating LCN2 levels in humans mediated by phosphatidylinositol 3-kinase (PI3K) and mitogen-activated protein kinase (MAPK)[107].

The Kousteni lab found LCN2 to be amongst the most highly secreted protein in a microarray of primary osteoblasts from *FoxO1$_{osb}$-/-* mice. Its expression was confirmed in bone and compared to all other tissue where it is at least 10-fold higher than any other tissue indicating the bone is the predominant tissue expressing LCN2 under baseline conditions[54]. Previously, LCN2 has displayed an important role in musculoskeletal health and disease. In 1995, Blaser and colleagues reported that very high concentrations of LCN2 were found in the synovial fluids (vicious fluids present in the cavities of moveable joints) of patients with inflammatory rheumatoid arthritis[108].

In addition, LCN2 transgenic mice were marked by a smaller phenotype, presented bone microarchitectural changes in bone endochondral and intramembranous bones, and further showed a reduced deposition in the osteoblast bone matrix and impairment in the expansion of bone marrow cavity[109]. In bone, LCN2 has been recognized as a mechano-responding gene regulating bone and energy homeostasis[110,111].

Chapter II: MC4R-Dependent Suppression of Appetite by Bone-Derived Lipocalin 2

Ioanna Mosialou, Steven Shikhel, Jian-Min Liu, Antonio Maurizi, Na Luo, Zhenyan He, Yiru Huang, Haihong Zong, Richard Friedman, Jonathan Barasch, Patricia Lanzana, Liyong Deng, Rudolph Leibel, Mishaela Rubin, Thomas Nicholas, Wendy Chung, Lori M. Zeltser, Kevin W. Williams, Jefferey E. Pessin &
Stravroula Kousteni. Nature. **546,** 440–440 (2017)

Preface

MC4R-Dependent Suppression of Appetite by Bone-Derived Lipocalin 2

Ioanna Mosialou[1], Steven Shikhel[1], Jian-Min Liu[1], Antonio Maurizi[1], Na Luo[1], Zhenyan He[2,3], Yiru Huang[2,3], Haihong Zong[4], Richard Friedman[5], Jonathan Barasch[6], Patricia Lanzana[7], Liyong Deng[7], Rudolph Leibel[7], Mishaela Rubin[8], Thomas Nicholas[9], Wendy Chung[7], Lori M. Zeltser[10], Kevin W. Williams[3], Jefferey E. Pessin[4] & Stravroula Kousteni[1]. Nature. **546,** 440–440 (2017)

[1]Department of Physiology and Cellular Biophysics, College of Physicians and Surgeons, Columbia University, New York, New York 10032, USA.

[2]Department of Neurosurgery, Zhujiang Hospital, Southern Medical University, Guangzhou 510515, China.

[3]Division of Hypothalamic Research, the University of Texas Southwestern Medical Center at Dallas, Dallas, Texas 75390-9077, USA.

[4]Department of Medicine and Molecular Pharmacology, The Albert Einstein College of Medicine, Bronx, New York, New York 10461, USA.

[5]Biomedical Informatics Shared Resource, Department of Biomedical Informatics, Herbert Irving Comprehensive Cancer Center, College of Physicians and Surgeons, Columbia University, New York, New York 10032, USA.

[6]Department of Medicine, College of Physicians and Surgeons, Columbia University, New York, New York 10032, USA.

[7]Naomi Berrie Diabetes Center and Division of Molecular Genetics, Department of Pediatrics, College of Physicians and Surgeons, Columbia University, New York, New York 10032, USA.

[8]Metabolic Bone Disease Unit, Department of Medicine, College of Physicians and Surgeons, Columbia University, New York, New York 10032, USA.

[9]Department of Medicine Nephrology, College of Physicians and Surgeons, Columbia University, New York, New York 10032, USA.

[10]Naomi Berrie Diabetes Center and Department of Pathology and Cell Biology, Columbia University, New York, New York 10032, USA.

Abstract

Bone has recently emerged as a pleiotropic endocrine organ that secretes at least two hormones, FGF23 and osteocalcin, which regulate kidney function and glucose homeostasis, respectively. These findings have raised the question of whether other bone-derived hormones exist and what their potential functions are. Here we identify, through molecular and genetic analyses in mice, lipocalin 2 (LCN2) as an osteoblast-enriched, secreted protein. Loss- and gain-of-function experiments in mice demonstrate that osteoblast-derived LCN2 maintains glucose homeostasis by inducing insulin secretion and improves glucose tolerance and insulin sensitivity. In addition, osteoblast-derived LCN2 inhibits food intake. LCN2 crosses the blood–brain barrier, binds to the melanocortin 4 receptor (MC4R) in the paraventricular and ventromedial neurons of the hypothalamus and activates an MC4R-dependent anorexigenic (appetite-suppressing) pathway. These results identify LCN2 as a bone-derived hormone with metabolic regulatory effects, which suppresses appetite in a MC4R-dependent manner, and show that the control of appetite is an endocrine function of bone.

Introduction

Central signals as well as several hormones and circulating peptides influence food intake and/or energy expenditure in a coordinated manner to regulate body weight. Those include, but are not limited to leptin, insulin, glucagon-like peptide-1, cholecystokinin and peptide YY, which are produced in distinct peripheral organs and influence food intake by signaling in the hypothalamus, the brainstem or afferent autonomic nerves[1,2,3,4,5,6.] It is conceivable that, in addition to these known signals, other hormones exist, which control food intake.

Bone has emerged as an endocrine organ that can regulate energy metabolism. A hormone secreted by osteoblasts, osteocalcin (*bglap*), promotes energy expenditure, insulin secretion and glucose homeostasis in mice and humans[7,8,9,10]. Another hormone, FGF23, which is secreted by osteoblasts and osteocytes, acts on the kidney to regulate phosphate metabolism[11]. The identification of osteocalcin as a regulator of energy metabolism indicates that other hormones synthesized by bone cells may potentially affect additional aspects of energy metabolism. Studies have suggested that osteoblasts have an anorexigenic function *in vivo*[12] and therefore we tried to identify anorexigenic signal(s) that originate from osteoblasts.

MC4R, which is expressed mainly in the paraventricular nucleus of the hypothalamus (PVH), regulates food intake, body weight and caloric efficiency in rodents and humans[13,14,15,16,17]. *MC4R* mutations in humans account for up to 5% of cases of childhood obesity and 0.5% to 2.5% of adult obesity, while deletion of *Mc4r* in mice results in hyperphagic obesity[18,19,20]. The anorexigenic signalling through MC4R is regulated by binding of MC4R to the anorexigenic α-melanocyte-stimulating hormone (α-MSH, the proteolytic cleavage product of pro-opiomelanocortin-α (Pomc)) and the orexigenic (appetite stimulating) Agouti-related protein (AGRP), which are released by different hypothalamic arcuate neurons. More recently, defensin β3, which is produced mainly in skin, was shown to be a MC4R ligand. Defensin β3

modulates MC4R signalling by inhibiting the action of α-MSH or AGRP[21]. These observations suggest that the list of MC4R-modulating proteins controlling food intake may not be complete.

We show that LCN2, a protein that was previously thought to be exclusively secreted by adipose tissue (an adipokine) and is associated with obesity, is expressed by osteoblasts, at levels that are at least tenfold higher in osteoblasts than in white adipose tissue or other organs. Osteoblast-derived LCN2 crosses the blood–brain barrier and suppresses appetite after binding to the MC4R in the hypothalamus. This result broadens our understanding of the control of appetite as well as the endocrine role of bone and identifies LCN2 as an osteoblast-derived hormone that activates the anorexigenic pathway in a MC4R-dependent manner.

Methods

Mice

To generate tissue-specific *Lcn2*-deficient mice, a targeting vector containing LoxP sites within introns 2 and 6, and designed to delete a 1.9 kb genomic fragment comprising *Lcn2* exons 3–6, was electroporated into 129/B6 ES cells. The neomycin-resistance gene flanked by two FRT sites and driven by the human β-actin promoter was used for positive selection. The diphtheria toxin A gene (DTA) driven by the PGK promoter is incorporated into the 3' end of the vector allowing for negative selection. After vector linearization with AsiSI and electroporation into 129/B6 ES cells, homologous recombinants were identified by Southern blot and PCR, and these were subsequently injected in C57BL/6 blastocysts to generate chimaeric mice that expressed the mutated allele. F1 heterozygotes originating from the intercross of chimaeric mice with wild-type C57BL/6 mice were screened for germline transmission of the mutant allele and bred with transgenic mice expressing the *Flp* recombinase under the control of the β-actin promoter to generate mice carrying the *Lcn2* floxed, Δneo/lacZ allele, *Lcn2^{fl/+}* (C57BL/6J: 75%; 129/B6: 25%). *Lcn2^{fl/+}* were crossed with *Col1a1-Cre*[25], *Bglap-Cre*[29], *Adipoq-Cre*[40] or *EIIa-Cre*transgenic mice to create mice with osteoblast-specific (*Lcn2*$_{osb}$^{+/−} and *Lcn2*$_{(OC)osb}$^{+/−}), adipocyte-specific (*Lcn2*$_{fat}$^{+/−}), or global deletion of *Lcn2*(*Lcn2*^{+/−} mice) (C57BL/6J: 87.5%; 129/B6: 12.5%). Of note, the GTex database artificially shows that the *Coll1a1* and *Bglap* genes are expressed in several tissues because bone as a positive control is not included in the expression panels of this database. *Lcn2*-heterozygous mice were intercrossed and animals homozygous for *Lcn2* deletion in osteoblasts (*Lcn2*$_{osb}$^{−/−} and *Lcn2*$_{(OC)osb}$^{−/−}), adipocytes (*Lcn2*$_{fat}$^{−/−}) or global deletion of *Lcn2* (*Lcn2*^{−/−} mice) were obtained. C57BL/6J, ROSA^{mT/mG} (stock number 007676), homozygous and heterozygous leptin-receptor-deficient mice, B6.BKS(D)-*Leprdb*/J (stock number 000697), and mice lacking *Mc4r*, B6;129S4-*Mc4r^{tm1Lowl}*/J (stock number 006414) were purchased from The Jackson Laboratory. *Foxo1*$_{osb}$^{−/−};*Lcn2*-reporter mice that had a double-fusion reporter gene that encodes luciferase-2 and mCherry (termed *Lcn2*–mCherry), *Pomc*–hrGFP, *Npy*–hrGFP and *Sim1*-

cre mice have been described[10,15,41,42,43]. All mice were housed under standard laboratory conditions (12 h on/off; lights on at 7:00) and temperature-controlled environment with food and water available *ad libitum*. In each experiment the mice used were of the same genetic background, as they were all littermates. 10–12-week-old male mice of all genotypes and female *Lcn2*^{−/−} mice were used in all experiments unless otherwise stated. Investigators were blinded during experiments and outcome assessment. Mouse genotypes were determined by PCR; primer sequences are available upon request. All animal procedures were approved by the Columbia University Institutional Animal Care and Use Committee.

Human samples

Men age ≥18 years old with type 2 diabetes were recruited through advertisement flyers. Type 2 diabetes was defined as HbA1c ≥ 6.5% (according to the IDF Diabetes Atlas 2015 (http://www.diabetesatlas.org)). Subjects were excluded if they had a history of disorders associated with altered skeletal structure or function such as chronic kidney disease, chronic liver disease, active malignancy, acromegaly, Cushing's syndrome, thyroid disease, hyper- or hypoparathyroidism or organ transplant. Additionally, subjects were excluded if they were currently using teriparatide, loop diuretics, anti-convulsive therapies, corticosteroids (>3 weeks over the past 3 years), thiazolidinediones or SGLT2 inhibitors. Bisphosphonate and/or denosumab use within the past 12 months were also exclusion criteria. Fasting morning blood was drawn and serum was stored at −80 °C. Patients with or without mutations in *MC4R* were enrolled in a study on the genetic basis of obesity. Participants had blood drawn after an overnight fast, and plasma and the buffy coat were separated. Genomic DNA was purified and the coding sequence of *MC4R* and at least 20 base pairs of flanking intronic sequence were Sanger sequenced and analysed for sequence variants using Sequencer. Primer sequences are available upon request. All studies were approved by

the Columbia University Medical Center Institutional Review Board and informed written consent was

obtained from all participants or their guardians.

Metabolic studies

Glucose tolerance (GTT), insulin tolerance (ITT) and glucose-stimulated insulin secretion (GSIS) tests were

performed as previously described10. For $Lepr^{db/db}$ mice, the dose of glucose during GTT was 1 g per kg

body weight and the dose of insulin during ITT was 2.5 U per kg body weight. Hyperglycemic clamps were

performed at Albert Einstein DRTC Animal Physiology Core, as previously described[44]. Insulin levels were

measure by the insulin ELISA kit (Crystal Chem). Urine elimination of catecholamines (epinephrine and

norepinephrine) was measured in acidified morning urine samples collected during three consecutive

days by EIA (Bi-CAT, Alpco Diagnostics). Creatinine (Microvue creatinine assay kit, Quidel corp.) was used

to normalize between urine samples. ELISAs were performed for measurement of LCN2 (R&D Systems)

and leptin (EMD Millipore) levels in the serum. TSE Labmaster (TSE systems) and Oxymax System

(Columbus Instruments) were used for indirect calorimetry and food-intake measurements. After at least

48-h acclimation to the chambers, data collected for a 48-h period were analysed as per the

manufacturer's recommendations. For fast–refeeding experiments, metabolic cages (Nalgene, Rochester,

NY) were used and food intake calculated as the change of powdered food weight. Mice were individually

housed, fed *ad libitum* and allowed to habituate to the cages for 3 days. Following the initial acclimation,

mice were fasted for 16 h and refed 2 h after the start of the light phase for four consecutive days.

Measurements of food intake after refeeding were collected from the last day. For pair-feeding

experiments, mice were individually housed starting at 4 weeks of age. Pair feeding started at 5 weeks of

age and continued for a period of 8 weeks. Food intake was measured daily, and $Lcn2_{osb}^{-/-}$ mice were

provided every day with the average amount of food consumed by the $Lcn2^{fl/fl}$ littermates that were

fed *ad libitum* on the previous day. Body composition was determined using Bruker Minispec nuclear magnetic resonance (Bruker Optics, Billerica, MA).

LCN2 treatment

Recombinant LCN2 was freshly diluted in phosphate-buffered saline at a concentration of 15 ng μl^{-1} and administered to mice daily intraperitoneally (i.p.) at a dose of 10 $\mu l\,g^{-1}$. Control, vehicle-treated mice, were injected with phosphate-buffered saline. In the study with C57BL/6J wild-type mice, daily injections were initiated at 9 weeks for a period of 16 weeks. GTT, ITT and GSIS tests were performed at 8, 9 and 10 weeks after treatment initiation. Food intake and serum insulin were measured at the end of the treatment period (15 weeks). In the study with *Lepr*$^{db/db}$ mice injections were initiated at 12 weeks of age for a period of 16 weeks. *Mc4r*$^{-/-}$ mice were injected daily with LCN2 for 8 weeks starting at 8 weeks of age. Mice were randomized so that body weight and body composition matched cohorts were used.

Recombinant protein and LCN2 protein identification

For the construction of the bacterial vector expressing LCN2 fused with GST, the cDNA encoding mature mouse LCN2 (residue 83–625) was subcloned into the BamHI/NotI sites of the pGEX-4T-3 vector (GE Healthcare). Purification of bacterially produced mouse recombinant LCN2 protein was performed as described[7]. In brief, the GST–LCN2 fusion protein was bacterially produced and purified on glutathione–sepharose 4B beads according to standard procedures. After extensive washes, LCN2 was cleaved out from the GST moiety using thrombin. A HiTrap Benzamidine column was subsequently used to deplete the thrombin from the preparation. Purity and identity of the protein was assessed by SDS–PAGE followed by Coomassie blue staining and microcapillary LC–MS/MS performed at Taplin Biological Mass Spectometry Facility (Harvard Medical School) as described below. Endotoxin concentration was determined as being below the detection limit.

For LCN2 protein identification by microcapillary LC–MS/MS, endogenous LCN2 protein was purified from flushed bone and adipocyte tissue extracts that were subjected to LCN2 antibody (AF1857, R&D) immunoprecipitation. Eluates from LCN2 immunoprecipitation along with purified recombinant protein were analysed by SDS–PAGE followed by Coomassie blue staining. Bands corresponding to the LCN2 protein were excised and sent to the Taplin Biological Mass Spectometry Facility (Harvard Medical School). Following in-gel trypsin digestion of the gel slice containing the LCN2 protein, the resulting peptides were extracted from the gel and separated on a nano-scale high-performance liquid chromatography (HPLC) capillary column. Eluted peptides were subjected to electrospray ionization and injection into an LTQ-Orbitrap mass spectrometer (Thermo Scientific). Peptides were detected, isolated and fragmented to produce a tandem mass spectrum of specific fragment ions for each peptide. Peptide sequences (and hence protein identity) were determined using the database search algorithm Sequest. Sequence coverage of the LCN2 recombinant protein was 71%, whereas coverage of bone or fat-derived LCN2 was 44.5% and 43% respectively. Owing to the absence of tryptic sites in the first 47 amino acids of the protein, the N terminus was absent from all analyses. Of note, LCN2 has no sequence or structural similarity to any of the known MC4R ligands, α-MSH, AGRP and defensin β3. This is consistent with the lack of sequence or structural similarity between α-MSH, AGRP and defensin β3. However, a search throughout the amino acid sequence of mouse LCN2 revealed the presence of an RGRW motif (amino acids 48–51) that biochemically resembles and may functionally mimic the binding motif of α-MSH to MC4R.

Intracerebroventricular infusions

Mice were anesthetized with avertin and placed on a stereotaxic instrument (Stoelting). The calvaria was exposed and a 0.7 mm hole was drilled upon bregma. A 28-gauge cannula (Brain infusion kit 2, Alzet) was implanted into the third ventricle. The cannula was secured to the skull with cyanoacrylate and attached

with tubing to a primed osmotic pump (Alzet) placed in the dorsal subcutaneous space of the mouse. The rate of delivery was 0.25 µl h^{-1} for 14 days.

For assessment of *Fos* induction by single-bolus injection, 12-week-old male mice were anesthetized by i.p. injection of ketamine/xylazine (100 mg per kg/10 mg per kg) and a chronic stainless steel guide cannula was implanted stereotaxically bilaterally into the PVH with the following coordinates: bregma −0.7 mm; midline ± 0.3 mm; dorsal surface 4.3 mm. Cannulas were secured to the skull with cyanocrylate adhesive gel. After a 12-day recovery and acclimation of mice to handling, mice were injected with saline (4 µl), LCN2 (0.125 mg ml^{-1}) or MT-II (0.125 mg ml^{-1}) through the internal/injector cannula using a 5-µl Hamilton syringe. After 1 h, mice were anesthetized with ketamine/xylazine and perfused transcardially with PBS and subsequently with 4% paraformaldehyde (PFA). Brains were post-fixed in 4% PFA/PBS for 16 h at 4 °C, cryoprotected in 30% sucrose/PBS overnight, embedded in cryomatrix and sectioned at 10 µm. For Fos immunostaining, goat anti-Fos (sc-52-G, Santa Cruz Biotechnology) and Alexa Fluor 488 (A11055, Life Technologies) antibodies were used. To quantify *Fos* expression and calculate the average number of Fos-responsive neurons in each mouse three sequential matched brain sections containing the PVH from each mouse were selected and Fos-positive neurons in the PVH were counted.

LCN2 brain measurements

Following 2 h of i.p. injection of *Lcn2*$^{-/-}$ mice with recombinant LCN2 or vehicle, blood vessels were extensively washed with PBS and the indicated brain regions were dissected out. Tissues were homogenized in ice-cold PBS supplemented with protease inhibitors and soluble fractions were used to measure LCN2 levels by ELISA (R&D Systems) normalized to total protein concentration as determined by DC Protein Assay (Bio-Rad Laboratories). For the detection of lower LCN2 values in the serum

of $Lcn2^{-/-}$ mice, a range of lower standards was used to generate the standard curve, ranging from 19.52 pg ml^{-1} to 2.5 ng ml^{-1}.

Gene-expression analyses

RNA isolation, cDNA preparation and real-time PCR analyses were carried out following standard protocols. For bone tissue analysis, bone-marrow cells were removed completely by extensively flushing the femurs with PBS. Trizol reagent was used for RNA extraction, random hexamers cDNA synthesis kit (Clontech Laboratories) for reverse transcription PCR and SYBR Green Master Mix (Bio-Rad Laboratories) for quantitative PCR. *Actb* was used as an internal control. Data are presented as fold change over control, unless otherwise indicated. Primer sequences are available upon request.

Histological analysis

Bone histomorphometry analyses were performed as previously described[45]. In brief, lumbar vertebrae were dissected, fixed, dehydrated and embedded in methyl metacrylate (MMA). Von Kossa, toluidine blue and tartrate-resistant acid phosphatase (TRAP) staining were used to measure bone volume over tissue volume (BV/TV), osteoblasts and osteoclasts number, respectively. For pancreas histological analysis, the procedure described previously10 was followed. In brief, samples were fixed in 10% neutral formalin, embedded in paraffin and sectioned at 5 μm. Immunohistochemistry was performed using guinea-pig anti-insulin (A0564, Dako), rabbit anti-glucagon (A0565, Dako) and rabbit anti-Ki67 (ab16667, Abcam) antibodies. DeadEnd Colorimetric TUNEL assay (Promega) was performed to assess apoptosis. Osteomeasure software and a Leica DM 5000B microscope outfitted with CCD camera (Sony) was used for pancreas and bone histomorphometric analysis. For cryosection preparation from tissues of reporter mice, tissues were isolated from mice perfused with 4% PFA/PBS, fixed in 4% PFA/PBS for 4–24 h at 4 °C, cryoprotected in 30% sucrose/PBS overnight, embedded in cryomatrix (Tissue-Tek) and sectioned at

10 μm. Bone samples were decalcified for 48 h before cryoprotection and embedding. Immunohistochemical analysis of samples from Lcn2–Luc2–mCherry and Cre-reporter mice was performed using anti-mCherry (ab167453, Abcam), anti-GFP (632375, Clontech Laboratories) and anti-RFP (600-401-379, Rockland Immunochemicals) antibodies, respectively. Alexa Fluor 488 and 594 (A11029 and A21207, Life Technologies) were used for signal detection. Experiments were repeated at least three times and representative images are presented.

Brain-binding assay

$Lcn2^{-/-}$ or $Mc4r^{-/-}$ brains were snap-frozen in liquid nitrogen, and 10-μm sections were prepared and desiccated overnight at 4 °C under vacuum. The following day brain sections were rehydrated in ice-cold binding buffer (50 nM Tris-HCl (pH 7.4), 10 nM $MgCl_2$, 0.1 mM EDTA and 0.1% BSA) for 15 min and incubated 1 h at room temperature in the presence of biotinylated LCN2 (25 pg ml^{-1}) or biotinylated GST as a control. After washing in harvesting buffer (50 mM Tris-HCl (pH 7.4)), samples were fixed in 4% PFA for 15 min, washed in PBS, and incubated with goat anti-biotin antibody (SP-3000, Vector Laboratories) overnight at 4 °C. The signal was visualized, after incubation with anti-goat Alexa Fluor 488 (A11055, Life technologies) followed by DAPI counterstaining, using an Olympus Bx53F microscope. To test for assay specificity, the procedure described above was performed in the presence of 100-fold excess of non-biotinylated LCN2 or GST (2.5 ng ml^{-1}). Experiments were repeated three times and representative images are presented.

Electrophysiology studies

Brain slices were prepared from young adult male mice (5–8 weeks old) as previously described[46,47]. In brief, male mice were deeply anaesthetized with an i.p. injection of 7% chloral hydrate and transcardially perfused with a modified ice-cold artificial CSF (ACSF) (described below). The mice were then decapitated,

and the entire brain was removed, and immediately submerged in ice-cold, carbogen-saturated (95% O_2 and 5% CO_2) ACSF (126 mM NaCl, 2.8 mM KCl, 1.2 mM $MgCl_2$, 2.5 mM $CaCl_2$, 1.25 mM NaH_2PO_4, 26 mM $NaHCO_3$ and 5 mM glucose). Coronal sections (250 µm) were cut with a Leica VT1000S vibratome and then incubated in oxygenated ACSF at room temperature for at least 1 h before recording. The slices were bathed in oxygenated ACSF (32 °C–34 °C) at a flow rate of ∼2 ml min^{-1}. All electrophysiology recordings were performed at room temperature.

The pipette solution for whole-cell recording was modified to include an intracellular dye (Alexa Fluor 350 hydrazide dye) for whole-cell recording: 120 mM K-gluconate, 10 mM KCl, 10 mM HEPES, 5 mM EGTA, 1 mM $CaCl_2$, 1 mM $MgCl_2$ and 2 mM MgATP, 0.03 mM Alexa Fluor 350 hydrazide dye (pH 7.3). Epifluorescence was briefly used to target fluorescent cells, at which time the light source was switched to infrared differential interference contrast imaging to obtain the whole-cell recording (Zeiss Axioskop FS2 Plus equipped with a fixed stage and a QuantEM:512SC electron-multiplying charge-coupled device camera). Electrophysiological signals were recorded using an Axopatch 700B amplifier (Molecular Devices), low-pass filtered at 2–5 kHz, and analysed offline on a PC with pCLAMP programs (Molecular Devices). Membrane potential and firing rate were measured by whole-cell current-clamp recordings from neurons in brain slices. Targeting of *Pomc* and *Npy* neurons was anatomically restricted to the arcuate nucleus of the hypothalamus, whereas *Sim1* neurons were targeted within the paraventricular nucleus of the hypothalamus. Recording electrodes had resistances of 2.5–5 MΩ when filled with the K-gluconate internal solution.

LCN2 (1.25 pM) was added to the ACSF for specific experiments. Solutions containing drug were typically perfused for 5 min. A drug effect was required to be associated temporally with peptide application, and the response had to be stable within a few minutes. A neuron was considered depolarized or hyperpolarized if a change in membrane potential was at least 2 mV in amplitude.

36

Cell culture and treatment

HEK293T (obtained from ATCC) and hypothalamic GT1-7 cells (obtained from The Salk Institute)[48] were maintained in DMEM (25 mM glucose) supplemented with 10% FBS and 100 U ml^{-1} penicillin and 100 µg ml^{-1}streptomycin and cultured at 37 °C in a 5% CO_2 atmosphere. INS1 cells (obtained from ThermoFisher Scientific) were maintained in RPMI supplemented with 10% FBS, 10 mM HEPES, 1 mM sodium pyruvate, 50 µM β-merchaptoethanol and 100 U ml^{-1} penicillin and 100 µg ml^{-1}streptomycin and cultured at 37 °C in a 5% CO_2 atmosphere. Cell lines were tested and found to be free of mycoplasma. GT1-7 cells were authenticated by examining the expression of their specific panel of genes as described in ref. 48. For LCN2/α-MSH treatment and gene expression analysis in GT1-7, cells were serum starved overnight in DMEM supplemented with 0.5% FBS before being treated with various concentrations of LCN2, α-MSH or vehicle for 4 h. Primary islets were isolated as described previously8. For isolation of primary osteoblasts, calvaria from 3-day-old mice were digested in 1 mg ml^{-1} collagenase (Worthington Biochemical) for 1 h at 37 °C with shaking, filtered, washed in αMEM and cultured in αMEM supplemented with 10% FBS and 100 U ml^{-1} penicillin and 100 µg ml^{-1} streptomycin. When cells reached confluence, medium was supplemented with 5 mM β-glycerolphosphate and 100 µg ml^{-1} ascorbic acid (mineralization medium) which was replaced every 2 days thereafter. All experiments were repeated at least three times in triplicate.

Binding assays

For binding assays, a 100-mm dish of HEK293T cells was transfected with 10 µg of the expression construct containing *MC4R*, *MC3R* or *MC1R*(purchased from Origene Technologies) using Lipofectamine 2000 (Invitrogen, Chicago, IL) according to the manufacturer's instructions. Transfection efficiency was tested by real-time PCR. Subsequently, 36 h after transfection, cells were dissociated with an enzyme-free cell-dissociation buffer (Life Technologies), washed with PBS and plated on white CoStar 96-well plates

pretreated with gelatin. For saturation binding assays and calculation of the dissociation constant, K_d, 24 h later cells were washed with binding medium (0.5% BSA in Ca^{2+}/Mg^{2+}PBS) and incubated with serial dilutions of biotinylated protein in binding medium for 2 h at 37 °C. Protein biotinylation was performed using the EZ-Link NHS-PEG$_4$-biotinylation kit from Fisher Scientific. Following washes with binding medium, cells were fixed with 4% PFA for 10 min, washed with binding medium supplemented with 0.3% Triton X-100 and further incubated for 30 min with extra-avidin peroxidase (Sigma-Aldrich) in binding buffer. Cells were extensively washed and bound peroxidase was quantified using TMB substrate (Thermo Fisher Scientific). The reaction was terminated by addition of TMB stop solution (Immunochemistry Technologies) and absorbance was read at 450 nm in a Fluostar Omega (BMG Labtech) microplate reader. Non-specific binding was determined in the presence of 100 µm non-biotinylated protein and specific binding was calculated by subtracting absorbance values for nonspecific binding from total binding values. Control experiments were performed using the maximum amount of biotinylated protein and HEK293T cells transiently transfected with the pcDNA3.1 vector alone, but no signal was detected. For competition binding assays, 50 nM and 10 nM of biotinylated LCN2 and α-MSH (Sigma-Aldrich), respectively, (corresponding to their $K_d$values) were added together with serial dilutions of non-biotinylated protein ranging from 10^{-11} to 10^{-5} M and the procedure described above for determination of binding affinities was followed. Recombinant human AGRP (aa 83–132) and mouse leptin proteins were purchased from R&D. The incubation time that is sufficient to ensure that equilibrium has been reached was determined by kinetic experiments. Biotinylated α-MSH (10 nM) was incubated in the presence of 10 nM LCN2 and specific binding was determined at various time points thereafter, For binding assays in GT1-7, cells were transiently transfected with 100 nM control siRNA (si-scramble) or siRNAs against *Mc4r* (Dharmacon) using Lipofectamine 2000. Silencing efficiency was tested by real-time PCR. Subsequently, 36 h after transfection, cells were dissociated, washed with PBS and plated on white CoStar 96-well plates. The cells were treated 24 h later with 60 ng ml^{-1} biotinylated LCN2 or equimolar amounts of α-MSH and binding

assays were performed as described above. Binding data were analysed using Graphpad Prism Software. All experiments were repeated four times in triplicate.

cAMP assays

For cAMP quantification in GT1-7, cells were serum starved overnight (0.5% FBS), pre-incubated in the presence of 0.5 mM IBMX for 30 min at 37 °C and then stimulated with various amounts of LCN2 in the presence of 0.5 mM IBMX for 15 min. cAMP concentration was measured by ELISA (Enzo Life Sciences) and data were normalized to total protein content measured by DC Protein Assay. α-MSH was used as a positive control. For determination of cAMP production in the presence of SHU9119 (Tocris, Bioscience), cells were pretreated with 10 µM of the antagonist for 1 h before LCN2 treatment. For determination of cAMP production in the absence of receptors, 48 h before LCN2 treatment (60 ng ml^{-1}), cells were transiently transfected with 100 nM ON-TARGETplus SMARTpool siRNA targeting *Mc4r* or *Slc22a17* or control (Dharmacon) using Lipofectamine 2000. For dose-response assays and calculation of EC$_{50}$, HEK293T cells were transiently transfected with 10 µg of pCRE/luciferase (pCRE–luc), a cAMP-inducible luciferase-expressing plasmid along with 10 µg of the expression construct containing *MC4R*, *MC3R* or *MC1R*. pRL-CMV Renilla (Promega) was used as an internal control. 24 h later, cells were dissociated, washed with PBS and plated on white CoStar 96-well plates. 48 h after transfection, cells were serum starved (0.5% FBS) overnight, pre-incubated in the presence of 0.5 mM IBMX for 30 min at 37 °C and then stimulated with increasing amounts of LCN2, α-MSH or leptin in the presence of 0.5 mM IBMX for 15 min at 37 °C. Luciferase activity was determined using the Dual-Glo Luciferase Assay System (Promega) and quantified using Fluostar Omega. Luciferase activity was normalized to renilla activity and is presented as relative luciferase activity over vehicle-treated cells. Control experiments were performed using HEK293T cells transiently transfected with pCRE-luc or the *MC4R*-expression construct alone but no

signal was detected. Data were analysed using Graphpad Prism Software. Experiments were repeated at least four times in triplicate.

Western blotting

For bone tissue analysis, bone-marrow cells were removed completely by flushing the femurs extensively with PBS. Tissue extracts from wild-type mice were analysed on SDS-polyacrylamide gel, transferred to a nitrocellulose membrane and probed with LCN2 (AF1857, R&D) and GAPDH (14C10, Cell Signaling Technology) antibodies following standard procedures. For signal-transduction pathways in GT1-7 cells, cells were serum starved overnight in DMEM supplemented with 0.5% FBS and then stimulated with various amounts of LCN2 for 5 or 15 min as indicated. Cells were lysed and analysed by western blotting using the following antibodies: anti-cFos (7963, Abcam) anti-pERK1/ERK2 (4370), anti-pAMPK (2531), anti-p-tyrosine (9416), anti-pCREB (9198), anti-ERK1/ERK2 (total ERK1/ERK2, 9102), anti-AMPK (total AMPK, 2532) and anti-CREB (4820) from Cell Signaling Technology. Anti-β-actin (sc-47778, Santa Cruz Biotechnology) was used as an internal loading control. Experiments were repeated at least three times and representative images are presented. Gel source data are provided in Supplementary Fig. 1.

Northern blotting

Trizol reagent was used for RNA extraction from tissues of C57BL/6J mice according to the manufacturer's instructions. For bone tissue analysis, bone-marrow cells were removed completely by flushing the femurs extensively with PBS. 10 µg total RNA was resolved on formaldehyde-agarose gels followed by transfer onto an Ambion BrightSTar-Plus membrane and hybridization with a ^{32}P-labelled probe in Ultrahyb (Ambion, Thermo Fisher Scientific). A β-actin-specific probe was used as an internal control. Uncropped images are provided in Supplementary Fig. 1.

Microarray analysis

Total RNA was extracted from primary osteoblasts isolated from mouse calvaria using Trizol reagent (Invitrogen). Microarray analysis was performed using the GeneChip 3' IVT express kit and mouse genome 430 2.0 array gene chips (Affymetrix) according to the manufacturer's instructions. In brief, antisense RNA was synthesized from 500 ng of RNA and was biotinylated followed by purification and fragmentation using the GeneChip 3' IVT express kit. Fragmented aRNA was hybridized to Affymetrix mouse genome 430 2.0 array gene chips. Following hybridization, chips were scanned with a GeneChip Scanner 3000 7G (Affymetrix). Data were normalized using the Mas5 method, and then $\log_2$ transformed. Data were deposited in Gene Expression Omnibus previously (accession number GSE43242). Differential expression was analysed using LIMMA. We focused on genes which code for secreted molecules (Gene Ontology49 Accession number GO:0005615 extracellular space) with Benjamini–Hochberg50 raw $P < 0.1$ FDR ≤ 0.33 and $|\log_2 FC \geq 2|$. For a given gene, only the transcript with the lowest P value is given in Extended Table 1.

Statistical analysis

Results are presented as mean ± s.e.m. Unpaired, two-tailed Student's t-test was performed for comparisons between two groups and one-way ANOVA for comparisons of more than two groups. For all experiments $*P \leq 0.05$ or $^{\#}P \leq 0.05$. Effect size between wild-type and $Lcn2_{osb}^{-/-}$ mice was calculated according to the formulae from ref. [51]. Sample-size determinations were based on the means and variances of preliminary data to achieve 80% power and a 5% experiment-wise error rate assuming either an analysis of covariance (ANCOVA) parametric design for cross-sectional comparisons or a repeated measures analysis of variance (rmANOVA) for metabolic studies in mice.

Data availability

All data supporting the findings of this study are available within the paper and Supplementary Information. Source Data for all figures are provided with the paper. Uncropped versions of the gel images are provided in Supplementary Fig. 1.

Results

LCN2 is an osteoblast-enriched hormone

Mice with osteoblast-specific knockdown of *Foxo1* (*Foxo1*$_{osb}$$^{-/-}$) show improved energy metabolism, in part owing to osteocalcin activation[10]. Therefore, we searched for osteoblast-secreted molecules that regulate energy homeostasis downstream of FOXO1. Among them, the gene that encodes LCN2, a 25 kDa, secreted glycoprotein, was one of the most highly upregulated in osteoblasts (Supplementary Table 1), bone and serum of *Foxo1*$_{osb}$$^{-/-}$ mice (Fig. 1a, b). Because LCN2 has been considered an adipokine that is associated with obesity[22,23,24], we analysed LCN2 expression in all tissues and identified bone as the predominant organ where *Lcn2* is expressed, with at least tenfold higher expression levels in bone than in white fat (Fig. 1c–e and Extended Data Fig. 1a, c). *Lcn2* expression increased with osteoblast differentiation similar to osteocalcin and alkaline phosphatase (Extended Data Fig. 1b). Therefore, LCN2 is an osteoblast-enriched, secreted protein that is upregulated in *Foxo1*$_{osb}$$^{-/-}$ mice, which have improved energy metabolism.

Osteoblast-derived LCN2 decreases food intake

To determine the cellular origin of LCN2, we generated mice that lacked LCN2 in osteoblasts (*Lcn2*$_{osb}$$^{-/-}$) or adipocytes (*Lcn2*$_{fat}$$^{-/-}$)[25,26](Extended Data Figs 1d–k, 2c). *Lcn2*$_{osb}$$^{-/-}$ and *Lcn2*$_{fat}$$^{-/-}$ mice showed a 67% and 27% decrease in serum levels of LCN2, respectively. Osteoblast-derived and fat-derived LCN2 is the same protein (Extended Data Fig. 2a, b).

Lcn2$_{osb}$$^{-/-}$ mice had compromised glucose metabolism, as was shown by decreased glucose tolerance, insulin sensitivity, a lack of insulin secretion after glucose or arginine challenge (Fig. 1f, h, j and Extended Data Fig. 3a, b), and 50% reduction in insulin levels (Fig. 2a). Islet numbers and size, β-cell mass and β-cell

43

proliferation were decreased in the pancreas of $Lcn2_{osb}^{-/-}$ mice without changes in apoptosis, islet architecture or differentiation (Extended Data Fig. 3c–g). None of these parameters were affected in $Lcn2_{fat}^{-/-}$ mice (Fig. 1g, i, k, 2b). In all experiments *Col1a1-Cre* mice were identical to wild-type littermates (Extended Data Fig. 3i–p).

In spite of low circulating insulin levels and decreased insulin sensitivity, $Lcn2_{osb}^{-/-}$ mice showed increased gonadal fat weight (16.5%), total fat mass (19.6%) and body weight (5%), which was an expected magnitude of change since lean and bone mass were unaltered (Fig. 2c–e). $Lcn2_{fat}^{-/-}$ mice did not show changes in fat or body weight (Fig. 2f–h). Expression of adipogenic factors increased, whereas expression of lipolytic factors decreased in $Lcn2_{osb}^{-/-}$ mice (Extended Data Fig. 3q). Energy expenditure and sympathetic nervous system activity were similar in $Lcn2_{osb}^{-/-}$ and control mice (Extended Data Fig. 3r–t). By contrast, 3-month-old $Lcn2_{osb}^{-/-}$ mice showed 16.4% increase in food intake, which persisted following normalization by body weight, whereas food intake was not affected in $Lcn2_{fat}^{-/-}$ mice (Fig. 2i, j and Extended Data Fig. 3u). During growth, food intake was increased by 23.7% in 3-week-old $Lcn2_{osb}^{-/-}$ mice and preceded the increase in body weight that manifested at 4 weeks of age (Fig. 2k, l). These observations, and the lack of *Adipoq-Cre* expression in bone-marrow adipocytes[27,28], indicate that neither bone marrow nor white fat contribute to an amount of LCN2 in circulation that can regulate appetite and glucose metabolism. These results also suggest that increased appetite accounts for the increase in body weight in $Lcn2_{osb}^{-/-}$ mice and may contribute to the development of glucose intolerance.

To examine this hypothesis, we pair-fed $Lcn2_{osb}^{-/-}$ mice with their wild-type littermates. Body weight, fat mass and insulin sensitivity were normalized, whereas serum insulin levels and insulin secretion after glucose load remained compromised in $Lcn2_{osb}^{-/-}$ mice and as a result their glucose intolerance persisted (Extended Data Fig. 4a–f). Therefore, we examined whether LCN2 signals in β-cells directly to affect β-cell functions. LCN2 stimulated insulin secretion directly in primary pancreatic islets (Extended Data Fig. 3h).

44

Therefore, the anorexigenic function of LCN2 influences fat mass, body weight and insulin sensitivity, whereas the ability of LCN2 to improve glucose tolerance probably reflects its direct action on pancreatic islets.

Inactivation of *Lcn2* in osteoblasts using another osteoblast-specific line expressing *Bglap-Cre*[29] (*Lcn2*$_{(OC)osb}$$^{-/-}$, Extended Data Fig. 2c) reproduced the metabolic phenotype of *Lcn2*$_{osb}$$^{-/-}$ mice (Extended Data Fig. 4g–q). Bone mass and osteocalcin expression and activity were not affected in *Lcn2*$_{osb}$$^{-/-}$ mice (Extended Data Fig. 4r–t), indicating that their metabolic phenotype is not secondary to a bone defect or changes in osteocalcin activity. Of note, osteocalcin does not regulate appetite[7].The biological significance of these observations was validated in humans. Serum levels of LCN2 inversely correlated with body weight and glycated haemoglobin (HbA$_{1c}$) in patients with type 2 diabetes mellitus (Fig. 2m, n).

A physiological role for LCN2 in feeding regulation was found, as there was a threefold increase in serum levels of LCN2 1–3 h after refeeding wild-type mice after overnight fasting (Fig. 2o). The increase in LCN2 was owing to LCN production by osteoblasts, as it correlated with a 1.6-fold increase in *Lcn2* expression in bone, but not in fat or other tissues (Extended Data Fig. 4u). Similarly, food intake was suppressed at 1–3 h after refeeding wild-type mice (Fig. 2p).

Lcn2$_{osb}$$^{-/-}$ mice had higher cumulative food intake at all examined time points after refeeding and twofold higher rate of food intake at 2 h after refeeding (Fig. 2q). Intraperitoneal administration of LCN2 to fasted *Lcn2*$_{osb}$$^{-/-}$ mice immediately after refeeding suppressed food intake within 1 h as efficiently as in wild-type mice. Thus, upregulation of *Lcn2* expression by osteoblasts following feeding is an acute anorexigenic signal to limit appetite after a meal in the mouse.

LCN2 suppresses food intake in lean and obese mice

We then investigated whether exogenous LCN2 could exert a sustained anorexigenic effect. Daily intraperitoneal administration of LCN2 (150 ng g^{-1}) to wild-type mice for 16 weeks increased serum LCN2 levels by twofold, an increase similar to that observed after postprandial upregulation of serum LCN2 levels (Extended Data Fig. 5a), and led to an 18% decrease in food intake (Fig. 3a). Fat mass, body weight and body-weight gain decreased by 32%, 9.4% and 34%, respectively (Fig. 3b, cand Extended Data Fig. 5b, c). Circulating insulin levels increased and glucose tolerance, insulin secretion and sensitivity and energy expenditure improved in LCN2-treated mice (Fig. 3d–f and Extended Data Fig. 5d–f). The identity and purity of the recombinant protein was verified by mass spectrophotometry (Extended Data Fig. 5g–h).

Treatment of mice with an inactive leptin receptor (*Lepr*$^{db/db}$ mice)[30] with LCN2 for 16 weeks suppressed food intake, gonadal fat and body-weight gain by 16.5%, 22% and 26%, respectively (Fig. 3g–i and Extended Data Fig. 5i). Glucose tolerance, insulin sensitivity and energy expenditure were improved in *Lepr*$^{db/db}$ mice treated with LCN2 (Fig. 3jand Extended Data Fig. 5j, k). These results indicate that LCN2 counteracts, at least in part, deleterious consequences of the lack of leptin signaling on appetite and energy expenditure. They also support observations that *Lcn2* expression is upregulated in obesity to counteract adiposity, inflammation and insulin resistance[22].

LCN2 acts on the hypothalamus to suppress appetite

Because *Lcn2*$_{osb}$$^{-/-}$ mice did not show changes in the expression of adipose- or gut-derived hormones that affect food intake, we tested whether LCN2, which is not expressed in the hypothalamus (Fig. 1c, d and Extended Data Fig. 1a, c), can cross the blood–brain barrier and signal directly in the brain to regulate food intake.

46

LCN2 or vehicle was delivered intraperitoneally to $Lcn2^{-/-}$ mice. Notably, hyperphagia and the entire metabolic phenotype—and lack of changes in bone mass—of the global $Lcn2^{-/-}$ mice are identical, including in their magnitude, to those observed in $Lcn2_{osb}^{-/-}$ mice (Extended Data Fig. 6h–s). LCN2, at a dose restoring normal serum levels (107 ng ml^{-1}), accumulated in the brainstem, thalamus and mostly in the hypothalamus of $Lcn2^{-/-}$ mice within 2 h of treatment at levels similar to those of wild-type mice (Extended Data Fig. 6t). Fasting and subsequent refeeding of wild-type mice led to a twofold increase in LCN2 levels in the hypothalamus (Extended Data Fig. 6u). Intracerebroventricular (ICV) infusions in $Lcn2^{-/-}$ mice, at a dose restoring normal LCN2 levels in the hypothalamus, normalized appetite in $Lcn2^{-/-}$ mice and decreased body-weight gain by 5% (Fig. 4a, b). There was no leakage of centrally delivered LCN2 into the circulation (Extended Data Fig. 6v). ICV infusion of LCN2 decreased appetite and body-weight gain in wild-type mice with similar amplitude as ICV infusion of leptin or melanotan II (MT-II), a potent synthetic analogue of α-MSH (Fig. 4c–f). Therefore, LCN2 suppresses appetite in the mouse by signaling directly in the brain.

LCN2 activates cAMP signaling in the hypothalamus

We investigated how LCN2 suppresses food intake after signaling in the hypothalamus. LCN2 did not induce phosphorylation of AMPK, ERK1, ERK2 or tyrosine kinase but activated cAMP as efficiently as 0.5 nM α-MSH, the equimolar amount of the most potent LCN2 dose (10 ng ml^{-1}) in mouse GT1-7 hypothalamic cells (Fig. 4g, h). LCN2 dose-dependently upregulated and subsequently downregulated cAMP activity. The same bell-shaped response curve was observed in the regulation of appetite after ICV infusion of increasing concentrations of LCN2 in wild-type mice (Fig. 4i). These responses suggest receptor desensitization as seen in the case of signaling that is mediated by G-protein-coupled receptors[31,32].

LCN2 activates MC4R signaling in the hypothalamus

Among all hypothalamic pathways that affect appetite, only the expression of downstream effectors of MC4R signalling was altered in $Lcn2_{osb}^{-/-}$ mice and in LCN2-treated wild-type mice (Extended Data Fig. 7a–d). Therefore, we analysed whether MC4R transduces LCN2 signals. Several lines of evidence supported this hypothesis. First, LCN2 dose-dependently induced cAMP activity in $Mc4r$-expressing HEK293T cells with an EC_{50} (the half-maximal response) of 1.41 ± 0.25 nM (Fig. 5a and Extended Data Figs 7h, 8i). Although α-MSH stimulated cAMP with an EC_{50} of 0.09 ± 0.01 nM, the potency of cAMP induction by LCN2 was higher compared to the effect of α-MSH in low, but physiologically relevant doses found in the brain (10^{-12} M and 10^{-11} M). Second, silencing $Mc4r$ or pharmacologically inhibiting its activity in GT1-7 cells abrogated LCN2-induced cAMP activity (Extended Data Fig. 7e–g). Third, LCN2 activated MC4R signalling in GT1-7 cells (Extended Data Fig. 7i–n). By contrast, among the two known LCN2 receptors, megalin (also known as $Lrp2$) is not expressed in GT1-7 cells, whereas silencing of $Slc22a17$ (known as 24p3R) did not affect LCN2 signalling (Extended Data Fig. 7o–t). Fourth, biotinylated LCN2, at a physiological dose in the hypothalamus (25 pg ml^{-1}), bound to PVH neurons and neurons in the ventromedial nucleus of the hypothalamus (VMH) of $Lcn2^{-/-}$ mice, where $Mc4r$ is expressed[33] (Fig. 5b and Extended Data Fig. 9a). Binding of LCN2–biotin was competitively displaced by an excess of unlabelled LCN2, and no signal was detected with GST–biotin. Binding of LCN2 was abolished in the hypothalamus of $Mc4r$-deficient mice (Fig. 5b), or in GT1-7 cells where $Mc4r$ was silenced by short-interfering RNA (siRNA) (Extended Data Fig. 7u). LCN2 binding was not detected in neurons of the arcuate nucleus of the hypothalamus.

LCN2 binds to MC4R in HEK293T cells with a dissociation constant (K_d) of 51.39 ± 4.78 nM and competed for binding with α-MSH with an inhibitor constant (K_i) of 46.34 ± 1.11 nM. By comparison, α-MSH bound to MC4R with a 4.5-fold higher affinity ($K_d = 11.93 \pm 1.23$ nM) than LCN2 and competed for binding with LCN2 with a K_i of 12.63 ± 1.10 nM (Fig. 5c–e and Extended Data Fig. 8i). Leptin and AGRP were used as a

48

negative and additional positive control, respectively. Similar to α-MSH, LCN2 bound to and activated cAMP signalling through the MC1 and MC3 receptors (Extended Data Fig. 8a–h). However, MC1R and MC3R do not regulate appetite[34,35]. Therefore, LCN2 binds to *Mc4r*-expressing hypothalamic neurons and activates MC4R signalling.

LCN2 activates PVH neurons of the hypothalamus

We investigated whether LCN2 signals directly in *Mc4r*-expressing cells. ICV administration of LCN2 induced, with similar potency to MT-II, *Fos* expression in PVH neurons of wild-type (36% of PVH neurons were activated by LCN2 and 35% activated by MT-II), but not *Mc4r*$^{-/-}$ mice (Fig. 5f and Extended Data Fig. 7v). To assess the effects on cellular activity of hypothalamic neurons, we targeted *Sim1*-expressing neurons in the PVH (PVH–*Sim1*) and *Pomc-* and *Npy*-expressing neurons in the arcuate nucleus for electrophysiological recordings (Extended data Fig. 9b–d). A subpopulation of PVH–*Sim1* neurons have been linked to *Mc4r* expression and activities related to energy balance and MC4R-mediated activation of PVH and anorexia[15,36,37]. Therefore, these functions of PVH–*Sim1* neurons help to better define the effect of LCN2 on melanocortin signalling. PVH-*Sim1* neurons were depolarized in the presence of LCN2 (1.25 pM; in control artificial cerebrospinal fluid (ACSF), resting membrane potential (RMP) = −50.8 ± 4.1 mV; in ACSF + LCN2, RMP = −43.2 ± 3.3 mV; $n = 8$ in each group, $P < 0.05$). The remaining 12 neurons from the PVH remained unchanged in response to LCN2 (1.25 pM; in control ACSF, RMP = −47.1 ± 2.8 mV; in ACSF + LCN2, RMP = −47.2 ± 2.7 mV; $n = 12$, $P > 0.05$) (Fig. 5g, j). LCN2 (1.25 pM) did not alter the resting membrane potential of any *Npy* neurons (in control ACSF, RMP = −43.5 ± 1.4 mV; in ACSF + LCN2, RMP = −43.5 ± 1.5 mV; $n = 26$, $P > 0.05$) and *Pomc* neurons (in control ACSF, RMP = −46.1 ± 2.1 mV; in ACSF + LCN2, RMP = −46.3 ± 2.2 mV; $n = 13$, $P > 0.05$) (Fig. 5h, i). These data support activation of PVH neurons by LCN2, which is independent of the activity within *Pomc* or *Npy*/*Agrp* neurons of the arcuate nucleus.

MC4R is necessary for regulation of appetite by LCN2

To determine whether MC4R mediates the anorexigenic function of LCN2 *in vivo* we treated *Mc4r*$^{-/-}$ and wild-type mice with LCN2. LCN2 suppressed appetite and decreased body weight in wild-type but not in *Mc4r*$^{-/-}$ mice (Fig. 6a–c). LCN2 treatment did not improve glucose metabolism in *Mc4r*$^{-/-}$ mice, although treatment improved energy expenditure, glucose tolerance and insulin sensitivity in wild-type mice (Extended Data Fig. 10a–d). Analysis of *Lcn2*$_{osb}$$^{+/-}$::*Mc4r*$^{+/-}$ mice showed a significant increase in appetite, body weight and fat mass, and decreased glucose tolerance and insulin sensitivity compared to *Lcn2*$_{osb}$$^{+/-}$ and *Mc4r*$^{+/-}$ mice (Fig. 6d–g and Extended Data Fig. 10e–k). Therefore, LCN2 suppresses appetite by signaling through MC4R.

To understand how LCN2 regulates MC4R signalling in humans, we measured LCN2 levels in the plasma of six patients with MC4R mutations and in six age-, gender- and body-mass-index-matched control subjects who had normal *MC4R* sequences (Fig. 6h, i and Extended Data Fig. 10l). LCN2 levels were two–fourfold increased in three out of the five young-adult patients and in the single pediatric patient with MC4R mutations, as expected for GPCR ligands when the GPCR carries inactivating mutations.

Discussion

We have identified a mode of endocrine regulation of energy metabolism by bone, which occurs through control of appetite. LCN2, which is secreted by osteoblasts, acts as a hormone that mediates an acute and chronic anorexigenic function of bone in lean and obese mice. Osteoblast-derived LCN2 crosses the blood–brain barrier, and binds to and activates MC4R in PVN neurons of the hypothalamus with potency similar to that of leptin and comparable to the potent α-MSH analogue, MT-II. In addition to appetite-suppressing activities, LCN2 regulates insulin secretion and increases insulin sensitivity and glucose tolerance.

At this time there is no experimental evidence to explain why bone would suppress food intake. It is possible that the food-suppressing function of the skeleton resembles the homeostatic role of leptin; a decrease in bone mass and *Lcn2* expression could allow an increase in food intake to restore nutrient uptake and maintain body growth through skeletal growth and/or increase in bone mass. Independent of the reasons for this regulation of energy intake, the underlying mechanisms that regulate appetite, and the abnormal glucose metabolism and obesity that are associated with metabolic disease, have not yet been fully elucidated. In that respect, the role of the skeleton in the control of energy intake and homeostasis may provide new insights into the pathogenesis of these diseases.

Note added in proof: Two earlier studies reported that *Lcn2* deficiency does not affect appetite[38,39]. The reasons for the different results are not clear, but maybe due to different methodology, including differences in generating the *Lcn2*-deficient mice. However, the effects of exogenous LCN2 support the conclusion drawn from our loss-of-function experiments.

References

1. Friedman, J. M. & Halaas, J. L. Leptin and the regulation of body weight in mammals. *Nature* **395**, 763–770 (1998)

2. Brüning, J. C. *et al.* Role of brain insulin receptor in control of body weight and reproduction. *Science* **289**, 2122–2125 (2000)

3. Drucker, D. J. The biology of incretin hormones. *Cell Metab.* **3**, 153–165 (2006)

4. Choudhury, A. I. *et al.* The role of insulin receptor substrate 2 in hypothalamic and β cell function. *J. Clin. Invest.* **115**, 940–950 (2005)

5. Batterham, R. L. *et al.* Critical role for peptide YY in protein-mediated satiation and body-weight regulation. *Cell Metab.* **4**, 223–233 (2006)

6. Coll, A. P., Farooqi, I. S. & O'Rahilly, S. The hormonal control of food intake. *Cell* **129**, 251–262 (2007)

7. Lee, N. K. *et al.* Endocrine regulation of energy metabolism by the skeleton. *Cell* **130**, 456–469 (2007)

8. Ferron, M. *et al.* Insulin signaling in osteoblasts integrates bone remodeling and energy metabolism. *Cell* **142**, 296–308 (2010)

9. Fulzele, K. *et al.* Insulin receptor signaling in osteoblasts regulates postnatal bone acquisition and body composition. *Cell* **142**, 309–319 (2010)

10. Rached, M. T. *et al.* FoxO1 expression in osteoblasts regulates glucose homeostasis through regulation of osteocalcin in mice. *J. Clin. Invest.* **120**, 357–368 (2010)

11. Bhattacharyya, N., Chong, W. H., Gafni, R. I. & Collins, M. T.Fibroblast growth factor 23: state of the field and future directions. *Trends Endocrinol. Metab.* **23**, 610–618 (2012)

12. Yoshikawa, Y. *et al.* Genetic evidence points to an osteocalcin-independent influence of osteoblasts on energy metabolism. *J. Bone Miner. Res.* **26**, 2012–2025 (2011)

13. Huszar, D. *et al.* Targeted disruption of the melanocortin-4 receptor results in obesity in mice. *Cell* **88**, 131–141 (1997)

14. Butler, A. A. & Cone, R. D. The melanocortin receptors: lessons from knockout models. *Neuropeptides* **36**, 77–84 (2002)

15. Balthasar, N. *et al.* Divergence of melanocortin pathways in the control of food intake and energy expenditure. *Cell* **123**, 493–505 (2005)

16. Liu, H. *et al.* Transgenic mice expressing green fluorescent protein under the control of the melanocortin-4 receptor promoter. *J. Neurosci.* **23**, 7143–7154 (2003)

17. Ste Marie, L., Miura, G. I., Marsh, D. J., Yagaloff, K. & Palmiter, R. D. A metabolic defect promotes obesity in mice lacking melanocortin-4 receptors. *Proc. Natl Acad. Sci. USA* **97**, 12339–12344 (2000)

18. Coll, A. P., Farooqi, I. S., Challis, B. G., Yeo, G. S. & O'Rahilly, S.Proopiomelanocortin and energy balance: insights from human and murine genetics. *J. Clin. Endocrinol. Metab.* **89**, 2557–2562 (2004)

19. Hinney, A. *et al.* Prevalence, spectrum, and functional characterization of melanocortin-4 receptor gene mutations in a representative population-based sample and obese adults from Germany. *J. Clin. Endocrinol. Metab.* **91**, 1761–1769 (2006)

20. Larsen, L. H. *et al.* Prevalence of mutations and functional analyses of melanocortin 4 receptor variants identified among 750 men with juvenile-onset obesity. *J. Clin. Endocrinol. Metab.***90**, 219–224 (2005)

21. Nix, M. A. *et al.* Molecular and functional analysis of human β-defensin 3 action at melanocortin receptors. *Chem. Biol.* **20**, 784–795 (2013)

22. Yan, Q. W. *et al.* The adipokine lipocalin 2 is regulated by obesity and promotes insulin resistance. *Diabetes* **56**, 2533–2540 (2007)

23. Lin, Y. *et al.* Hyperglycemia-induced production of acute phase reactants in adipose tissue. *J. Biol. Chem.* **276**, 42077–42083 (2001)

24. Soukas, A., Cohen, P., Socci, N. D. & Friedman, J. M. Leptin-specific patterns of gene expression in white adipose tissue. *Genes Dev.* **14**, 963–980 (2000)

25. Dacquin, R., Starbuck, M., Schinke, T. & Karsenty, G. Mouse α1(I)-collagen promoter is the best known promoter to drive efficient Cre recombinase expression in osteoblast. *Dev. Dyn.* **224**, 245–251 (2002)

26. Kalajzic, Z. *et al.* Directing the expression of a green fluorescent protein transgene in differentiated osteoblasts: comparison between rat type I collagen and rat osteocalcin promoters. *Bone***31**, 654–660 (2002)

27. Qiang, G. *et al.* Lipodystrophy and severe metabolic dysfunction in mice with adipose tissue-specific insulin receptor ablation. *Mol. Metab.* **5**, 480–490 (2016)

28. Scheller, E. L., Cawthorn, W. P., Burr, A. A., Horowitz, M. C. & MacDougald, O. A. Marrow adipose tissue: trimming the fat. *Trends Endocrinol. Metab.* **27**, 392–403 (2016)

29. Zhang, M. *et al.* Osteoblast-specific knockout of the insulin-like growth factor (IGF) receptor gene reveals an essential role of IGF signaling in bone matrix mineralization. *J. Biol. Chem.* **277**, 44005–44012 (2002)

30. Coleman, D. L. Obese and diabetes: two mutant genes causing diabetes-obesity syndromes in mice. *Diabetologia* **14**, 141–148 (1978)

31. Kelly, E., Bailey, C. P. & Henderson, G. Agonist-selective mechanisms of GPCR desensitization. *Br. J. Pharmacol.* **153** (Suppl 1), S379–S388 (2008)

32. Gainetdinov, R. R., Premont, R. T., Bohn, L. M., Lefkowitz, R. J. & Caron, M. G. Desensitization of G protein-coupled receptors and neuronal functions. *Annu. Rev. Neurosci.* **27**, 107–144 (2004)

33. Garfield, A. S. *et al.* A neural basis for melanocortin-4 receptor-regulated appetite. *Nat. Neurosci.* **18**, 863–871 (2015)

34. Myers, M. G., Jr & Olson, D. P. Central nervous system control of metabolism. *Nature* **491**, 357–363 (2012)

35. Cone, R. D. Anatomy and regulation of the central melanocortin system. *Nat. Neurosci.* **8**, 571–578 (2005)

36. Berglund, E. D. *et al.* Melanocortin 4 receptors in autonomic neurons regulate thermogenesis and glycemia. *Nat. Neurosci.* **17**, 911–913 (2014)

37. Kublaoui, B. M., Holder, J. L., Jr, Gemelli, T. & Zinn, A. R. Sim1 haploinsufficiency impairs melanocortin-mediated anorexia and activation of paraventricular nucleus neurons. *Mol. Endocrinol.* **20**, 2483–2492 (2006)

38. Law, I. K. *et al.* Lipocalin-2 deficiency attenuates insulin resistance associated with aging and obesity. *Diabetes* **59**, 872–882 (2010)

39. Guo, H.,*et al.* Lipocalin-2 deficiency impairs thermogenesis and potentiates diet-induced insulin resistance in mice. *Diabetes* **59**, 1376–1385 (2010)

40. Eguchi, J. *et al.* Transcriptional control of adipose lipid handling by IRF4. *Cell Metab.* **13**, 249–259 (2011)

41. Paragas, N. *et al.* The Ngal reporter mouse detects the response of the kidney to injury in real time. *Nat. Med.* **17**, 216–222 (2011)

42. Parton, L. E. *et al.* Glucose sensing by POMC neurons regulates glucose homeostasis and is impaired in obesity. *Nature* **449**, 228–232 (2007)

43. van den Pol, A. N. *et al.* Neuromedin B and gastrin-releasing peptide excite arcuate nucleus neuropeptide Y neurons in a novel transgenic mouse expressing strong Renilla green fluorescent protein in NPY neurons. *J. Neurosci.* **29**, 4622–4639 (2009)

44. DeFronzo, R. A., Tobin, J. D. & Andres, R. Glucose clamp technique: a method for quantifying insulin secretion and resistance. *Am. J. Physiol.* **237**, E214–E223 (1979)

45. Kode, A. *et al.* FOXO1 orchestrates the bone-suppressing function of gut-derived serotonin. *J. Clin. Invest.* **122**, 3490–3503 (2012)

46. Sohn, J. W. *et al.* Serotonin 2C receptor activates a distinct population of arcuate pro-opiomelanocortin neurons via TRPC channels. *Neuron* **71**, 488–497 (2011)

47. Williams, K. W. *et al.* Xbp1s in Pomc neurons connects ER stress with energy balance and glucose homeostasis. *Cell Metab.* **20**, 471–482 (2014)

48. Mellon, P. L. *et al.* Immortalization of hypothalamic GnRH neurons by genetically targeted tumorigenesis. *Neuron* **5**, 1–10 (1990)

49. Ashburner, M. *et al.* Gene ontology: tool for the unification of biology. *Nat. Genet.* **25**, 25–29 (2000)

50. Benjamini, Y. & Hochberg, Y. Controlling the false discovery rate: a practical and powerful approach to multiple testing. *J. R. Stat. Soc. B* **57**, 289–300 (1995)

51. Cohen J. in *Statistical Power Analysis for the Behavioral Sciences* 24–27 (Lawrence Erlbaum Associates, 1988)

Figures

**Figure 1: LCN2 regulates glucose homeostasis through its expression in osteoblasts.**
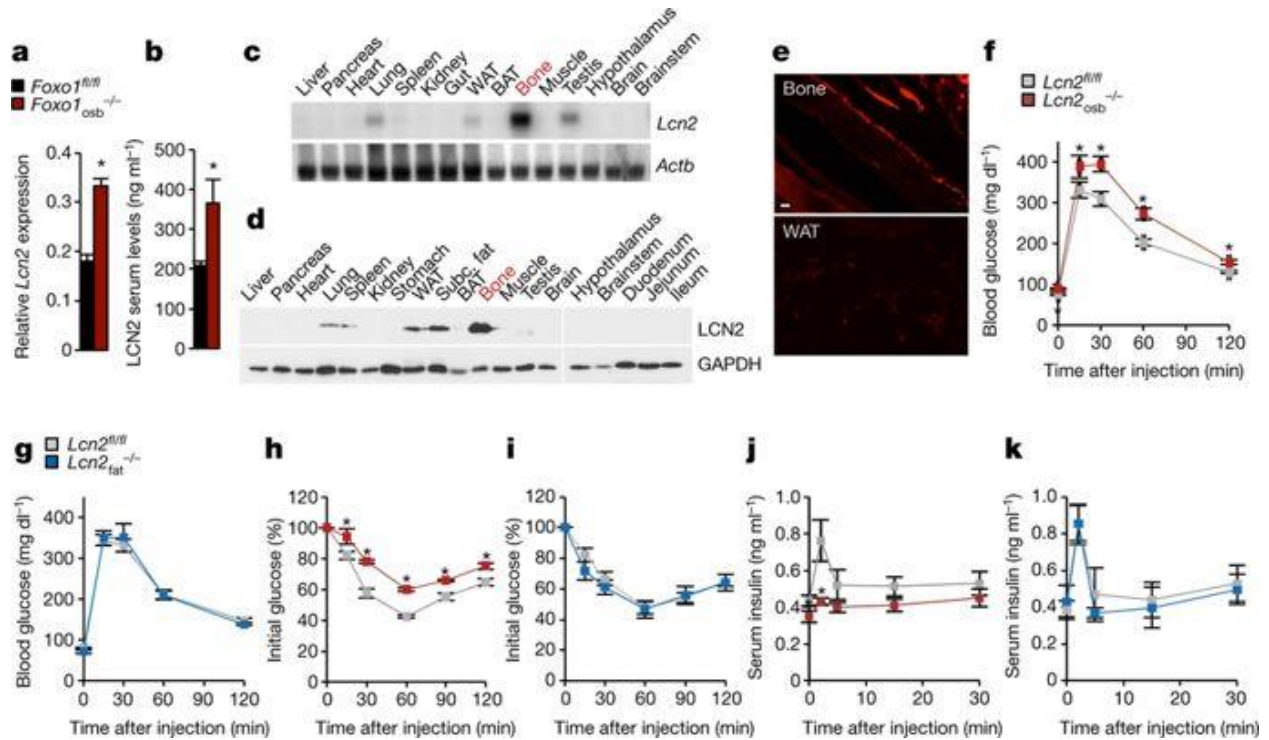
a, mRNA expression of *Lcn2* in bone. **b**, Serum levels of LCN2 in mice. **c**, **d**, mRNA and protein expression of LCN2 in wild-type (WT) tissues. BAT, brown adipose tissue; subc. fat, subcutaneous fat; WAT, white adipose tissue. **c**, Northern blot analysis of *Lcn2* levels. *Actb* was used as a loading control. **d**, Western blot analysis of LCN2 levels. GAPDH was used as a loading control. **e**, LCN2 in bone and fat tissues of *Lcn2–mCherry* mice. Scale bar, 40 μm. **f**, **g**, Glucose-tolerance test of osteoblast-specific (**f**) or adipocyte-specific (**g**) *Lcn2*-knockout mice compared to wild-type (*Lcn*^fl/fl) littermates. **h**, **i**, Insulin-tolerance test of osteoblast-specific (**h**) or adipocyte-specific (**i**) *Lcn2*-knockout mice compared to wild-type (*Lcn*^fl/fl) littermates. **j**, **k**, Glucose-stimulated insulin secretion in osteoblast-specific (**j**) or adipocyte-specific (**k**) *Lcn2*-knockout mice or wild-type littermates. Data are mean ± s.e.m.; $n = 10$ (**a**, **b**), $n = 12$ (**f**), $n = 7$ (**g**, **k**), $n = 6$ (**h**) and $n = 8$ (**i**, **j**) mice per group; representative of three independent experiments. In **f**, **h**, **j**, the effect size (d) > 0.84; *$P < 0.05$ (Student's *t*-test).

**Figure 2: Inactivation of *Lcn2* in osteoblasts increases food intake.**
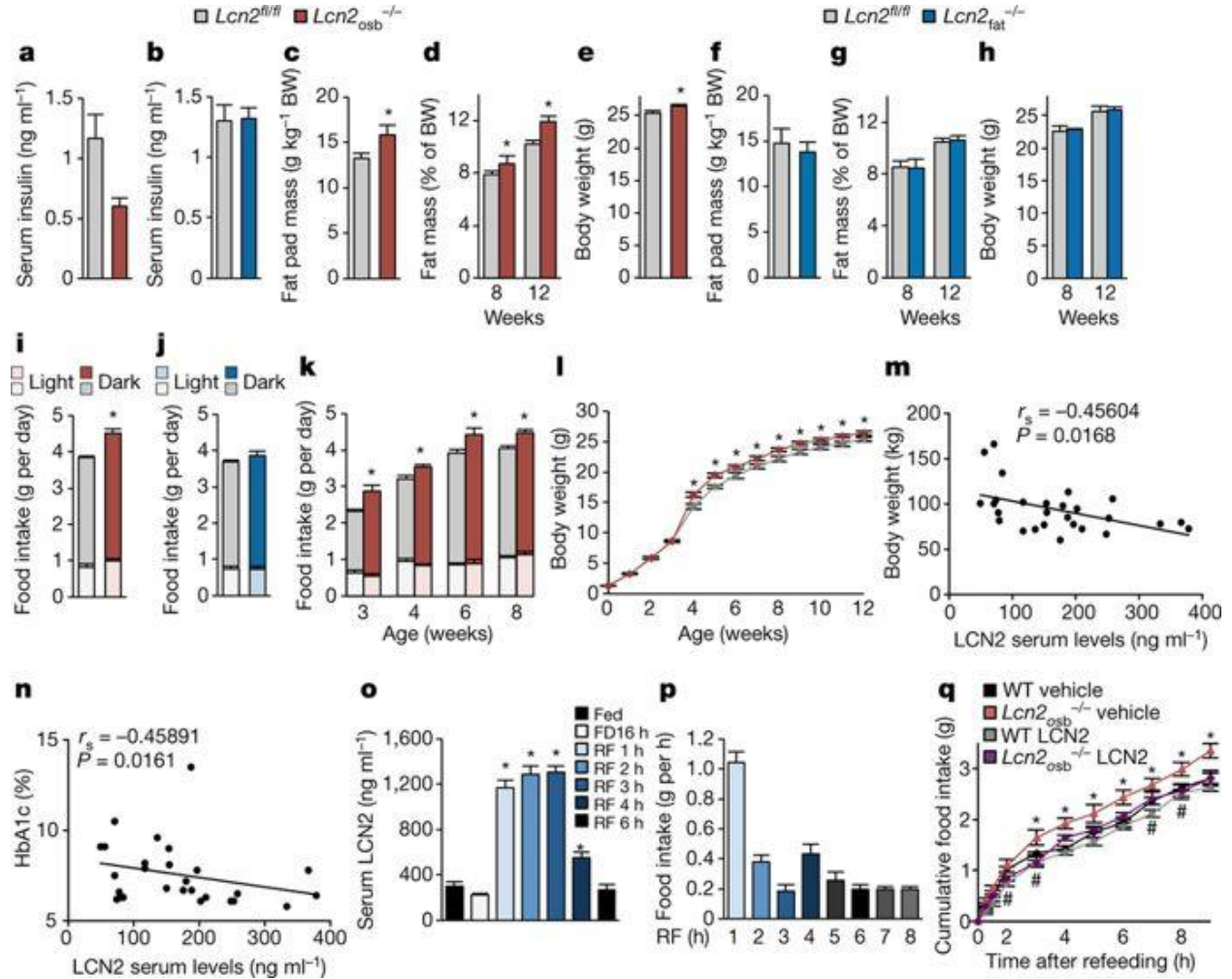
a, **b**, Serum insulin levels of osteoblast-specific (**a**) or adipocyte-specific (**b**) *Lcn2*-knockout mice compared to wild-type (*Lcn*^fl/fl) littermates. **c–l**, Analysis of fat pad mass (**c, f**), body fat mass (**d, g**), body weight (BW; **e, h, l**) and cumulative food intake (**i, j, k**) of *Lcn2*osb^−/− (**c–e, i, k, l**) and *Lcn2*fat^−/− (**f–h, j**) mice. **m, n** Body weight (**m**) and HbA1c (**n**) inversely correlate with serum LCN2 levels in patients with type 2 diabetes. **o, p**, LCN2 serum levels (**o**) and food intake (**p**) in wild-type mice that were fast (FD) or fasted and refed (RF). **q**, Food intake in *Lcn2*osb^−/− mice that were fasted and refed after intraperitoneal LCN2 administration. Data are mean ± s.e.m.; $n = 11$ (**a, c, o**), $n = 10$ (**b, d**), $n = 13$ (**e**), $n = 8$ (**f, h**), $n = 7$ (**g, j**), $n = 9$ (**i, l, p**), $n = 5$ (**k**) and $n = 4$ (**q**) mice per group; representative of three independent experiments; $d > 0.96$ (**a, c, d, i, k**) and $d > 0.74$ (**e, l**). **a, c, d, e, i, k, l, o**, *$P < 0.05$ (Student's *t*-test). **q**, *$P < 0.05$, vehicle-treated *Lcn2*osb^−/− versus vehicle-treated wild-type mice and LCN2-treated *Lcn2*osb^−/−mice (ANOVA); and #$P < 0.05$, LCN2-treated wild-type mice versus vehicle-treated wild-type mice (Student's *t*-test)

57

**Figure 3: LCN2 suppresses food intake in lean and obese mice.**
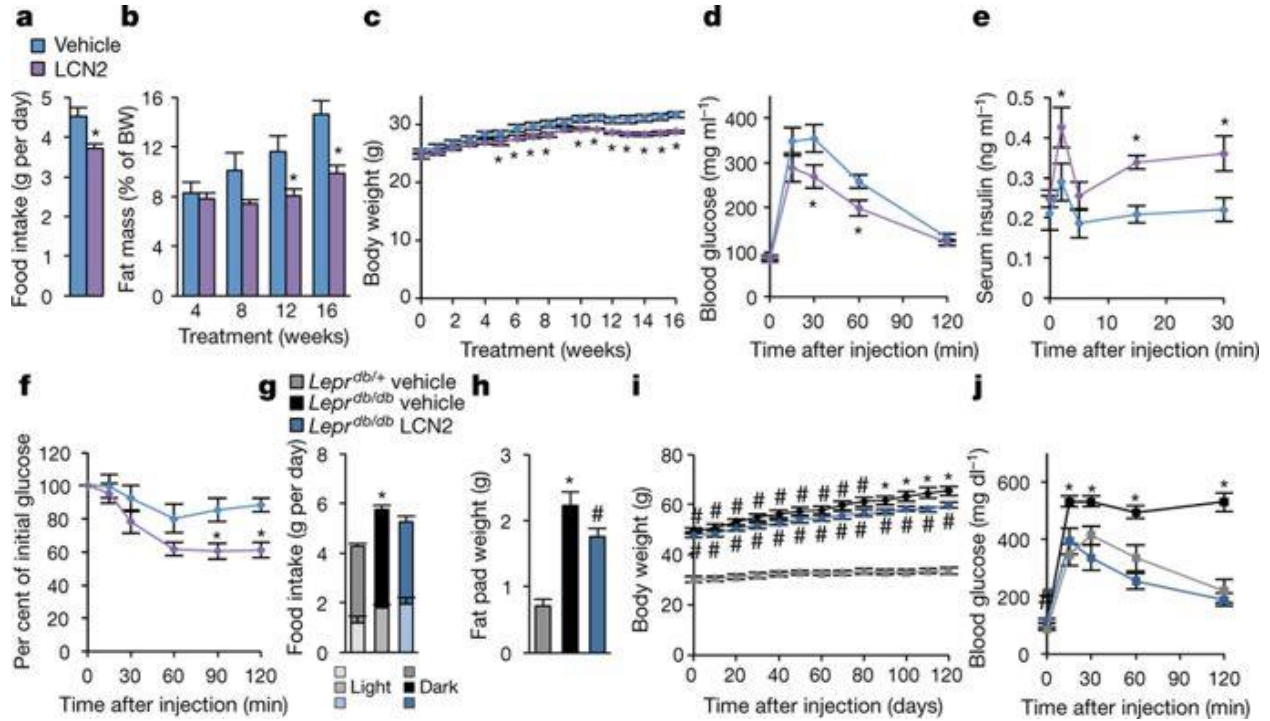
a, Daily food intake of wild-type mice treated with vehicle or LCN2. **b**, **c**, **h**, **i**, Analysis of fat mass (**b**, **h**) and body weight (**c**, **i**) of wild-type or *Lepr*^{db/db} mice treated with vehicle or LCN2. **g**, Cumulative (for the two phases, dark and light) daily food intake of wild-type or *Lepr*^{db/db} mice treated with vehicle or LCN2 during different light phases of the day. **d**–**f**, **j**, Glucose-tolerance test (**d**, **j**), glucose-stimulated insulin secretion (**e**), insulin-tolerance test (**f**) of wild-type or *Lepr*^{db/db} mice treated with LCN2. Data are mean ± s.e.m.; *n* = 8 wild-type and *n* = 6 *Lepr*^{db/db} mice; representative of three independent experiments. **a**–**g**, *P* < 0.05 (Student's *t*-test). **h**–**j**, #*P* < 0.05, *Lepr*^{db/db} versus *Lepr*^{db/+} mice treated with vehicle (Student's *t*-test). *P* < 0.05, *Lepr*^{db/db} vehicle versus *Lepr*^{db/+} (vehicle) and *Lepr*^{db/db} (LCN2) groups (ANOVA).

**Figure 4: LCN2 signals directly in the brain to suppress food intake.**
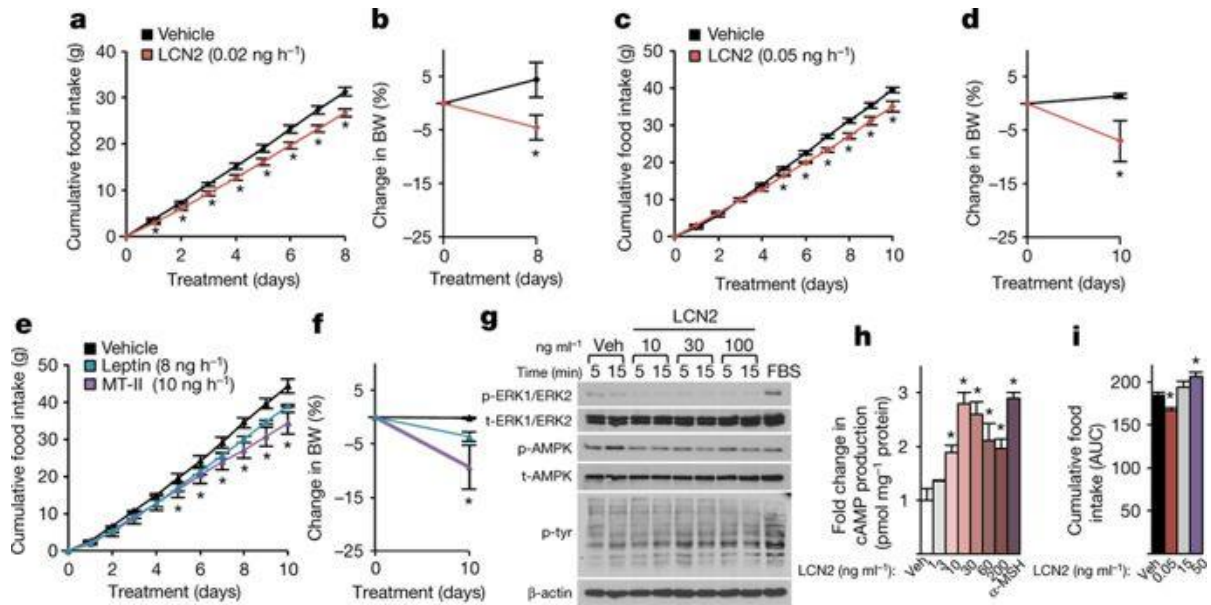
a–f, i, Change in food intake (**a**, **c**, **e**, **i**) and body weight (**b**, **d**, **f**) in *Lcn2*$^{-/-}$ or wild-type mice during ICV administration of LCN2 (**a–d**, **i**), leptin or MT-II (**e**, **f**). AUC, area under the curve. **g**, Western blot analysis of phosphorylated (p-) or total (t-) AMPK, ERK1/ERK2 and tyrosine kinase (tyr). β-actin was used as a loading control. Veh, vehicle; FBS, fetal bovine serum. **h**, cAMP production in GT1-7 cells after treatment with LCN2 or α-MSH. In **i**, data from **c** for vehicle and low-LCN2 are included. Data are mean ± s.e.m.; $n = 6$ (**a**, **b**), $n = 10$ (**c**, **d**, **i**) and $n = 5$ (**e**, **f**) mice per group; $n = 3$ (**h**); representative of three independent experiments. *$P < 0.05$ (Student's *t*-test).

Figure 5: LCN2 binds to and signals through MC4R in the hypothalamus.
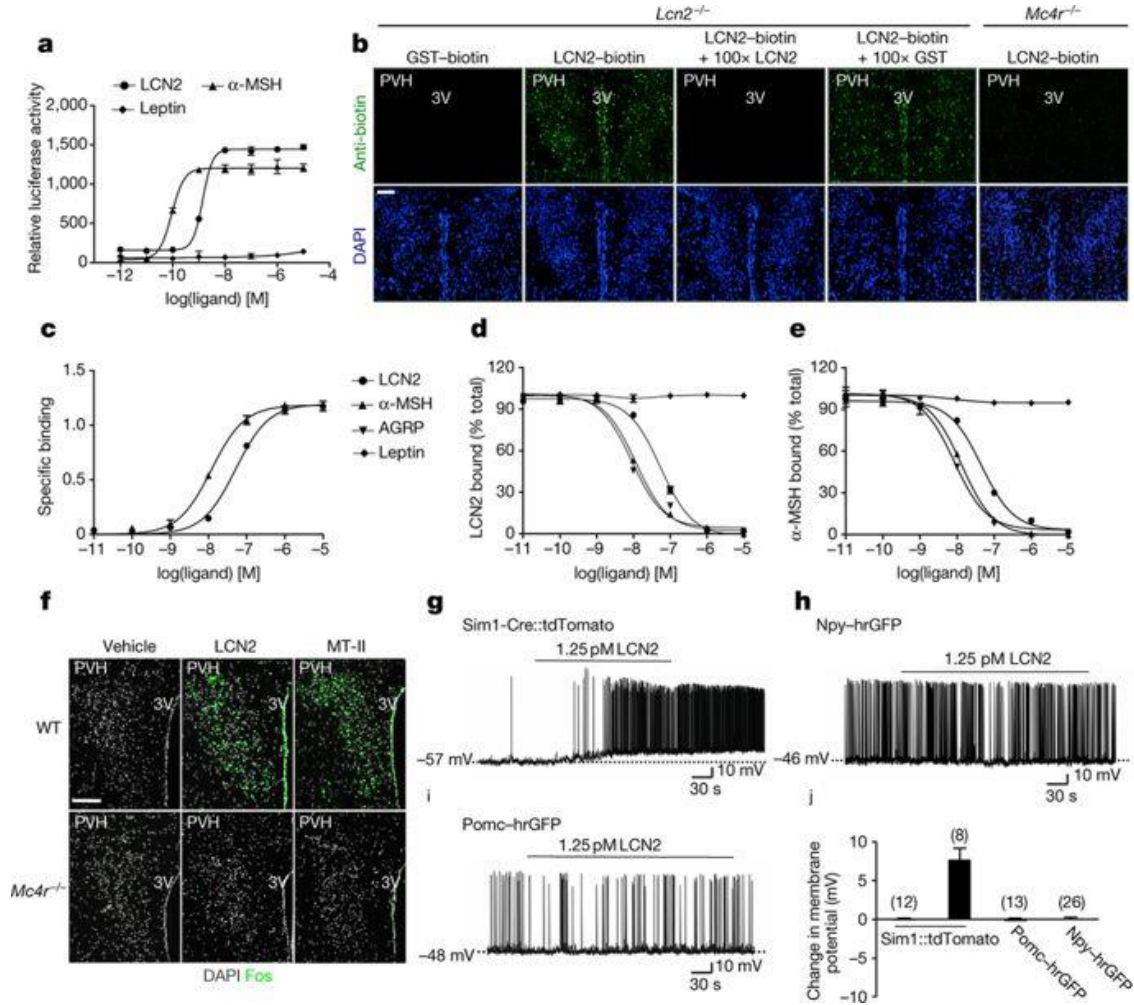
a, cAMP production of HEK293T cells overexpressing MC4R after treatment with LCN2, leptin or α-MSH **b**, Binding of biotinylated LCN2 or GST (control) to hypothalamic sections from $Lcn2^{-/-}$ or $Mc4r^{-/-}$ mice in the presence or absence of 100-fold excess of non-biotinylated LCN2 or GST. PVH, paraventricular nucleus of the hypothalamus; 3V, third ventricle. **c–e**, Saturation (**c**) and competitive binding (**d**, **e**) assay curves of LCN2 and α-MSH in $Mc4r$-transfected HEK293T cells. Leptin and AGRP were used as a negative and additional positive control, respectively. **f**, Fos expression in the PVH of wild-type and $Mc4r^{-/-}$ mice treated with LCN2 or MT-II. **g–j**, Representative traces (**g–i**) and change in resting membrane potential (**j**) of neurons after LCN2 treatment. LCN2 treatment induced depolarization in a $Sim1$-cre::tdTomato (**g**) but not Npy–hrGFP (humanized renilla green fluorescent protein) (**h**) or $Pomc$–hrGFP (**i**) neuron. Scale bars, 100 μm. Data are mean ± s.e.m.; representative of three independent experiments. *$P < 0.05$ (Student's t-test).

Figure 6: MC4R mediates suppression of appetite by osteoblast-derived LCN2.
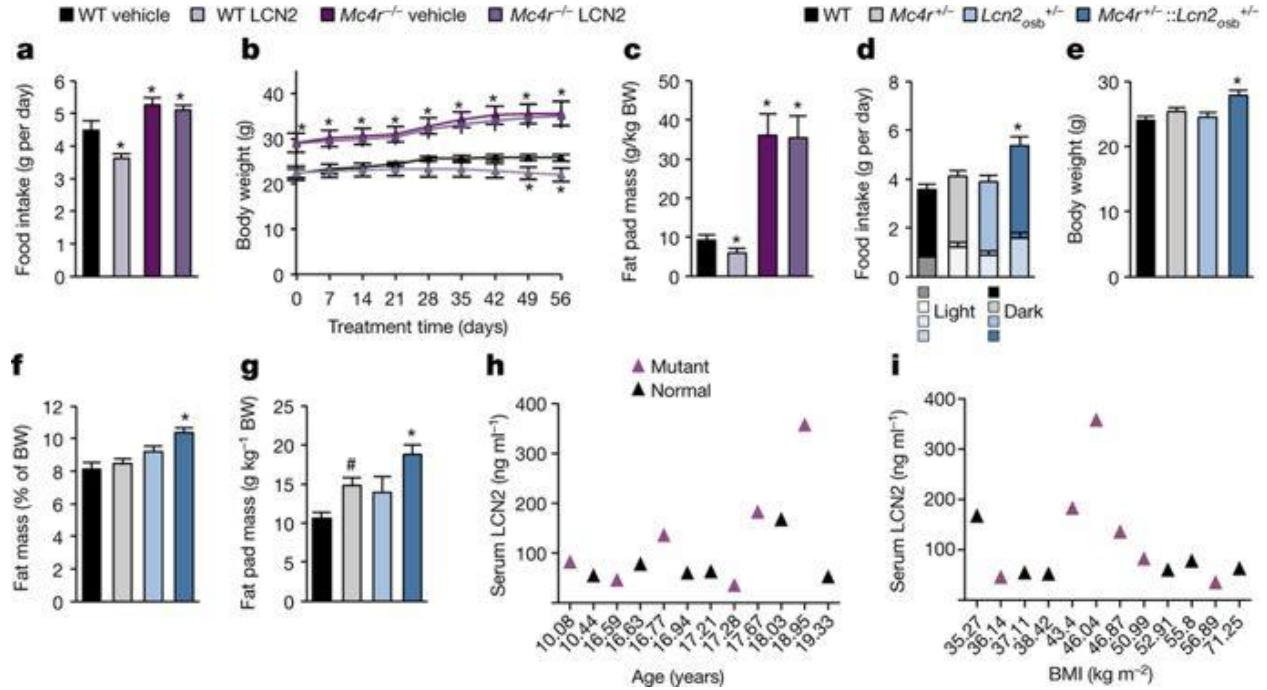
a–f, Analysis of food intake (**a**, **d**), body weight (**b**, **e**), fat pad mass (**c**, **g**) and body fat mass (**f**) in $Mc4r^{-/-}$ mice treated with LCN2 for 8 weeks(**a–c**) or in $Mc4r^{+/-}$, $Lcn2_{osb}^{+/-}$, $Mc4r^{+/-}::Lcn2_{osb}^{+/-}$ and wild-type littermates (**d–g**). **h**, **i**, LCN2 plasma levels in patients with mutated and normal $MC4R$ at different ages (**h**) and body-mass indexes (**i**). Data are mean ± s.e.m.; $n = 5$ wild-type and $n = 8$ $Mc4r^{-/-}$ mice (**a–c**), $n = 7$ wild-type, $Mc4r^{+/-}$ and $Mc4r^{+/-}::Lcn2_{osb}^{+/-}$ mice and $n = 5$ $Lcn2_{osb}^{+/-}$ mice (**d–g**); representative of three independent experiments. **a–c**, *$P < 0.05$, vehicle-treated wild-type mice compared to the other groups; **d–g**, *$P < 0.05$, $Mc4r^{+/-}::Lcn2_{osb}^{+/-}$ mice versus wild-type, $Mc4r^{+/-}$ and $Lcn2_{osb}^{+/-}$ mice (ANOVA); #$P < 0.05$, $Mc4r^{+/-}$ versus wild-type mice (Student's t-test).

Supplemental Figures

Extended Data Figure 1 | Identification of *Lcn2* as an osteoblast enriched gene and generation of mice lacking *Lcn2* in osteoblasts (*Lcn2*osb−/−) and adipocytes (*Lcn2*fat−/−).
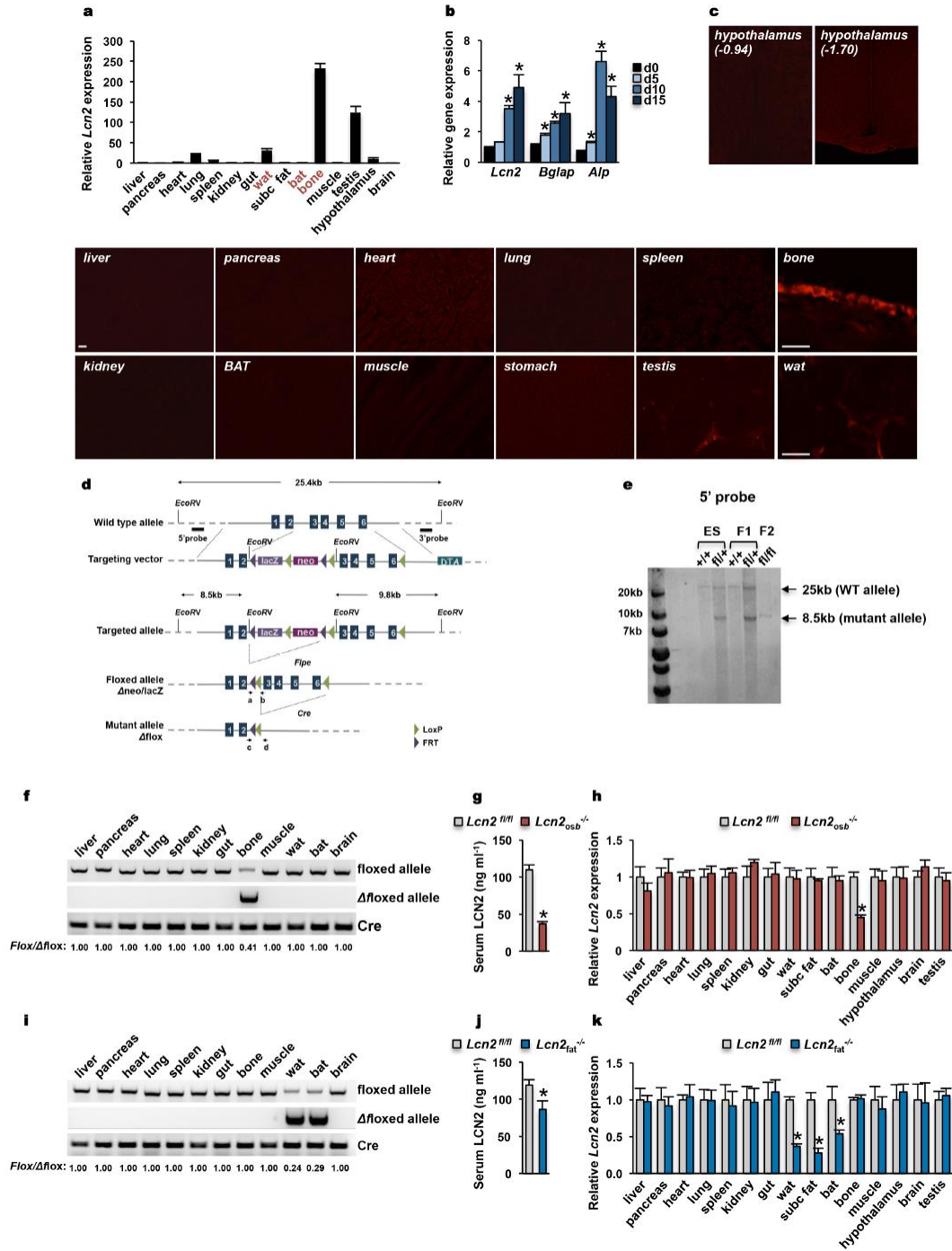
a, Real-time PCR analysis of *Lcn2* expression levels in the indicated tissues from wild-type mice. **b**, *Lcn2*, *Bglap and Alp* expression levels in differentiating osteoblasts (day 0–day 15). **c**, Lack of *Lcn2* expression in indicated tissues of the *Lcn2*–mCherry-reporter mouse. Scale bars, 40 μ m. **d**, Targeting strategy used to generate a floxed allele of *Lcn2*. The targeting vector, which contains loxP sites within introns 2 and 6, is designed to delete a 1.9 kb genomic fragment containing *Lcn2* exons 3– 6. Location of probes used for Southern blotting (5' and 3') and primers used for PCR to detect the floxed (a and b) and mutant allele (c and d) are indicated. **e**, Southern-blot analysis on DNA from targeted embryonic stem (ES) cells and mice from F1 and F2 generation showing germline transmission of the mutated allele.

Extended Data Figure 2 | Osteoblast-specific activation of Cre in *Col1a1-Cre* and *Bglap-Cre* mice.
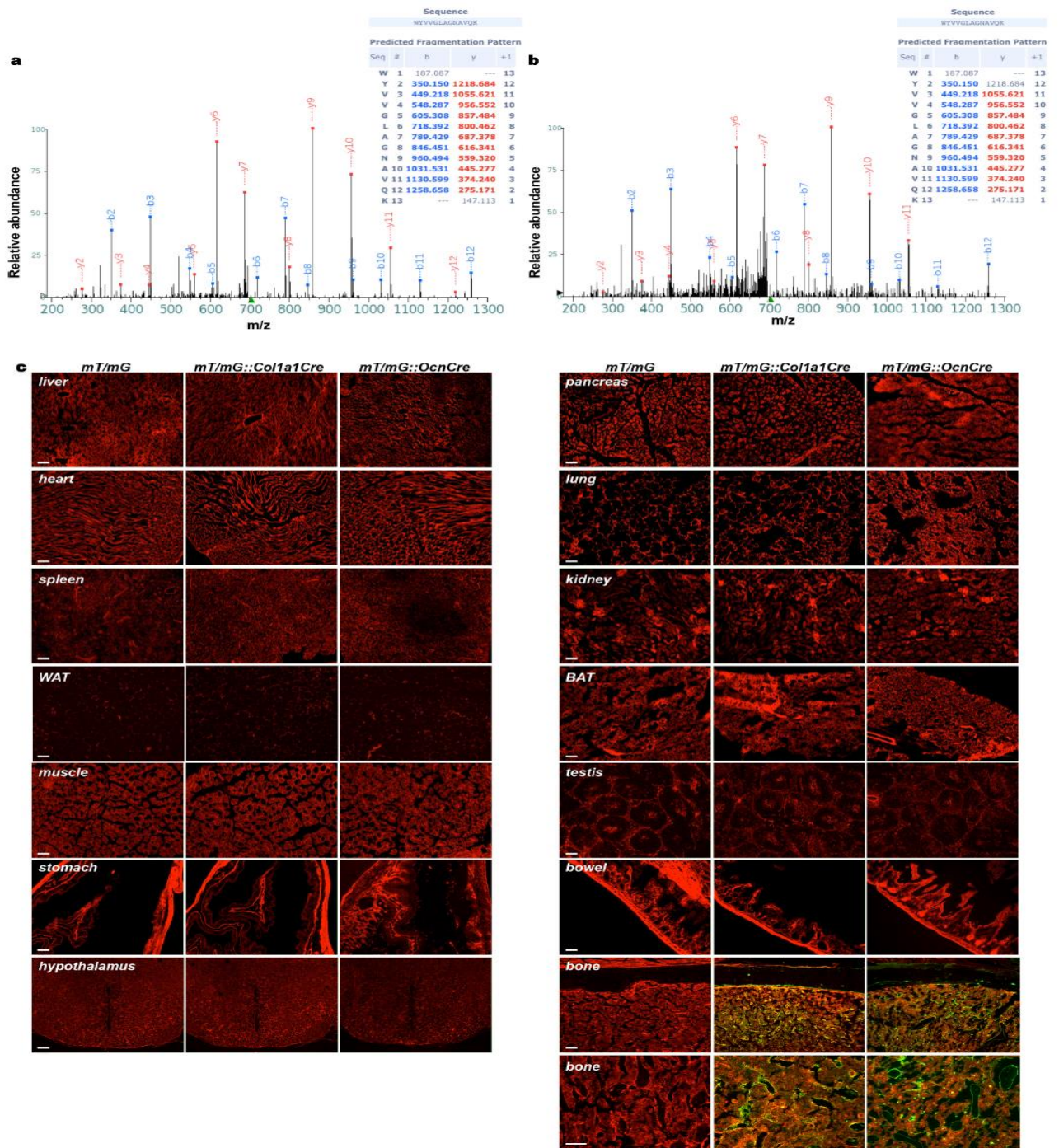
a, **b**, Tandem mass spectrum of an eluted peptide fragment of bone-derived (**a**) and fat-derived (**b**) LCN2. **c**, Specific expression of *Cre* in osteoblasts, but not any other tissues in mT/mG::Col1a1-Cre mice and in mT/mG::Bglap-Cre mice. Scale bars, 100 μ m. Results are representative of three independent experiments.

Extended Data Figure 3 | LCN2 regulates glucose homeostasis through its expression in osteoblasts.
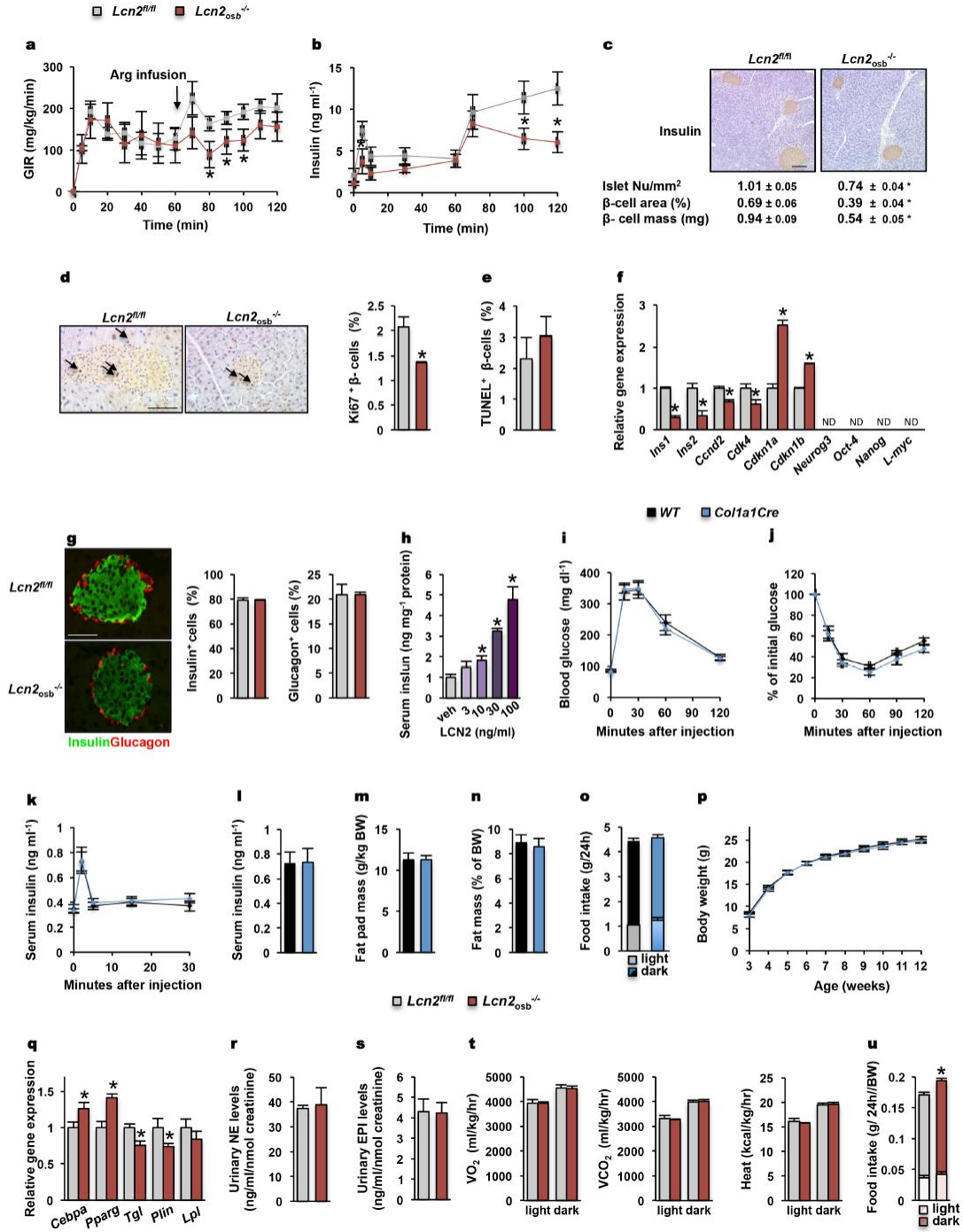
a, **b**, Glucose infusion rate (**a**) and serum insulin levels (**b**) during hyperglycaemic clamp. **c**, Insulin staining and islet histomorphometry of pancreatic sections. **d**, Ki67 immunostaining and histomorphometric analysis of Ki67-immunoreactive cells in pancreatic islets (arrows indicate Ki67-positive cells). **e**, Histomorphometric analysis of TUNEL-positive β -cells in the pancreas. **f**, Expression of insulin genes, cell cycle genes and β -cell dedifferentiation markers in pancreatic islets. **g**, Insulin and glucagon immunostaining and histomorphometric analysis of insulin- and glucagon-immunoreactive cells in pancreatic islets of *Lcn2*osb −/− mice and their *Lcn2fl/fl* littermates. **h**, Insulin secretion in pancreatic islets treated with increasing doses of LCN2. **i–p**, Glucose tolerance (**i**), insulin tolerance (**j**) and glucose-stimulated insulin secretion (**k**), random-fed serum-insulin levels (**l**), fat pad mass (**m**), fat mass (**n**),food intake (**o**) and body weight (**p**) are not altered in *Col1a1-Cre* mice compared to their wild-type littermates. **q**, Expression levels of *Cebpa*, *Pparg*, *Tgl* (also known as *Pnpla2*), *Plin1* (also known as *Plin*) and *Lpl* in white adipose tissue. **r**, **s**, Urinary levels of norepinephrine (**r**) and epinephrine (**s**) in *Lcn2*osb −/− mice and *Lcn2fl/fl* littermates. **t**, **u**, Indirect calorimetry measurements (**t**) and daily food intake normalized to body weight (**u**) in *Lcn2*osb −/− mice and *Lcn2fl/fl* littermates. Scale bars, 200 μ m (**c**), 100 μ m (**d**) and 50 μ m (**g**). Data are mean ± s.e.m.; $n = 5$ (**a**, **b**, **e**, **r–t**), $n = 8$ (**c**, **d**, **q**), $n = 7$ (**i–p**), $n = 3$ (**g**) and $n = 9$ (**u**) mice per group. Results are representative of three independent experiments. * $P < 0.05$ (Student's *t*-test).

Extended Data Figure 4 | The anorexigenic function of LCN2 influences fat mass, body weight and insulin sensitivity identically in Lcn2osb −/− and Lcn2(OC)osb −/− mice.
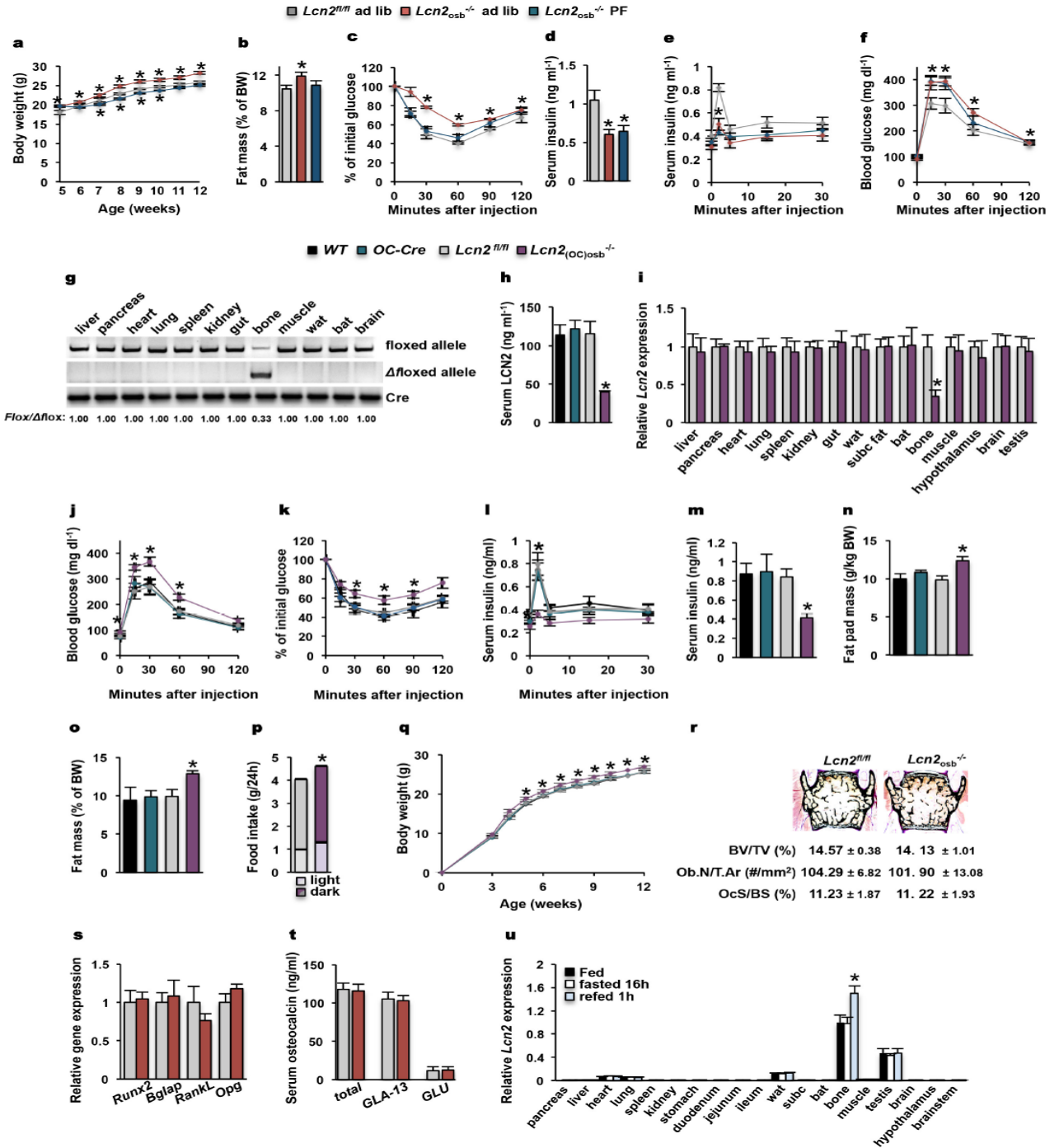
a–f, Body weight (**a**), fat mass (**b**), insulin tolerance (**c**), serum insulin levels (**d**), glucose-stimulated insulin secretion (**e**) and glucose tolerance (**f**) in pair-fed *Lcn2*osb −/− and *Lcn2fl/fl* littermates.

Data from Figs 2l, 2d, 1h, 2a, 1j and 1f, respectively, for fed *Lcn2*osb −/− mice are included for comparison. **g**, Detection of the *Lcn2* floxed (primers a–b) and mutant allele, Δ flox, (primers c–d) in genomic DNA isolated from tissues of *Lcn2*(OC)osb −/− mice. **h**, **i**, Serum levels of LCN2 (**h**) and tissue expression of *Lcn2* (**i**) in *Lcn2*(OC)osb −/− mice and their *Lcn2fl/fl* littermates. **j–q**, glucose tolerance (**j**), insulin tolerance (**k**), glucose-stimulated insulin secretion (**l**), random-fed serum-insulin levels (**m**), fat pad mass (**n**), fat mass (**o**), food intake (**p**) and body weight (**q**) in *Lcn2*(OC)osb −/− mice and their *Lcn2fl/fl* littermates. **r**, Histomorphometric analysis of bone mass and Von Kossa staining of vertebral sections. BV/TV, bone volume over tissue volume; Ob.N./T.Ar, osteoblast numbers per trabecular area; OcS/BS, osteoclast surface per bone surface. **s**, Expression levels of osteoblastogenic and osteoclastogenic genes in bone in *Lcn2*osb −/− mice and their *Lcn2fl/fl* littermates. **t**, Serum osteocalcin levels in *Lcn2*osb −/− mice and their *Lcn2fl/fl* littermates. **u**, *Lcn2* expression levels in indicated tissues following fasting–refeeding of wild-type mice. Data are mean ± s.e.m.; *n* = 6 (a–f, r), *n* = 3 (s), *n* = 10 (t) and *n* = 5 (u) mice per group; *n* = 3 wild-type, *n* = 7 *Bglap-Cre*, *n* = 7 *Lcn2*(OC)osb −/− and *n* = 6 *Lcn2fl/fl* mice (**h–q**). Results are representative of three independent experiments. * *P* < 0.05 (Student's *t*-test).

Extended Data Figure 5 | Exogenous LCN2 decreases body-weight gain and increases energy expenditure in lean and obese mice.
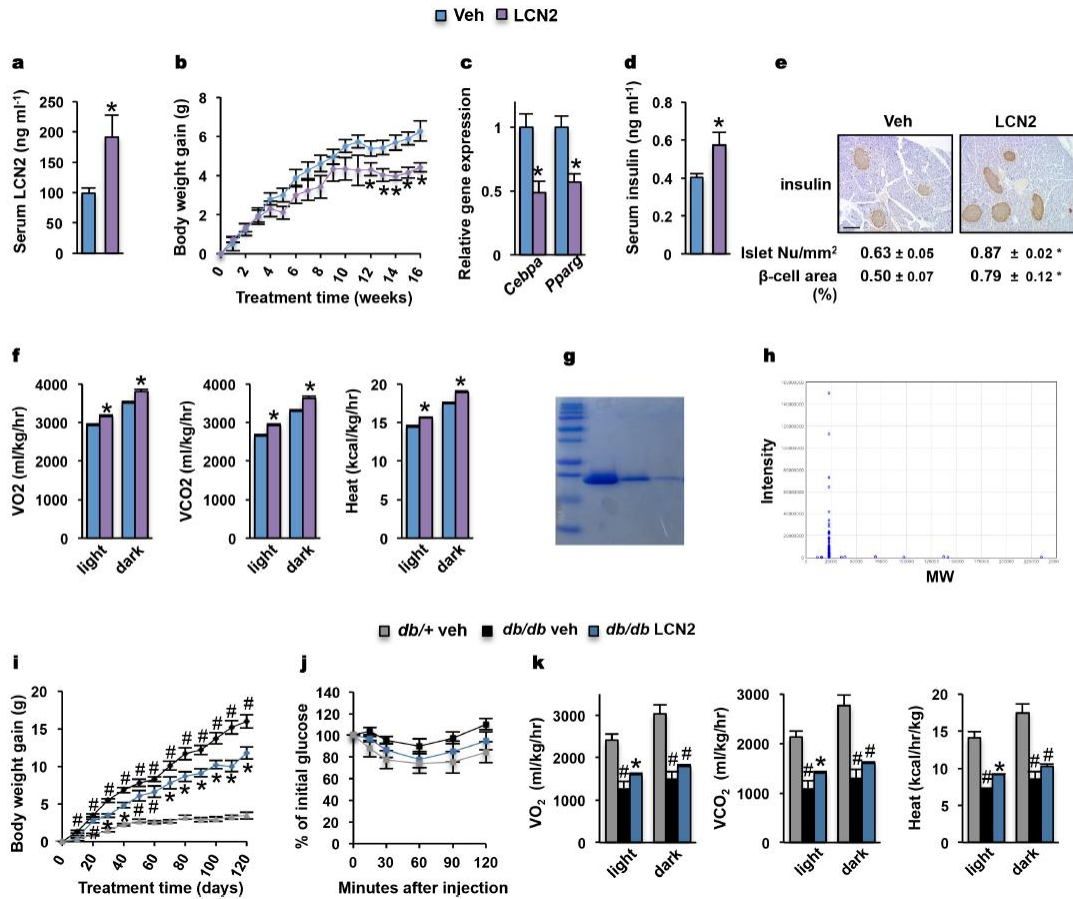
a–f, Wild-type mice were treated with LCN2 (150 ng g−1 per day) or vehicle for 16 weeks. **a**, Serum levels of LCN2. **b**, Body-weight gain. **c**, Expression levels of *Cebpa* and *Pparg* in white adipose tissue. **d**, Serum insulin levels. **e**, Pancreas insulin staining and islet histomorphometry. Scale bar, 200 μm. **f**, Indirect calorimetry measurements. **g**, **h**, Coomassie blue staining (**g**) and mass spectrometry analysis (**h**) of recombinant mouse LCN2. Body-weight gain (**i**), insulin tolerance (**j**) and indirect calorimetry (**k**) measurements of *Leprdb/db* mice treated with LCN2 (150 ng g−1 per day) or vehicle for 16 weeks. *n* = 8 mice wild-type and *n* = 6 *Leprdb/db* mice per group. Results are representative of three independent experiments. Data are mean ± s.e.m.; * *P* < 0.05 (**a–f**; Student's *t*-test). #*P* < 0.05 (**i–k**) for *Leprdb/db* (vehicle or LCN2 treated) versus *Leprdb/+* (vehicle) groups (Student's *t*-test). * *P* < 0.05 (**i–k**) *Leprdb/db* (LCN2) versus *Leprdb/+* (vehicle) and *Leprdb/db* (vehicle) groups (ANOVA).

Extended Data Figure 6 | Increased food intake, compromised glucose metabolism and normal bone mass in *Lcn2−/−* mice.

	LCN2 (pg/mg proteins)		
	LCN2 −/−	LCN2 −/−	LCN2 +/+
	veh	LCN2	veh
serum (ng/ml)	0.06 ± 0.04	107.05 ± 6.46	138.39 ± 22.64
cortex	0.00	5.67 ± 0.50	6.76 ± 0.56
cerebellum	0.00	8.44 ± 0.63	7.25 ± 1.53
thalamus	0.00	8.93 ± 1.13	6.32 ± 0.47
brainstem	0.00	16.96 ± 1.18	14.73 ± 0.55
hypothalamus	0.00	27.52 ± 0.60	28.16 ± 1.13

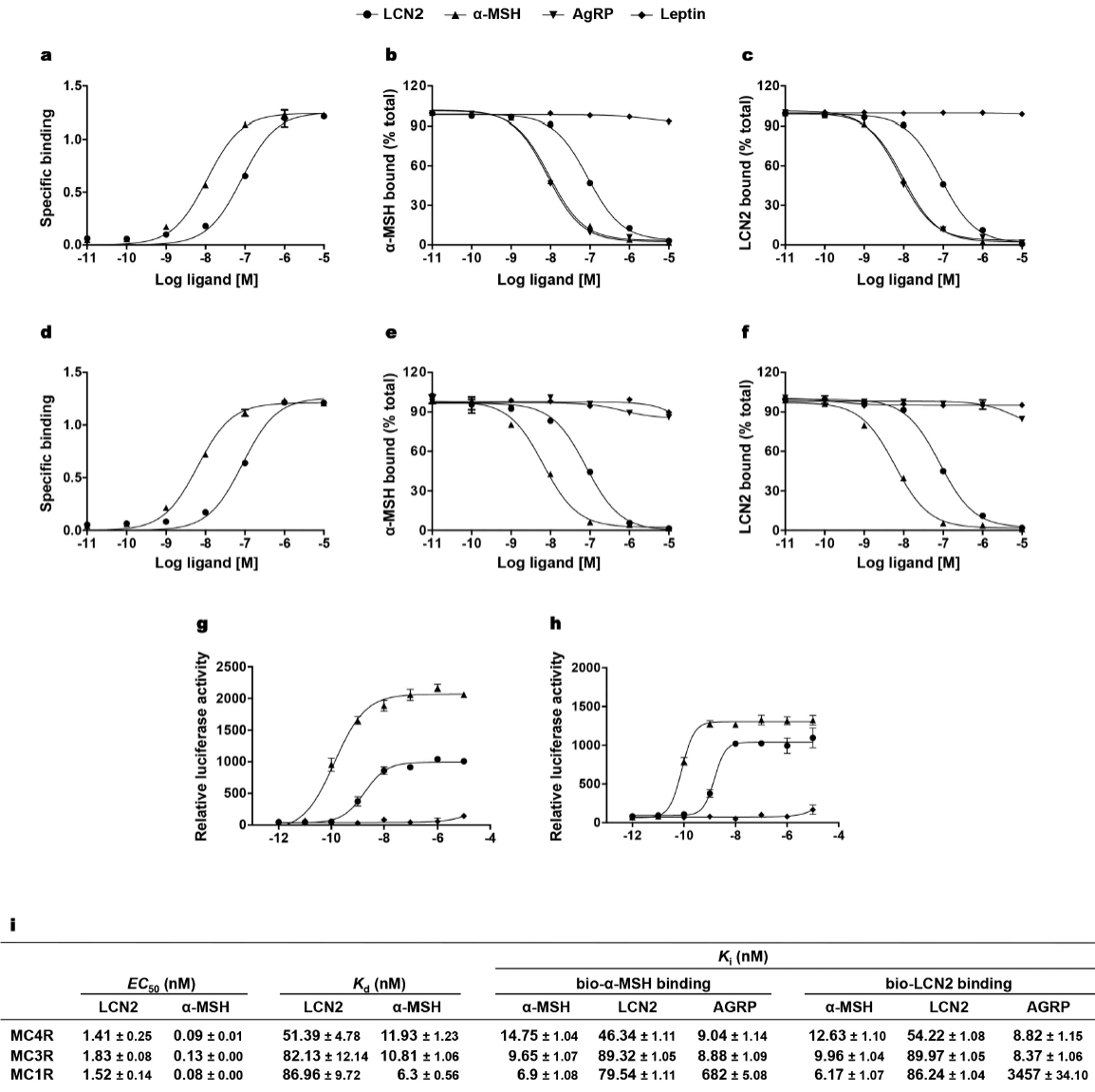|	veh	LCN2
	LCN2 (pg/mg proteins)	
serum (ng/ml)	0.06 ± 0.07	0.06 ± 0.15
cortex	0.00	0.00
cerebellum	0.00	0.00
thalamus	0.00	0.00
brainstem	0.00	0.00
hypothalamus	0.00	17.54 ± 3.53

a, Serum levels of leptin in *Lcn2osb −/−* mice and their *Lcn2fl/fl* littermates. **b**, Expression levels of leptin in white adipose tissue. **c–g**, Expression levels of the gastrointestinal hormones that regulate appetite *Cck* (**c**), *Pyy* (**d**), *Glp1* (also known as *Zglp1*; **e**), *Gip* (**f**) and ghrelin (*Ghrl*; **g**) under fed (F), 16-h fasted (FD) and re-fed (RF) (2 h after 16-h fasting) conditions for *Lcn2osb −/−* mice and their *Lcn2fl/fl* littermates. **h**, Detection of the *Lcn2* mutant allele, Δ flox, (primers c–d) in genomic DNA isolated from tissues of *Lcn2−/−* mice. **i**, **j**, Serum levels of LCN2 (**i**) and tissue expression of *Lcn2* (**j**) in *Lcn2−/−* mice and their *Lcn2+/+* littermates. **k–s**, Analysis of *Lcn2−/−* mice and their *Lcn2+/+* littermates. **k**, Glucose tolerance test. **l**, Insulin tolerance test. **m**, Glucose-stimulated insulin secretion. **n**, Fat pad mass. **o**, Fat mass. **p**, Food intake. **q**, Body weight. **r**, Bone histomorphometric analysis. **s**, Expression levels of osteoblastogenic and osteoclastogenic genes in bone. **t**, **u**, LCN2 crosses the blood–brain barrier to regulate food intake. **t**, LCN2 levels in the brain and serum of *Lcn2−/−* and wild-type littermates 2 h after i.p. administration of LCN2. **u**, LCN2 levels in the brain of wild-type mice 3 h after refeeding. **v**, LCN2 levels in the brain and serum of *Lcn2−/−* mice following ICV administration of 0.02 ng h−1 LCN2 or vehicle for 8 days. Data are mean ± s.e.m.; n = 10 (**a, b, i**), n = 5 (**c–g, k, l, p, r, s**), n = 7 (**m–o, q**), n = 4 (**j, t**) and n = 3 (**u, v**) mice per group. Results are representative of three independent experiments. * $P < 0.05$ (Student's *t*-test).

Extended Data Figure 7 | MC4R, but not SLC22A17, is required for the stimulation of cAMP activity and anorexigenic gene expression induced by LCN2.
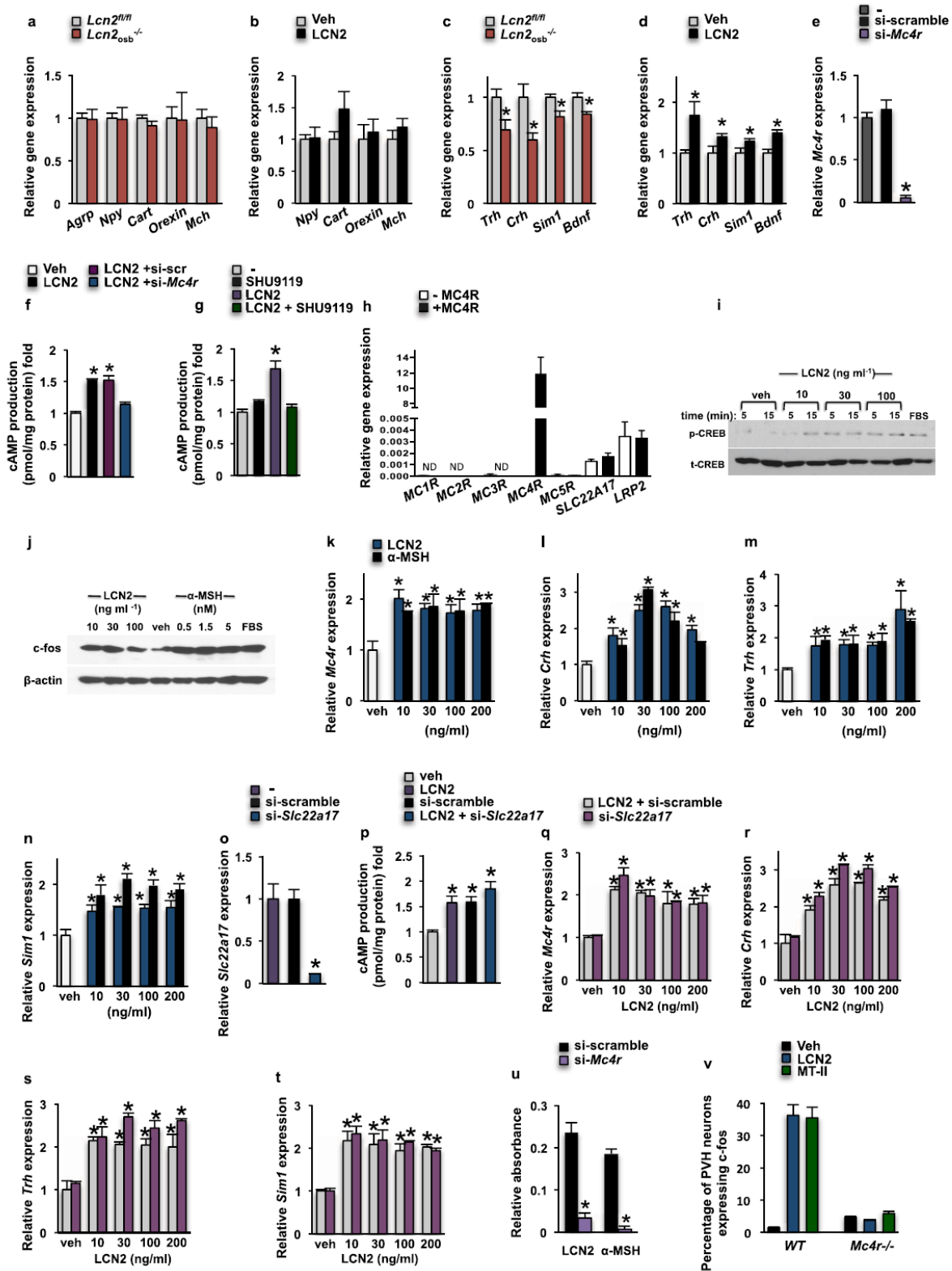
a–d, Expression levels of neuropeptides regulating appetite in the hypothalamus of *Lcn2fl/fl* and *Lcn2*osb −/− mice (**a**, **c**) and wild-type mice injected daily i.p. with LCN2 (150 ng g−1 per day) or vehicle for 16 weeks (**b**, **d**). **e**, **o**, *Mc4r* (**e**) or *Slc22a17* (**o**) expression levels in GT1-7 hypothalamic cells following transfection with *Mc4r* or *Slc22a17* siRNA. si-scramble, Scramble siRNA. **f**, **g**, **p**, cAMP production in GT1-7 cells treated with LCN2 following pretreatment with the SHU9119 inhibitor (**g**) or silencing of *Mc4r* (**f**) or *Slc22a17* (**p**) expression. **h**, Expression levels of melanocortin receptors and LCN2 receptors in HEK293T cells transfected with an *MC4R* expression vector or empty vector. ND, not detected. **i**, **j**, Western blot analysis of CREB phosphorylation (**i**) and *FOS* induction (**j**) in GT1-7 cells treated with LCN2, vehicle or α -MSH. **k–t**, Expression levels of *Mc4r* and targets in GT1-7 cells treated with LCN2 or α -MSH for 4 h (**k–n**) and after silencing of *Slc22a17* (**q–t**). **u**, Binding of biotinylated LCN2 and α -MSH in GT1-7 cells transiently transfected with *Mc4r* siRNA or scramble siRNA. **v**, Quantification of *Fos*-expressing neurons in the PVH of wild-type and *Mc4r*−/− mice injected with LCN2 or MT-II. Data are mean ± s.e.m. of triplicates. *n* = 9 (**a**) and *n* = 7 (**b–d**) mice per group. Results are representative of three independent experiments. * *P* < 0.05 (Student's *t*-test).

Extended Data Figure 8 | Binding affinity and activation potency of LCN2 on MC3R and MC1R.

	EC_{50} (nM)		K_d (nM)		K_i (nM)					
					bio-α-MSH binding			bio-LCN2 binding		
	LCN2	α-MSH	LCN2	α-MSH	α-MSH	LCN2	AGRP	α-MSH	LCN2	AGRP
MC4R	1.41 ± 0.25	0.09 ± 0.01	51.39 ± 4.78	11.93 ± 1.23	14.75 ± 1.04	46.34 ± 1.11	9.04 ± 1.14	12.63 ± 1.10	54.22 ± 1.08	8.82 ± 1.15
MC3R	1.83 ± 0.08	0.13 ± 0.00	82.13 ± 12.14	10.81 ± 1.06	9.65 ± 1.07	89.32 ± 1.05	8.88 ± 1.09	9.96 ± 1.04	89.97 ± 1.05	8.37 ± 1.06
MC1R	1.52 ± 0.14	0.08 ± 0.00	86.96 ± 9.72	6.3 ± 0.56	6.9 ± 1.08	79.54 ± 1.11	682 ± 5.08	6.17 ± 1.07	86.24 ± 1.04	3457 ± 34.10

a–f, Saturation (**a**, **d**) and competition binding (**b**, **c**, **e**, **f**) assay curves of LCN2 and α -MSH in HEK293T cells transfected with *MC3R* (**a–c**) or *MC1R* (**d–f**). Displacement of biotinylated α -MSH (**b**, **e**) or biotinylated LCN2 (**c**, **f**) by the indicated proteins. **g**, **h**, cAMP production in HEK293T cells transfected with *MC3R* (**g**) or *MC1R* (**h**) along with a cAMP/luciferase reporter and treated for 15 min as indicated. Results are representative of three independent experiments. Data are mean ± s.e.m.; **i**, EC50, *K*d and *K*i of LCN2, α MSH and AGRP on melanocortin receptors expressed in HEK293T cells.

Extended Data Figure 9 | Binding and activation of PVH neurons by LCN2.
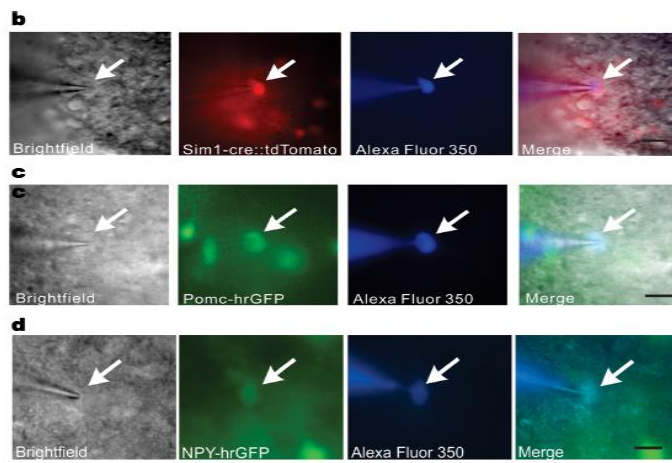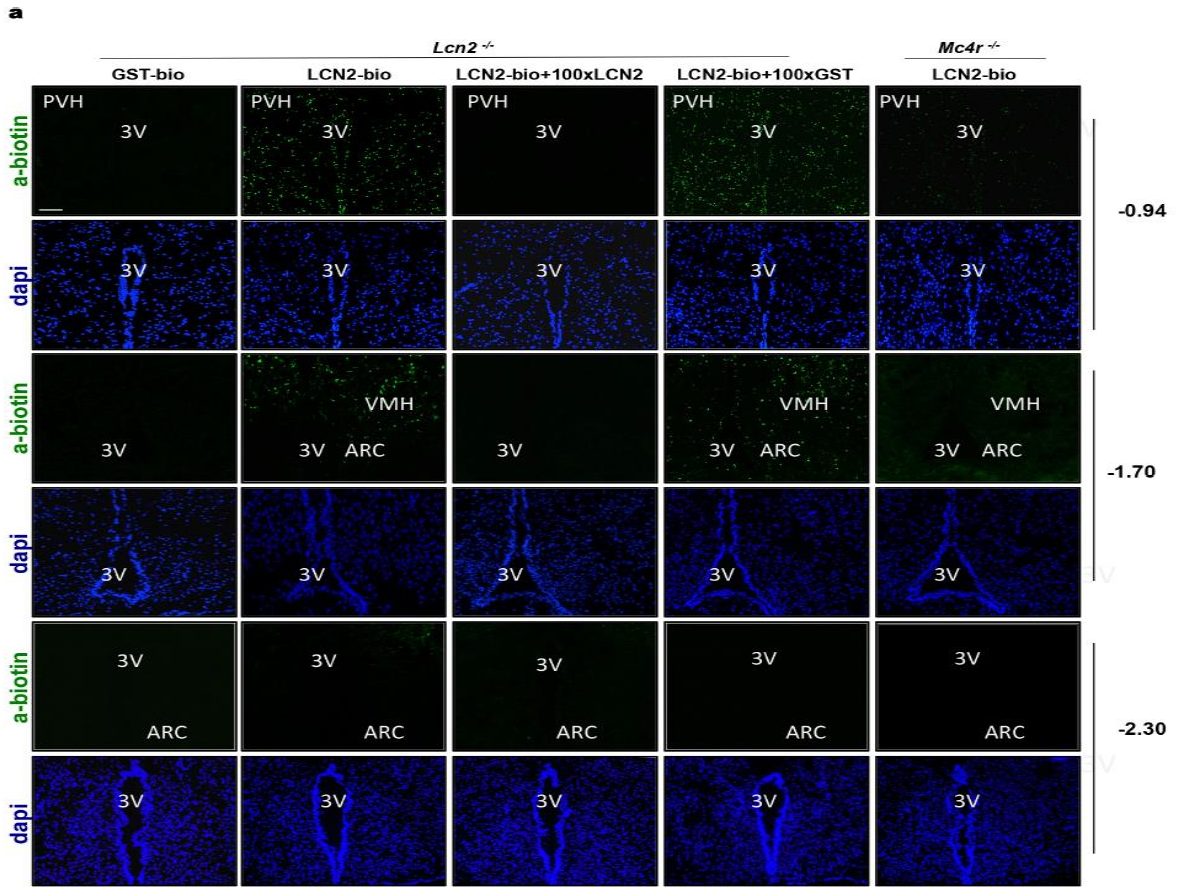
a, Binding of biotinylated LCN2 to PVH and VMH neurons, but not neurons in the arcuate nucleus (ARC) in hypothalamic sections of *Lcn2−/−* and *Mc4r−/−* mice. Competition with unlabelled LCN2 or GST. **b–d**, Bright-field images of a targeted (as indicated by the arrows) neurons. **b**, A *Sim-1* neuron from a *Sim-1* cre::tdTomato mouse. **c**, A *Pomc* neuron from *Pomc*–hrGFP mouse. **d**, A *Npy* neuron from *Npy*–hrGFP mouse. The same neuron is shown in red (Alexa Fluor 594, tdTomato), green (FITC, hrGFP) and blue (Alexa Fluor 350, DAPI), as well the merged image. Scale bars, 100 μm (**a**) and 50 μm (**b–d**).

Extended Data Figure 10 | MC4R is required for the improvement in glucose metabolism and energy expenditure by LCN2.

MC4R results	Sex	Age	BMI (Kg/m²)	LCN2 (ng/ml)
Normal	f	18.0	35.3	168.207
Normal	m	16.9	52.9	60.616
Normal	m	19.3	38.4	52.957
Normal	f	17.2	71.3	63.658
Normal	f	16.6	55.8	78.465
Normal	f	10.4	37.1	55.056
p.Phe202Leu	m	19.0	46.0	358.713
p.Cys271Arg	m	17.3	56.9	35.927
p.Asp146His	f	17.7	43.4	183.602
p.Leu139CysfsTer22	f	16.6	36.1	46.553
p.Ile251TrpfsTer34	f	16.8	46.9	136.504
p.Ile251TrpfsTer34	f	10.1	51.0	82.991
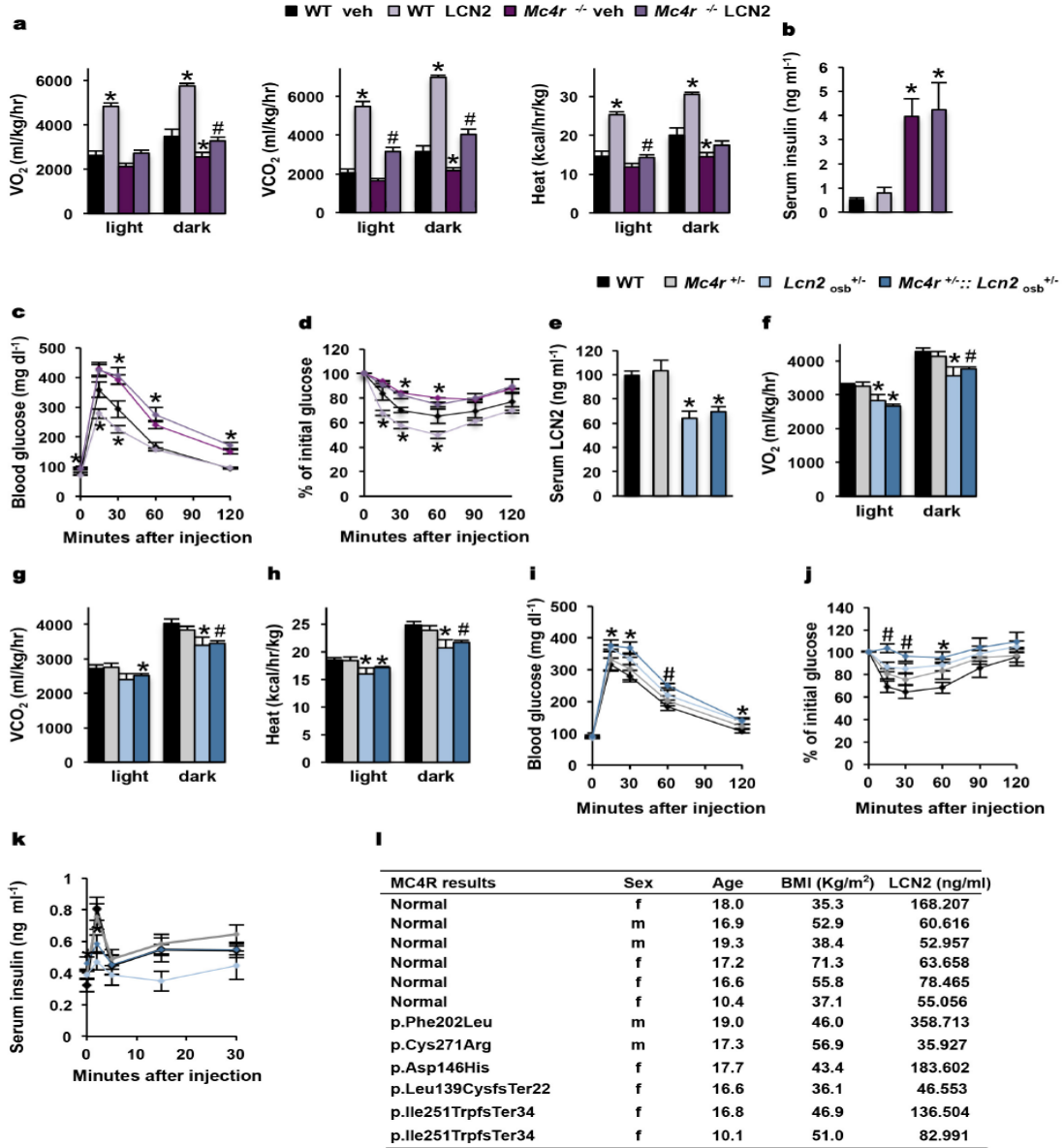
a–d, *Mc4r–/–* and wild-type littermates were treated with LCN2 (150 ng/g/day) or vehicle for 8 weeks. **a**, Indirect calorimetry measurements. **b**, Serum insulin levels. **c**, Glucose tolerance test. **d**, Insulin tolerance test. **e–k**, Serum levels of LCN2 (**e**), indirect calorimetry measurements (**f–h**), glucose tolerance test (**i**), insulin tolerance test (**j**) and glucose-stimulated insulin secretion (**k**) in *Mc4r+/–*, *Lcn2*osb +/–, *Mc4r+/–*::*Lcn2*osb +/– and wild-type littermates. Data are mean ± s.e.m.; *n* = 5 wild-type and *n* = 7 *Mc4r–/–* mice (**a–d**). **l,** LCN2 plasma levels in patients with mutated and normal *MC4R* sequences. *n* = 6 wild-type, *Mc4r+/–* and *Mc4r+/–*::*Lcn2*osb +/– mice and *n* = 5 *Lcn2*osb +/– mice (**e–k**). Results are representative of three independent experiments. * *P* < 0.05 indicated genotypes or treatments versus wild-type mice (Student's *t*-test). #*P* < 0.05 when comparing either *Mc4r–/–* (vehicletreated) and *Mc4r–/–* (LCN2-treated) groups (**a**) or *Mc4r+/–*::*Lcn2*osb +/– mice versus wild-type, *Mc4r+/–* and *Lcn2*osb +/– mice (**f–k**) (ANOVA).

Chapter III: Upregulation of Lipocalin-2 is a protective mechanism to counteract metabolic dysregulation in obesity

Steven Shikhel, Ioanna Mosialou, Mishaela Rubin, Cyrille Confavreux & Stavroula Kousteni

Preface

The completion of this work is owed to the contribution of the people represented on the authorship list

Upregulation of Lipocalin2 is a protective mechanism to counteract metabolic dysregulation in obesity

Steven Shikhel[1], Ioanna Mosialou[1], Mishaela Rubin[2], Cyrille Confavreux[3] & Stavroula Kousteni[1]

[1]Department of Physiology and Cellular Biophysics, College of Physicians and Surgeons, Columbia University, New York, New York 10032, USA.

[2]Metabolic Bone Disease Unit, Department of Medicine, College of Physicians and Surgeons, Columbia University, New York, New York 10032, USA.

[3]Depeartment of Rheumatology, Hospices Civils de Lyon, Lyon, France.

Abstract

Regulation of food intake is a recently identified endocrine function of bone that is mediated by Lipocalin 2 (LCN2). Osteoblast-secreted LCN2 suppresses food intake, induces satiety after feeding and decreases fat mass while improving glucose tolerance, insulin secretion and sensitivity. We now show that serum LCN2 levels correlate with insulin levels and β-cell function, indices of healthy glucose metabolism, in genetic and diet-induced mouse models of obesity and in obese, healthy or pre-diabetic patients. However, LCN2 serum levels also correlate with body mass index (BMI) and insulin resistance in the same patients; and are increased in obese mice. To dissect this apparent discrepancy, we examined LCN2 effects in hyperphagia and β -cell function mouse models of obesity or β -cell destruction. Silencing *Lcn2* expression increases hyperphagia, fat and body weight and worsens β -cell function and general metabolic dysfunction in obese, leptin receptor-deficient mice. Conversely, LCN2 increases β-cell numbers and promotes β-cell function after streptozotocin-induced β -cell failure by (STZ) and acts as a growth factor necessary for β -cell adaptation to higher metabolic load in mice. These results support a protective role for LCN2 in obesity-induced glucose intolerance and insulin resistance that stem from its ability to decrease food intake and promote adaptive β-cell proliferation.

Introduction

The discovery of multiple endocrine functions of bone established a new paradigm in which proteins secreted from osteoblasts can act on distal organs to coordinate whole-body energy metabolism[1-6]. The function of osteoblasts on regulating energy metabolism have solely been attributed to osteocalcin which subsequently raised the question of whether multiple bone-derived hormones exist and whether osteoblasts elicit unanticipated endocrine functions[7]. In response to this question, a known hormone with a previously unidentified action in bone was found to mediate a new metabolic function of osteoblasts: regulation of food intake. Lipocalin-2 (LCN2) is a hormone preferentially expressed by osteoblasts in at least 10-fold higher levels as compared to other tissues at basal states. Its inactivation in osteoblasts in mice increases food intake by 16%, fat mass, and body weight and leads to glucose intolerance and insulin resistance, a decrease in circulating insulin levels, islet number and size, β-cell mass and β-cell proliferation, and lack of insulin secretion following a glucose challenge. In addition, chronic administration of exogenous LCN2 in lean and obese mice decreases food intake, fat mass, and body weight gain, supporting a beneficial role for LCN2 in energy metabolism[8] Osteoblastic expression and circulating LCN2 levels increase rapidly after a meal in mice indicating an acute physiological role of LCN2 in the regulation of feeding. The postprandial increase in LCN2 is required for suppression of food intake and termination of the meal. This effect is conserved in humans. Healthy women Postprandial LCN2 regulation is conserved in humans since LCN2 levels were elevated in normal weight women following a meal[9].

Several studies have reported a beneficial role for LCN2 in energy metabolism which include protection from diet-induced obesity, fatty liver disease, atherogenic dyslipidemia and insulin resistance, suppression of hepatic gluconeogenesis and, promotion of adaptive thermogenesis through activation of brown adipose tissue and fatty acid oxidation[9-12]. In addition, postprandial LCN2 positively correlates with energy

expenditure and improved fatty acid oxidation following a high-fat-meal in women with normal BMI[9]

Although circulating levels of LCN2 increase with body weight and insulin reistance in mouse models of obesity and insulin resistance, and in human subjects, the role of LCN2 is not well understood[9, 13-22]. Furthermore, serum LCN2 is decreased in long-term type 2 diabetes patients and are inversely correlated with body weight and glycated hemoglobin in diabetic patients[23]. These observations suggest a complex etiology regulating LCN2 serum levels in lean and obese subjects with or without diabetes and prompted us to interrogate what serum levels of LCN2 may reflect in each situation.

Observations relevant to the mode of LCN2 regulation provide insight into its role throughout the pathophysiology of diabetes. Besides its functions in suppressing appetite and favoring glucose metabolism, LCN2 acts as an acute phase protein in tissues in which it is minimally expressed in the basal states, such as kidney and liver[24-31]. LCN2 production is stimulated by both pro- and anti-inflammatory cytokines; which had led to several ascribed functions and roles in various pathological setting of LCN2[32-34]. Whether modulation of LCN2 in these contexts is deleterious or protective is currently unclear. It appears to depend on cell context and confounding associated comorbidities[35]. Nonetheless, LCN2 is upregulated by pro-inflammatory cytokines in the obese state to resolve inflammation in adipocytes and macrophages[14-15]. Interestingly, expression of *Mc4r*, the receptor of LCN2 in the hypothalamus mediating its anorexigenic effect, increases during inflammation; and, MC4R antagonism improves food intake in both acute and chronic inflammatory diseases presumably by counteracting the functions of LCN2[36-37]. In addition, LCN2 could play a protective role in obesity by promoting β-cell proliferation and function[38]. These observations suggest that elevated LCN2 levels in obesity may be a compensatory homeostatic response to counteract hyperglycemia and insulin resistance by suppressing body weight and by promoting β -cell proliferation, at least at the early stages of the disease.

We have found that serum LCN2 levels correlate with insulin levels and β -cell function, in genetic and diet-induced mouse models of obesity and in obese, pre-diabetic patients. However, LCN2 serum levels

also correlate with body mass index (BMI) and insulin resistance in the same patients; and are increased in obese mice. Increasing *Lcn2* through genetic means improves metabolic function while silencing *Lcn2* increases hyperphagia, body weight and worsens metabolic dysfunction as indicated by increased blood glucose, a higher impairment in glucose stimulated insulin secretion and a decrease in insulin levels. In addition, a beneficial effect of LCN2 on β-cell function was observed in mouse models of β-cell failure due to toxicity or high fat diet. These results support a protective role for LCN2 in obesity-induced glucose intolerance and insulin resistance.

Methods

Human study participants and sample collection

Pre-diabetic women were recruited as part of the NANTOS study. Pre-diabetes was defined as %HbA1c between 5.7 and 6.4. Subjects were excluded if they had a history of disorders associated with altered skeletal structure or function such as chronic kidney disease, chronic liver disease, active malignancy, acromegaly, Cushing's syndrome, thyroid disease, hyper- or hypoparathyroidism or organ transplant. Additionally, subjects were excluded if they were currently using teriparatide, loop diuretics, anti-convulsive therapies, corticosteroids (>3 weeks over the past 3 years), thiazolidinediones or SGLT2 inhibitors. Bisphosphonate and/or denosumab use within the past 12 months were also exclusion criteria. Fasting morning blood was drawn and serum was stored at −80 °C. Age and anthropometric characteristics such as height, body weight, and waist circumference were recorded. Body mass index was calculated as ratio of body weight(kg) to height squared(m^2). Homeostatic model assessment (HOMA) is a method to quantify insulin resistance (HOMA-IR) and beta-cell function (HOMA-B) using glucose and insulin measurements. HOMA-R was calculated by multiplying fasting glucose by fasting glucose and dividing by constant 22.5 (HOMA-IR = FPG*FPI/22.5). HOMA-B = (20*FPI) / (FPG − 3.5) %. (Turner et al., 1979; Mathews et al., 1985).

Exclusion criteria included if previous use of teriparatide or rhPTH, glucocorticoid use within the past 2 years, pregnancy or breastfeeding within the past 6 months, a history of Cushing's syndrome, uncontrolled thyroid disease, malabsorption syndrome, significant liver disease, creatinine clearance <30 mL/min, other chronic disorders of mineral metabolism such as Paget's disease, and osteogenesis imperfecta. Postmenopausal status was defined as having no menstrual period for more than 1 year in both groups. The study was approved by the institutional review boards of CUMC; all subjects gave written informed consent.

Mice

Lcn2fl/+ mice were generated as previously described[8]. *Lcn2fl/+* mice were crossed with *Col1a1-Cre* or *EIIa-Cre* transgenic mice to generate osteoblast specific or global deletion of *Lcn2* mice. *Lcn2*-heterozygous mice were intercrossed and animals homozygous for *Lcn2* deletion in osteoblasts ($Lcn2_{osb}^{-/-}$) or global deletion of *Lcn2*($Lcn2^{-/-}$ mice) were obtained. C57BL/6J, homozygous and heterozygous leptin-receptor-deficient mice, B6.BKS(D)-*Leprdb*/J (stock number 000697), leptin-deficient mice, B6.Cg-*Lepob*/J (stock number 000632) and mice lacking *Mc4r*, B6;129S4-*Mc4r^{tm1Lowl}*/J (stock number 006414) were purchased from The Jackson Laboratory. High fat diet fed mice were given a 60% fat diet for 16 weeks (Research Diets D12492). All mice were housed under standard laboratory conditions (12 h on/off; lights on at 7:00) and temperature-controlled environment with food and water available *ad libitum* unless otherwise specified. In each experiment the mice used were of the same genetic background, as they were all littermates. 10–12-week-old male mice of all genotypes and female $Lcn2^{-/-}$ mice were used in all experiments unless otherwise stated. Investigators were blinded during experiments and outcome assessment. Mouse genotypes were determined by PCR; primer sequences are available upon request. All animal procedures were approved by the Columbia University Institutional Animal Care and Use Committee.

RNA Isolation

RNA isolation, cDNA preparation and real-time PCR analyses were carried out following standard protocols. For bone tissue analysis, bone-marrow cells were removed completely by extensively flushing the femurs with PBS. Trizol reagent was used for RNA extraction, random hexamers cDNA synthesis kit (Clontech Laboratories) for reverse transcription PCR and SYBR Green Master Mix (Bio-

Rad Laboratories) for quantitative PCR. *Actb* was used as an internal control. Data are presented as fold change over control, unless otherwise indicated. Primer sequences are available upon request.

Metabolic tests

Glucose tolerance (GTT), insulin tolerance (ITT) and glucose-stimulated insulin secretion (GSIS) tests were performed as previously describes[45]. For *Lepr*[db/db] mice, the dose of glucose during GTT was 1 g per kg body weight and the dose of insulin during ITT was 2.5 U per kg body weight. Insulin levels were measure by the insulin ELISA kit (Crystal Chem).

STZ

To check whether enhanced lipocalin-2 serum levels could ameliorate hyperglycemia caused by pancreatic b-cell failure, 9-week old male mice (8 per group) were injected with a single high dose of STZ (150mg/kg of body weight) to induce b-cell death and subsequently injected daily with 150ng/g recombinant lcn-2, one week following STZ injection. Blood glucose was measured every 48h with a glucometer. STZ induced diabetes (fed blood glucose>250mg/dl) in 50% of the mice injected by day 2 , 56.25% by day 4 and 62.5% by day 6 which remained stable thereafter, with blood glucose levels raging from 400-500mg/dl.

siRNA

siRNA against LCN2 was delivered to *Lepr*[db/db] mice as a complex with a polymer-based reagent (In vivo JetPei) every two days for 30 days by subcutaneous injections.

Statistics

Authors must fully describe all statistical tests used during the analysis in the methods, and the statistical test used must also be reported in the relevant figure legend. We encourage authors to describe methods used to assess whether the data met the assumptions of the statistical test utilized (e.g., normal distribution). Authors must specify whether statistical tests are one-sided or two-sided. When making multiple comparisons on a single data set, authors should choose statistical tests that account for multiple groups (such as ANOVA rather than a series of *t* tests). The statistical analysis should also correct for repeated measures when comparing multiple measurements within subjects. A statement describing inclusion/exclusion criteria must be included in Methods if any samples were excluded from the analysis. Error bars must be defined, either in Methods or in the legends themselves; e.g., "Data represent mean ± SEM." Variance around the mean and statistical analysis should not be presented if fewer than 3 independent samples are included.

Results

LCN2 correlates with β-cell function and insulin resistance in pre-diabetic women

To elucidate the connection between LCN2 and obesity in the development of diabetes, we examined potential correlations between serum LCN2 levels, glucose tolerance and insulin sensitivity in a 5-year prospective study of obese pre-diabetic women (n=88). Subjects characteristics are summarized in Table1.

Spearman's correlation showed a positive association between serum LCN2 levels and BMI (r=0.3*), waist circumference (r=0.29*), serum insulin levels (r=0.39) and HOMA-B (r=0.39*). At the same time, LCN2 levels positively correlated with HOMA-IR (r=0.37*) and inversely correlated with serum adiponectin levels (r=-0.29*), which are both indices of insulin resistance (Table 2 and Suppl. Figure 1A-F).

The correlations between serum LCN2 levels and BMI, Waist Circumference and HOMA-IR became stronger when BMI was segregated into obese (BMI>30 kg/mg^2 (n=39)) and severely obese (BMI>35kg/mg^2 (n=25)) groups (Table 3). A logistic regression analysis, showed that an increase of HOMA-IR by 1SD, or 34% above the mean, increased the likelihood of belonging in the highest quartile of serum LCN2 levels (Odds ratio (OR) = 2.81 [1.46-5.40], p=0.002).

Subsequently, we examined whether baseline serum LCN2 levels could predict diabetes progression in the same group of obese pre-diabetic women. A prospective analysis at the end of the 5-year follow-up study indicated that whereas HOMA-IR was associated with the risk of becoming diabetic, as this was defined by HbA1c levels above 6.5%, baseline fasting LCN2 serum level was not associated with the risk of developing diabetes (OR=0.98 per 1 SD increase [0.86-1.23]; p=0.56) (Table 4).

In a separate cohort of post-menopausal women (n=97), LCN2 increases in type-2-diabetics (T2D) and with BMI classification in non-diabetics (Table 5). LCN2 serum levels are elevated in diabetics (87.28 ng/ml±5.15), as compared to non-diabetic lean controls subjects (58.58 ng/ml±7.61) (Fig. 1A). Also, in non-diabetic subjects increasing BMI is associated with rising LCN2 levels (Fig. 1B). The magnitude of

increase in T2D was independent of BMI as LCN2 serum levels were elevated among all BMI groups of T2D (Fig. 1C). A decrease in HbA1c with increasing LCN2 levels was previously shown in T2D men of similar age[8].

Therefore, while the increased LCN2 levels are indicative of the onset of insulin resistance in the pre-diabetic state they are indicative of a better metabolic regulation in the presence of insulin resistance in T2D. This biphasic opposite association of serum LCN2 levels with disease severity in the two stages of the disease possibly reflects its inability to predict diabetes onset and its unlikely involvement as a causative factor in disease progression. On the contrary, and in light of our previous observations of a beneficial role for LCN2 in obesity and glucose metabolism in mice, the increase in LCN2 levels with the onset of insulin resistance most probably reflects a compensatory protective response for LCN2 increasing as glucose metabolism deteriorates to subsequently improve b-cell function and decrease hyperglycemia.

Serum LCN2 levels are increased in mouse models of obesity

To better understand the role LCN2 and the impact of modulating circulating LCN2 levels in the pathophysiology of diabetes we took advantage of genetic and diet-induced mouse models of obesity and diabetes. Our previous observations in diabetic and obese pre-diabetic subjects prompted us to examine whether LCN2 serum levels are elevated in obese or diabetic mouse models including the leptin-receptor deficient, leptin-deficient, MC4R-deficient and high-fat-diet-fed mice. Circulating LCN2 levels are increased in leptin-deficient (*Lepr^{db/db}*) mice (Fig. 2A), leptin deficient (*Lepr^{ob/ob}*) mice (Fig. 2B) and 16-week old obese insulin resistant *Mc4r-/-* mice (Fig.2C), as compared to wild-type controls. Placing wild-type mice on a 60% high-fat-diet (HFD) for 16-weeks results in a 25% increase in serum LCN2 compared to littermate controls on regular-chow-diet (RCD) (Fig. 2D). The increase in circulating LCN2 levels was evident as early as five weeks of age in *Lepr^{db/db}* mice (Fig. 2E) whereas circulating LCN2 levels remained normal in 2-month-old MC4R-/- mice but started increasing at three months of age (Fig. 2F). While being

92

fed an ad libitum HFD, LCN2 levels started to increase at four weeks and became significantly different at ten weeks compared to mice on RCD (Fig. 2G). The observed difference in kinetics of LCN2 levels likely coincides with the differential onset of insulin resistance in each mouse model. These results recapitulate our findings in prediabetic subjects showing an increase in LCN2 serum levels in response to the development of impaired glucose metabolism.

The increase in circulating LCN2 levels, thus far, has been difficult to attribute to changes of transcriptional activity. Significant increases of LCN2 expression are seen in tissues when compared to their baseline which express low levels of LCN2. However, their total input is exceedingly small when compared to bone (Fig 2 H-M). Forthcoming analysis will be targeted to increasing sample size and evaluating protein content in each tissue, serum, and whole blood to evaluate the role of secretory events.

The correlational observations made in obese and diabetic mouse models cannot resolve whether elevation of circulating LCN2 is a compensatory or driving response as insulin resistance and adiposity increase. To examine the specific effect of increased osteoblast and circulating LCN2 level in a genetic mouse model, transgenic mice overexpressing LCN2 in osteoblasts (*Col1a1-Lcn2^{Tg}*) were generated (Suppl Fig 3A). Transgenic *Col1a1-Lcn2^{Tg}* mice display a 50% increase in systemic LCN2 levels as compared to wild type littermates (Fig. 3A) resulting in a 12.5% reduction in food intake, total fat mass and body weight, lower fed and fasting blood glucose levels, improved insulin sensitivity and increased energy expenditure (Fig3. B-J). The effect of increased LCN2 levels on glucose and energy metabolism agrees with our previous observations in wild-type mice treated with intermittent injections of recombinant LCN2[8]. The improvement in metabolic parameters in the transgenic mice remained until at least six months of age, the latest time point these mice were monitored, suggesting that sustained elevated LCN2 levels, do not lead to obesity and insulin resistance.

LCN2 silencing worsens hyperphagia, glucose intolerance and LCN2 silencing worsens hyperphagia, glucose intolerance

Elevating LCN2 via genetic (*Col1a1-Lcn2^{Tg}*) and pharmacological means, as previously seen by treatment of rLCN to WT and *Lepr$^{db/db}$*, is non-pathogenic and provides beneficial effects on metabolic function by decreasing food intake and improving beta-cell function. Therefore, we aimed to lower LCN2 levels in *Lepr$^{db/db}$* where circulating LCN2 levels are elevated and assess whether this increase is driving the increase in adiposity and hyperglycemia, or is a compensatory, protective mechanism against weight gain, hyperglycemia, β-cell failure, and glucose intolerance. For this purpose, *Lcn2* expression was silenced in *Lepr$^{db/db}$* mice by systemic delivery of LCN2 siRNA every two days for 30 days by subcutaneous injections. This regime decreased circulating LCN2 levels by 50% (Fig. 4A), normalizing it to those of wild-type mice. A decrease in Lcn2 expression was observed in bone (30%), liver (50%) and adipose tissue (60%) (Fig. 4B).

Lepr$^{db/db}$ mice given siRNA for LCN2 subcutaneously displayed worsened metabolic health. Food intake increased by 24% which correlates with a 50% increase in body weight and a corresponding 44% increase in gonadal fat pad weight (Fig. 4 C-E). In agreement with the hyperphagia, expression of anorexigenic downstream targets of the melanocortin 4 receptor (MC4R) pathway genes like Trh, Crh, Sim1 and BDNF was decreased in the hypothalamus of *Lcn2* silenced *Lepr$^{db/db}$* mice following (Fig 4. F). Fed and fasting blood glucose levels increased by 50% while insulin levels decreased (Fig. 4G-I). Also, silencing *Lcn2* further impaired glucose stimulated insulin secretion (Fig. 4J).

We have previously observed a direct effect of LCN2 treatment on islet size and function in vivo and in vitro[8]. To better understand the mechanism by which glucose metabolism becomes further compromised in diabetic mice following LCN2 silencing, pancreas histology was performed. Islet number, size and mass are all reduced following reduction in LCN2 in *Lepr$^{db/db}$* mice compared to controls (Fig. 4K).

Similarly, using a second model of decreased LCN2 levels, the *Lcn2$_{osb}$-/-* mice which have 68% less

circulating LCN2 levels, on HFD, resulted in further worsened body weight gain, fat pad mass, glucose levels, glucose intolerance and insulin resistance as compared to wild-type littermate controls (Fig 5A-D). The human and mouse data reported here, together with our previous genetic and pharmacological manipulations of LCN2, support a protective role for increased levels of endogenous LCN2 to counteract the adverse effects of hyperphagia and hyperglycemia on obesity and insulin resistance.

LCN2 promotes adaptive β-cell proliferation and function in mouse models of diabetes and obesity.

Serum LCN2 levels are positively associated with insulin levels and β-cell function in obese, pre-diabetic patients and in mouse models of obesity. In addition to limiting appetite, LCN2 may function to improve glucose handling by increasing β-cell mass and function. Indeed, our previous observations showed that LCN2 acts directly on mouse pancreatic islets to increase insulin secretion, and promote β-cell proliferation[8]. To test this hypothesis, we examined whether LCN2 acts as a growth factor to increase mass and functionality of β-cells as a compensatory mechanism of hyperglycemia. First, we evaluated a model of extreme hyperglycemia caused by pancreatic β-cell failure. Mice were injected with a single high dose of streptozotocin (STZ) to induce β -cell death. LCN2 was administered eight days after STZ injection. At this time point, STZ induced a 75% loss in β -cells resulting in blood glucose levels to rise above 250 ng/ml (Fig. 6A-E). The dose of LCN2 administered was the same to the one that improves glucose metabolism and insulin sensitivity in healthy, wild type mice[8]. Treatment with rLCN2 increased β -cell area, islet number and β-cell mass while lowered fed and fasted glucose by 50% (Fig. 6A-E). Glucose tolerance improved with rLCN2 treatment. There was a 3-fold increase in serum insulin levels which could explain the improved glucose tolerance in rLCN2-treated diabetic mice (Fig. 6F, G). In spite of the massive destruction of β-cells, this dose of LCN2 prevented STZ-induced lethality (Fig. 6H). All mice treated with LCN2 survived through the two months of treatment whereas only 20% of mice given vehicle were alive.

95

Subsequently, we examined whether LCN2 is necessary for β-cell adaption to higher metabolic load. We used a short-term physiological intervention model, where mice are placed on a high-fat-diet for seven days. This model has previously been shown to induce b-cell proliferation before noticeable changes in insulin resistance and can be used to identify early drivers of b-cell proliferation[39]. β-cells and control mice were placed on a regular-chow-diet (RCD) or a high-fat-diet (HFD, consisting of 60% kcal from fat) for seven days. After the seventh day mice were euthanized and pancreata were processed for histological analysis. Body weight and glucose increased comparably in both WT and *Lcn2-/-* (Fig. 7A, B). However, whereas insulin significantly increased 2-fold in the WT mice, the *Lcn2-/-* failed to increase insulin production to meet increased metabolic demands (Fig. 7C). The *Lcn2-/-* have less of the smallest islets indicating a potential lack of ability for hyperplasia. Subsequently, after seven days of HFD, a group of mice were fasted overnight and a glucose-tolerance-test was performed which *Lcn2-/-* have worsened glucose tolerance. These results indicate that LCN2 is required to mount the early protective response of β-cells proliferation to suppress hyperglycemia in mice fed HFD.

Discussion

LCN2 is secreted by osteoblasts to suppress appetite and improve glucose metabolism in lean and obese mice. Herein, we show that obese mice have increased circulating levels of LCN2 to protect against hyperglycemia and metabolic deregulation by maintaining β-cell function. From our studies in obese, pre-diabetic and diabetic patients we observe a positive correlation between serum LCN2 levels with HOMA-B and insulin levels but also with HOMA-IR and BMI.

The increase in LCN2 is in agreement with the elevated circulating LCN2 levels that have been reported in obese and insulin resistant states in mice and humans. The clinical[9-12] studies are cross-sectional thus showing causality is hard and difficult to make a confident conclusion. Several indications suggest that, at least at the early stages of the disease, LCN2 up-regulation may be a consequence of hyperglycemia and a protective mechanism against inflammation-induced insulin resistance and hyperglycemia. Indeed, circulating LCN2 levels are not associated with insulin resistance in non-diabetic, healthy men and women in our studies or in reported observations[12] but increase in T2D and are inversely correlated with body weight and glycated hemoglobin within long-term diabetic patients[23] possibly reflecting an exhaustion of LCN2 response, while disease remains. LCN2 levels in T2D are positively associated with the indexes of insulin secretion and insulin resistance but negatively associated with fasting plasma glucose suggesting that increased LCN2 levels may contribute to enhance insulin secretion in diabetes and ameliorate hyperglycemia[22].

The increase in serum LCN2 levels with increasing adiposity follows a pattern similar to that of the anorexigenic adipokine leptin; where the serum concentration increase is associated with the development of leptin resistance[40]. Inflammation has been proposed as a potential unifying mechanism behind the pathogenesis of obesity and insulin resistance. Nevertheless, given that LCN2 is up-regulated by pro- and anti-inflammatory cytokines and a positive correlation between LCN2 levels and C-reactive

protein (CRP) concentrations in obese humans has been shown[13-15], the underlying chronic low-grade inflammation in obesity may be the trigger for LCN2 upregulation.

This study and the work of others in mouse models support the notion that the positive correlation of LCN2 with adiposity, insulin resistance, and hyperglycemia observed in humans in a beneficial compensatory response to combat hyperglycemia by improving islet function. LCN2 serum levels are elevated in mouse models of obesity. Silencing Lcn2 expression in leptin receptor-deficient mice deceased circulating LCN2 levels and lead to worsening of their metabolic phenotype by increasing hyperphagia, insulin resistance and glucose intolerance. Similar to our finding's, others have shown that *Lcn2* expression is upregulated in the obese state to counteract and resolve increases in diet-induced inflammation due to increased adiposity[13-15]. Also, because exogenous LCN2 suppresses appetite and improves glucose metabolism and energy expenditure in obese *Lepr*$^{db/db}$ mice, it's likely LCN2 plays a protective role in the development of obesity and insulin resistance.

Our observations showing that osteoblast-derived LCN2 exerts a beneficial influence on energy metabolism are in agreement with several studies in mice lacking Lcn2 in all cells. These studies showed that LCN2 promotes insulin sensitivity and glucose homeostasis by various mechanisms such as promoting adaptive thermogenesis and suppressing hepatic gluconeogenesis; decreasing gonadal fat and body weight, improving insulin sensitivity; suppressing a pro-atherogenic metabolic profile; and, by activating brown adipose tissue and fatty acid oxidation thus promoting oxidative metabolism[9-12].

Interestingly, improved fatty acid oxidation has also been reported in normal-weight women whom LCN2 serum levels correlate with energy expenditure measured after a high-fat meal[9]. In contrast, one study reported that Lcn2 deficiency protects mice from developing age- and obesity-induced insulin resistance[41]; whereas a second study reported small effects of LCN2 in glucose intolerance and lack of an effect in age- or obesity-induced insulin resistance[42]. These studies were performed using mice in which

Lcn2 has been inactivated by deletion of either exons 1 to 5[43] or exons 2 to 5[44].

In contrast, we inactivated Lcn2 by deletion of exons 3-6. It is possible that deletion of different exons of Lcn2 accounts for differences in the potency of the metabolic phenotype developed. However, the effects of exogenous LCN2 support the conclusion drawn from our loss-of-function experiments. Moreover, recent studies in humans have noted that circulating LCN2 levels are decreased in type 2 diabetic patients[23] suggesting that the favorable effects of LCN2 in energy metabolism may be conserved in humans.

In addition to the previously well-characterized anorexigenic effects of osteoblast-secreted LCN2[8], we show here a distinct beneficial role of LCN2 on beta cell function. Data from obese pre-diabetic and diabetic patients and mouse models of beta cell failure due to toxicity or high-fat-diet support this initial hypothesis. These results are complemented by our previous observations that treatment lean and obese *Lepr*^{db/db} mice, with exogenous LCN2, increased b-cell proliferation, b-cell mass, and blood insulin levels and that these effects result from direct actions of LCN2 on mouse pancreatic islets inducing beta cell proliferation and insulin secretion[8].

References

1. Lee NK, Sowa H, Hinoi E, Ferron M, Ahn JD, Confavreux C, Dacquin R, Mee PJ, McKee MD, Jung DY, Zhang Z, Kim JK, Mauvais-Jarvis F, Ducy P, Karsenty G. Endocrine regulation of energy metabolism by the skeleton. Cell 2007; 130:456-469

2. Ferron M, Hinoi E, Karsenty G, Ducy P. Osteocalcin differentially regulates beta cell and adipocyte gene expression and affects the development of metabolic diseases in wild-type mice. Proc Natl Acad Sci U S A 2008; 105:5266-5270

3. Ferron, M. *et al. Insulin signaling in osteoblasts integrates bone remodeling and energy metabolism*. *Cell* **142**, 296–308 (2010)

4. Kousteni, S. 2012. FoxO1, the transcriptional chief of staff of energy metabolism. *Bone*. 50, 2 (2012), 437–443.

5. Oury F, Ferron M, Huizhen W, Confavreux C, Xu L, Lacombe J, Srinivas P, Chamouni A, Lugani F, Lejeune H, Kumar TR, Plotton I, Karsenty G. Osteocalcin regulates murine and human fertility through a pancreas-bone-testis axis. J Clin Invest 2013; 123:2421-2433

6. Mera P, Laue K, Ferron M, Confavreux C, Wei J, Galan-Diez M, Lacampagne A, Mitchell SJ, Mattison JA, Chen Y, Bacchetta J, Szulc P, Kitsis RN, de Cabo R, Friedman RA, Torsitano C, McGraw TE, Puchowicz M, Kurland I, Karsenty G. Osteocalcin Signaling in Myofibers Is Necessary and Sufficient for Optimum Adaptation to Exercise. Cell Metab 2016; 23:1078-1092

7. Yoshikawa Y, Kode A, Xu L, Mosialou I, Silva BC, Ferron M, Clemens TL, Economides AN, Kousteni S. Genetic evidence points to an osteocalcin-independent influence of osteoblasts on energy metabolism. J Bone Miner Res 2011; 26:2012-2025

8. Mosialou I, Shikhel S, Liu JM, Maurizi A, Luo N, He Z, Huang Y, Zong H, Friedman RA, Barasch J, Lanzano P, Deng L, Leibel RL, Rubin M, Nicholas T, Chung W, Zeltser LM, Williams KW, Pessin JE, Kousteni S. MC4R-dependent suppression of appetite by bone-derived lipocalin 2. Nature 2017; 543:385-390

9. Paton CM, Rogowski MP, Kozimor AL, Stevenson JL, Chang H, Cooper JA. Lipocalin-2 increases fat oxidation in vitro and is correlated with energy expenditure in normal weight but not obese women. Obesity (Silver Spring) 2013; 21:E640-648

10. Guo H, Jin D, Zhang Y, Wright W, Bazuine M, Brockman DA, Bernlohr DA, Chen X. Lipocalin-2 deficiency impairs thermogenesis and potentiates diet-induced insulin resistance in mice. Diabetes 2010; 59:1376-1385

11. Guo H, Bazuine M, Jin D, Huang MM, Cushman SW, Chen X. Evidence for the regulatory role of lipocalin 2 in high-fat diet-induced adipose tissue remodeling in male mice. Endocrinology 2013; 154:3525-3538

12. Zhang Y, Guo H, Deis JA, Mashek MG, Zhao M, Ariyakumar D, Armien AG, Bernlohr DA, Mashek DG, Chen X. Lipocalin 2 regulates brown fat activation via a nonadrenergic activation mechanism. J Biol Chem 2014; 289:22063-22077

13. Yan QW, Yang Q, Mody N, Graham TE, Hsu CH, Xu Z, Houstis NE, Kahn BB, Rosen ED. The adipokine lipocalin 2 is regulated by obesity and promotes insulin resistance. Diabetes 2007; 56:2533-2540

14. Wang Y, Lam KS, Kraegen EW, Sweeney G, Zhang J, Tso AW, Chow WS, Wat NM, Xu JY, Hoo RL, Xu A. Lipocalin-2 is an inflammatory marker closely associated with obesity, insulin resistance, and hyperglycemia in humans. Clinical chemistry 2007; 53:34-41

15. Zhang J, Wu Y, Zhang Y, Leroith D, Bernlohr DA, Chen X. The role of lipocalin 2 in the regulation of inflammation in adipocytes and macrophages. Mol Endocrinol 2008; 22:1416-1426

16. Moreno-Navarrete, J.M., Manco, M., Ibáñez, J., García-Fuentes, E., Ortega, F., Gorostiaga, E., Vendrell, J., Izquierdo, M., Martínez, C., Nolfe, G., Ricart, W., Mingrone, G., Tinahones, F. and Fernández-Real, J.M. Metabolic endotoxemia and saturated fat contribute to circulating NGAL concentrations in subjects with insulin resistance. *International journal of obesity (2010)*. 34, 2, 240–9.

17. Liu X, Hamnvik OP, Petrou M, Gong H, Chamberland JP, Christophi CA, Kales SN, Christiani DC, Mantzoros CS. Circulating lipocalin 2 is associated with body fat distribution at baseline but is not an independent predictor of insulin resistance: the prospective Cyprus Metabolism Study. Eur J Endocrinol 2011; 165:805-812

18. Jin, D., Guo, H., Bu, S.Y., Zhang, Y., Hannaford, J., Mashek, D.G. and Chen, X. 2011. Lipocalin 2 is a selective modulator of peroxisome proliferator-activated receptor-gamma activation and function in lipid homeostasis and energy expenditure.*FASEB journal : official publication of the Federation of American Societies for Experimental Biology*. 25, 2 (Feb. 2011), 754–64.

19. Koiou, E., Tziomalos, K., Katsikis, I., Kandaraki, E.A., Kalaitzakis, E., Delkos, D., Vosnakis, C. and Panidis, D. 2012. Weight loss significantly reduces serum lipocalin-2 levels in overweight and obese women with polycystic ovary syndrome.*Gynecological endocrinology : the official journal of the International Society of Gynecological Endocrinology*. 28, 1 (Jan. 2012), 20–4 Huang et al., 2012;

20. Huang Y, Yang Z, Ye Z, et al. Lipocalin-2, glucose metabolism and chronic low-grade systemic inflammation in Chinese people. *Cardiovasc Diabetol*. 2012;11:11. Published 2012 Jan 31. doi:10.1186/1475-2840-11-11

21. Rashad NM, El-Shal AS, Etewa RL, Wadea FM. Lipocalin-2 expression and serum levels as early predictors of type 2 diabetes mellitus in obese women. IUBMB Life 2017; 69:88-97

22. Wang W, Ye S, Qian L, Xing Y, Ren A, Chen C, Li S, Xu J, Liu Q, Dong L, Xiao C, Zhou W. Elevated serum lipocalin 2 levels are associated with indexes of both glucose and bone metabolism in type 2 diabetes mellitus. Endokrynologia Polska 2018;Elevated serum lipocalin 2 levels are associated with indexes of both glucose and bone metabolism in type 2 diabetes

23. De la Chesnaye E, Manuel-Apolinar L, Zarate A, Damasio L, Espino N, Revilla-Monsalve MC, Islas-Andrade S. Lipocalin-2 plasmatic levels are reduced in patients with long-term type 2 diabetes mellitus. International journal of clinical and experimental medicine 2015; 8:2853-2859

24. Paragas N, Kulkarni R, Werth M, et al. α-Intercalated cells defend the urinary system from bacterial infection. *J Clin Invest*. 2014;124(7):2963-76.

25. Karoui, K. et al. 2016. Endoplasmic reticulum stress drives proteinuria-induced kidney lesions via Lipocalin 2. *Nature Communications*. 7, 1 (2016), 10330.

26. Borkham-Kamphorst, Erawan & Drews, Falko & Weiskirchen, Ralf. (2011). Induction of lipocalin-2 expression in acute and chronic experimental liver injury moderated by pro-inflammatory cytokines interleukin-1? through nuclear factor-?B activation. Liver international : official journal of the International Association for the Study of the Liver. 31. 656-65. 10.1111/j.1478-3231.2011.02495.x.

27. Borkham-Kamphorst, Erawan & van de Leur, E & Zimmermann, HW & Karlmark, KR & Tihaa, L & Haas, U & Tacke, F & Berger, Thorsten & Mak, TW & Weiskirchen, R. (2013). Protective effects of Lipocalin-2 (LCN2) in acute and chronic liver injury indicate a novel function in liver homeostasis. Zeitschrift für Gastroenterologie. 51. 10.1055/s-0032-1331904.

28. Labbus, Kirsten & Henning, Marc & Borkham-Kamphorst, Erawan & Geisler, Cordelia & Berger, Thorsten & W Mak, Tak & Knuchel, Ruth & Meyer, Helmut & Weiskirchen, Ralf & Henkel, Corinna. (2012). Proteomic profiling in Lipocalin 2 deficient mice under normal and inflammatory conditions. Journal of proteomics. 78. 10.1016/j.jprot.2012.11.021.

29. Asimakopoulou, Anastasia & Borkham-Kamphorst, Erawan & Henning, Marc & Yagmur, Eray & Gassler, Nikolaus & Liedtke, Christian & Berger, Thorsten & W. Mak, Tak & Weiskirchen, Ralf. (2014). Lipocalin 2 (LCN2) regulates PLIN5 expression and intracellular lipid droplet formation in the liver. Biochimica et Biophysica Acta (BBA) - Molecular and Cell Biology of Lipids. 1841. 10.1016/j.bbalip.2014.07.017.

30. Asimakopoulou, Anastasia & Fülöp, Annabelle & Borkham-Kamphorst, Erawan & Van de Leur, Eddy & Gassler, Nikolaus & Berger, Thorsten & Beine, Birte & Meyer, Helmut & W. Mak, Tak & Hopf, Carsten & Henkel, Corinna & Weiskirchen, Ralf. (2017). Altered mitochondrial and peroxisomal integrity in lipocalin-2-deficient mice with hepatic steatosis. Biochimica et Biophysica Acta (BBA) - Molecular Basis of Disease. 1863. 10.1016/j.bbadis.2017.04.006.

31. Ye, Dewei & Yang, Kangmin & Zang, Shufei & Lin, Zhuofeng & Chau, Hau-Tak & Wang, Yudong & Zhang, Jialiang & Shi, Junping & Xu, Aimin & Lin, Shaoqiang & Wang, Yu. (2016). Lipocalin-2 Mediates Nonalcoholic Steatohepatitis by Promoting Neutrophil-Macrophage Crosstalk via The Induction of CXCR2. Journal of Hepatology. 65. 10.1016/j.jhep.2016.05.041.

32. Li, Chen & R Chan, Yvonne. (2011). Lipocalin 2 regulation and its complex role in inflammation and cancer. Cytokine. 56. 435-41. 10.1016/j.cyto.2011.07.021.

33. Xiao, Xia & Yeoh, Beng San & Vijay-Kumar, Matam. (2017). Lipocalin 2: An Emerging Player in Iron Homeostasis and Inflammation. Annual review of nutrition. 37. 10.1146/annurev-nutr-071816-064559.

34. Moschen, Alexander & E. Adolph, Timon & Gerner, Romana & Wieser, Verena & Tilg, Herbert. (2017). Lipocalin-2: A Master Mediator of Intestinal and Metabolic Inflammation. Trends in Endocrinology & Metabolism. 28. 10.1016/j.tem.2017.01.003.

35. Fadel, Fatina & Abdel Rahman, Azza & Farouk, Mohamed & A Habib, Sonia & H Ibrahim, Mona & S Sleem, Zeinab & M Bazaraa, Hafez & M.A. Soliman, Mohamed. (2012). Plasma neutrophil gelatinase-associated lipocalin as an early biomarker for prediction of acute kidney injury after cardio-pulmonary bypass in pediatric cardiac surgery. Archives of medical science : AMS. 8. 250-5. 10.5114/aoms.2012.28552.

36. Caruso, C. et al. Activation of melanocortin 4 receptors reduces the inflammatory response and prevents apoptosis induced by lipopolysaccharide and interferon-gamma in astrocytes. Endocrinology 148, 4918-4926, doi:10.1210/en.2007-0366 (2007).

37. Dwarkasing J, Marks D, Witkamp R, Norren K (2015). Hypothalamic inflammation and food intake regulation during chronic illness. Peptides. 77. 10.1016/j.peptides.2015.06.011.

38. Chang SY, Kim DB, Ko SH, Jo YH, Kim MJ. Induction mechanism of lipocalin-2 expression by co-stimulation with interleukin-1β and interferon-γ in RINm5F beta-cells. Biochemical and Biophysical Research Communications,Volume 434, Issue 3,2013,Pages 577-583.

39. Stamateris, Rachel & Sharma, Rohit & A Hollern, Douglas & Alonso, Laura. (2013). Adaptive -cell proliferation increases early in high-fat feeding in mice, concurrent with metabolic changes, with induction of islet cyclin D2 expression. American journal of physiology. Endocrinology and metabolism. 305. 10.1152/ajpendo.00040.2013.

40. Fruhwürth, Stefanie & Vogel, Heike & Schürmann, Annette & Williams, Kevin Jon. (2018). Novel Insights into How Overnutrition Disrupts the Hypothalamic Actions of Leptin. Frontiers in Endocrinology. 9. 10.3389/fendo.2018.00089.

41. Law, Ivy & Xu, Aimin & S L Lam, Karen & Berger, Thorsten & W Mak, Tak & Vanhoutte, Paul & T C Liu, Jacky & Sweeney, Gary & Zhou, Mingyan & Yang, Bo & Wang, Yu. (2010). Lipocalin-2 Deficiency Attenuates Insulin Resistance Associated With Aging and Obesity. Diabetes. 59. 872-82. 10.2337/db09-1541.

42. Jun LS, Siddall CP, Rosen ED. 2011. A minor role for lipocalin 2 in high fat diet-induced glucose intolerance. Am J Physiol Endocrinol Metab 301:E825–E835

43. Berger, T., Togawa, A., Duncan, G.S., Elia, A.J., You-Ten, A., Wakeham, A., Fong, H.E., Cheung, C.C., and Mak, T.W. (2006). Lipocalin 2-deficient mice exhibit increased sensitivity to Escherichia coli infection but not to ischemiareperfusion injury. Proc. Natl. Acad. Sci. USA 103, 1834–1839.

44. Flo TH, Smith KD, Sato S, Rodriguez DJ, Holmes MA, Strong RK, Akira S, Aderem A. Lipocalin 2 mediates an innate immune response to bacterial infection by sequestrating iron. Nature 2004; 432:917-921

45. Rached MT, Kode A, Silva BC, Jung DY, Gray S, Ong H, Paik JH, DePinho RA, Kim JK, Karsenty G, Kousteni S. FoxO1 expression in osteoblasts regulates glucose homeostasis through regulation of osteocalcin in mice. J Clin Invest 2010; 120:357-368

Figures

Figure 1: LCN2 increases with changes in BMI and diabetes status.
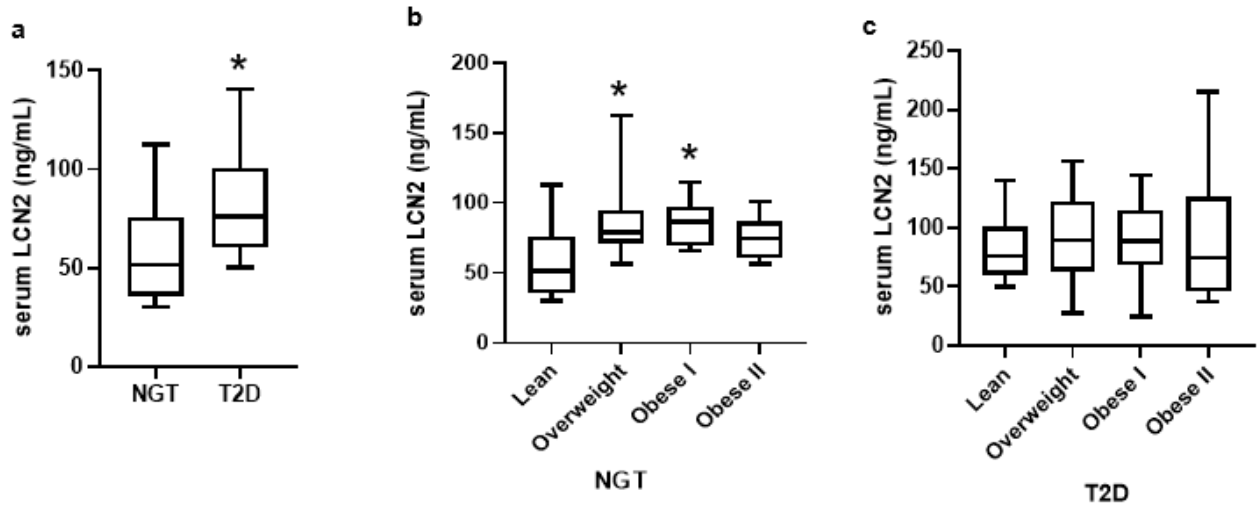
(a-c) Serum LCN2 of female subjects of varying BMI and diabetes status. Serum LCN2 levels in **(a)** lean healthy (n=11) and lean T2D (n=54) females **(b)** female subjects with NGT segregated by BMI, lean (n=11), overweight (n=14), Obese I (n=8), Obese II (n=10) **(c)** female subjects with T2D segregated by BMI, lean (n=10), overweight (n=11), Obese I (n=15), Obese II (n=14). Data are mean ± s.e.m. *$P < 0.05$ (ANOVA)

Figure 2: LCN2 serum levels increase in mouse models of obesity.

106
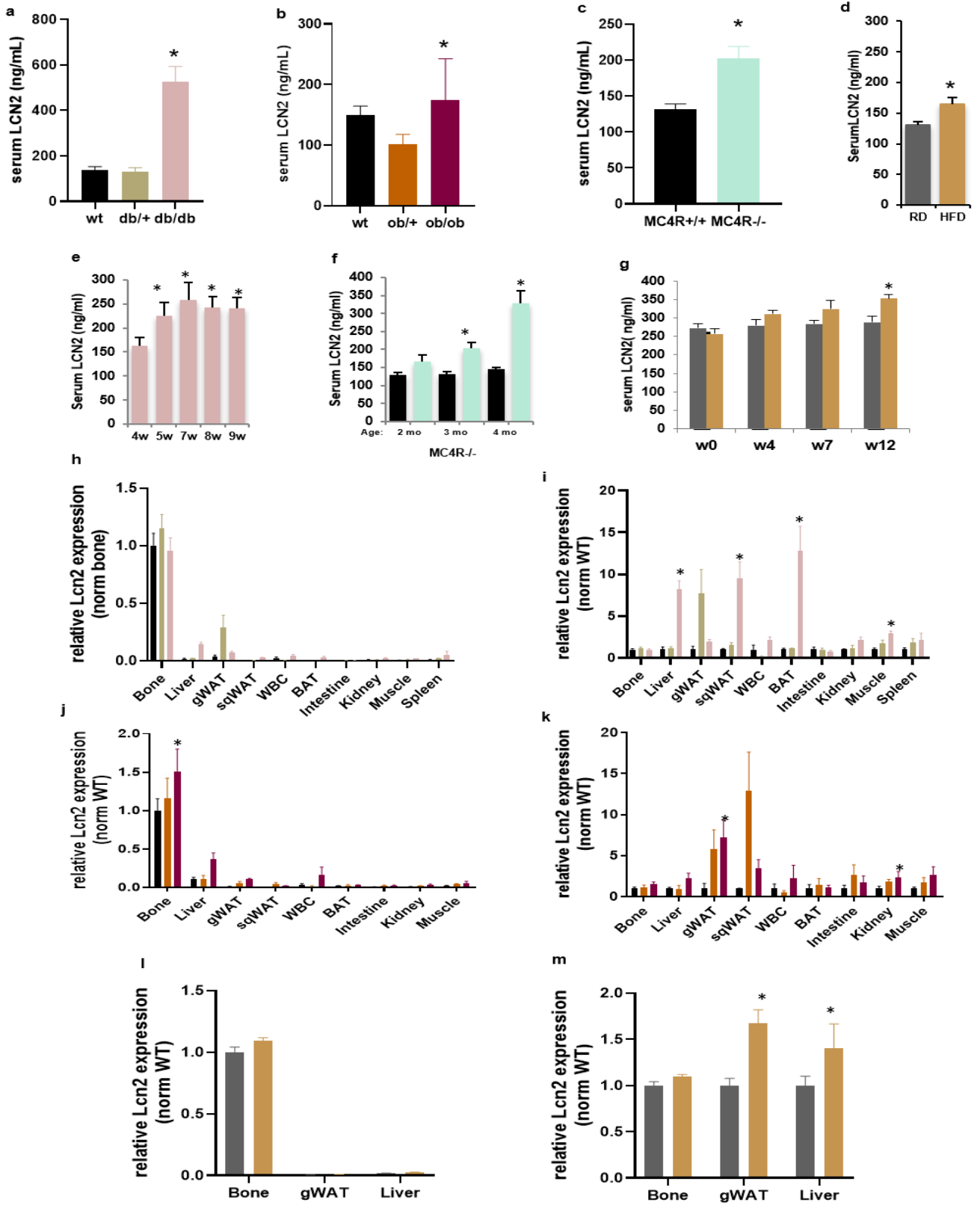
(a–g), Analysis of serum levels of LCN2 in mouse models of obesity **(a)** wild-type (n=12), $Lepr^{d/+}$(n=6)*, $Lepr^{db/db}$(n=9), **(b)** wild-type (n=4), $Lepr^{ob/+}$(n=3)*, $Lepr^{ob/ob}$(n=3), **(c)** $Mc4R+/+$(n=5) and $Mc4R-/-$ (n=9), **(d)** regular-chow diet (RD) (n=XX), high-fat diet (HFD) (n=X), **(e)** $Lepr^{db/db}$ (n=5), **(f)** $Mc4R+/+$(n=5) and $Mc4R-/-$ (n=9), **(g)** regular-chow diet (RD) (n=8), high-fat diet (HFD) (n=6), **(h-m)** mRNA expression analysis of *Lcn2* in mouse models of obesity **(h-i)** wild-type (n=3-9), $Lepr^{d/+}$(n=7-10)*, $Lepr^{db/db}$(n=4-9) of bone, liver, gonadal white adipose tissue (gWAT), subcutaneous white adipose tissue (sqWAT), white blood cells (WBC), brown adipose tissue (BAT), intestine, kidney, muscle, spleen, **(j-k)** wild-type (n=4), $Lepr^{ob/+}$(n=3)*, $Lepr^{ob/ob}$(n=3) of bone, liver gWAT, sqWAT, WBC, BAT, intestine, kidney, muscle **(l-m)** regular-chow diet (RD) (n=8), high-fat diet (HFD) (n=6) of bone, gWAT, liver. Data are mean ± s.e.m. *$P < 0.05$ (Student's *t*-test).

Figure 3: Transgenic mice expressing increased _Lcn2_ in osteoblasts have lower body weight and improved glucose metabolism
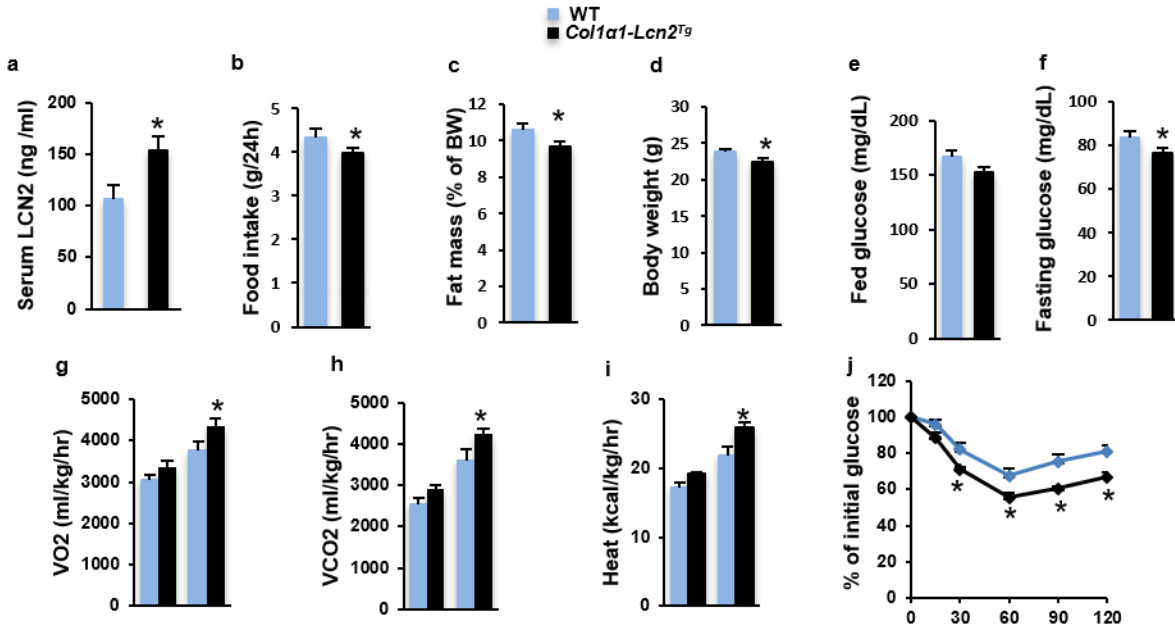
(a-j) analysis of metabolic phenotype of wild-type and _Col1α1-Lcn2^Tg_ mice **(a)** serum levels of LCN2 **(b)** food intake **(c)** fat mass as percent of BW **(d)** body weight **(e)** fed glucose **(f)** fasting glucose **(g)** volume of oxygen consumption **(h)** volume of CO_2 production **(i)** heat production **(j)** insulin tolerance test. Data are mean ± s.e.m. *$P < 0.05$ (Student's _t_-test).

Figure 4: LCN2 silencing worsens hyperphagia and glucose intolerance and in obese mice
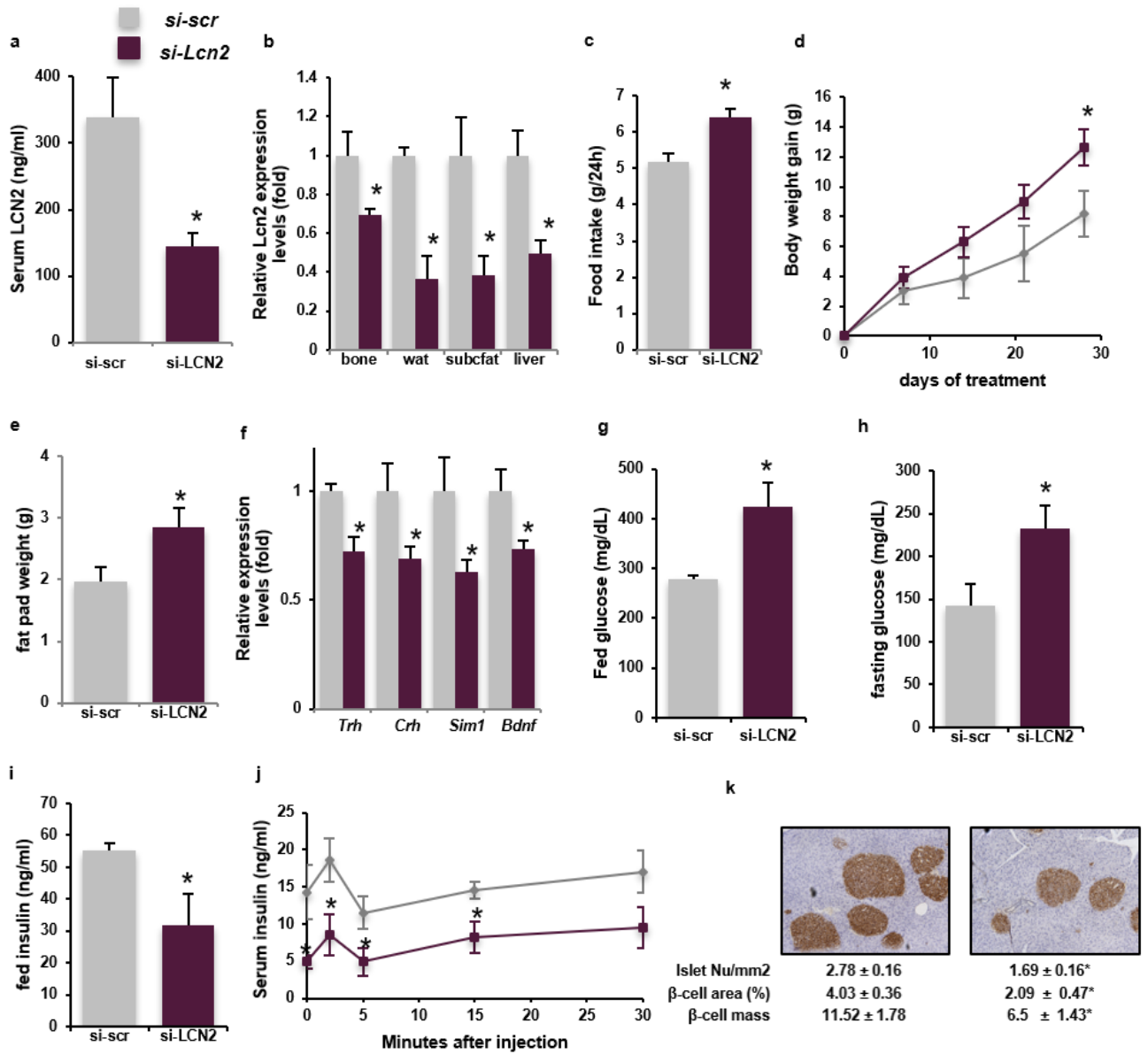
(a-k) analysis of metabolic phenotype of 12-week old male *Lepr^db/db* treated with *si-scrambled (si-scr)*(n=4) or *si-LCN2* (n=5) for 30 days **(a)** serum levels of LCN2 **(b)** relative *Lcn2* expression levels **(c)** food intake **(d)** body weight following treatment **(e)** fat pad weight **(f)** expression of Mc4r targets, *Trh, Crh, Sim1* and *Bdnf* **(g)** fed glucose **(h)** fasting glucose **(i)** fed insulin **(j)** glucose-stimulated insulin secretion **(k)** Pancreas insulin staining and islet histomorphometry. Data are mean ± s.e.m. *$P < 0.05$ (Student's *t*-test).

Figure 5: *Lcn2* deficiency exacerbates diet-induced obesity
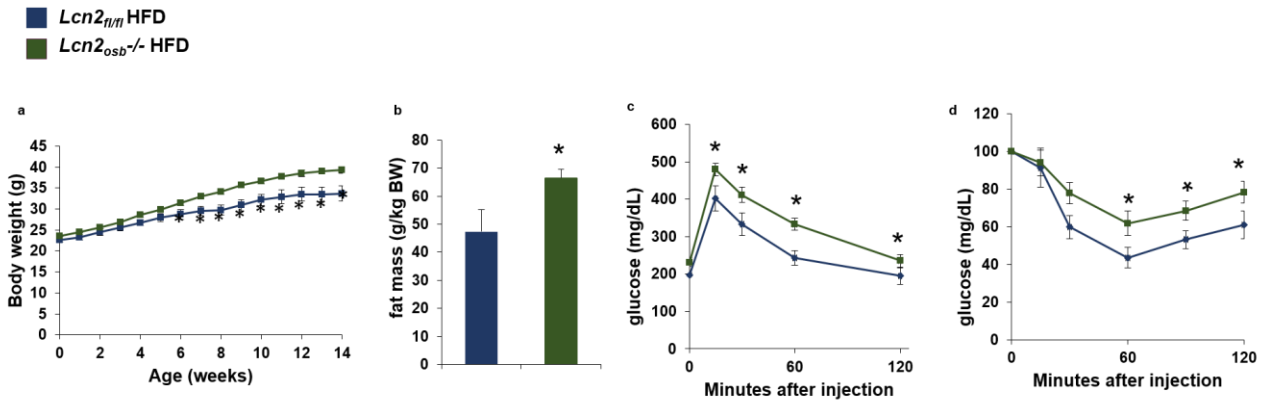
(a-d) analysis of metabolic phenotype of 22-week old male *Lcn2 fl/fl* (n=8) and *Lcn2osb-/-* (n=8) mice fed HFD for 14 weeks **(a)** body weight **(b)** fat mass **(c)** glucose-tolerance test **(d)** insulin tolerance test. Data are mean ± s.e.m. *$P < 0.05$ (Student's *t*-test).

Figure 6: LCN2 promotes β-cell proliferation and function following STZ treatment
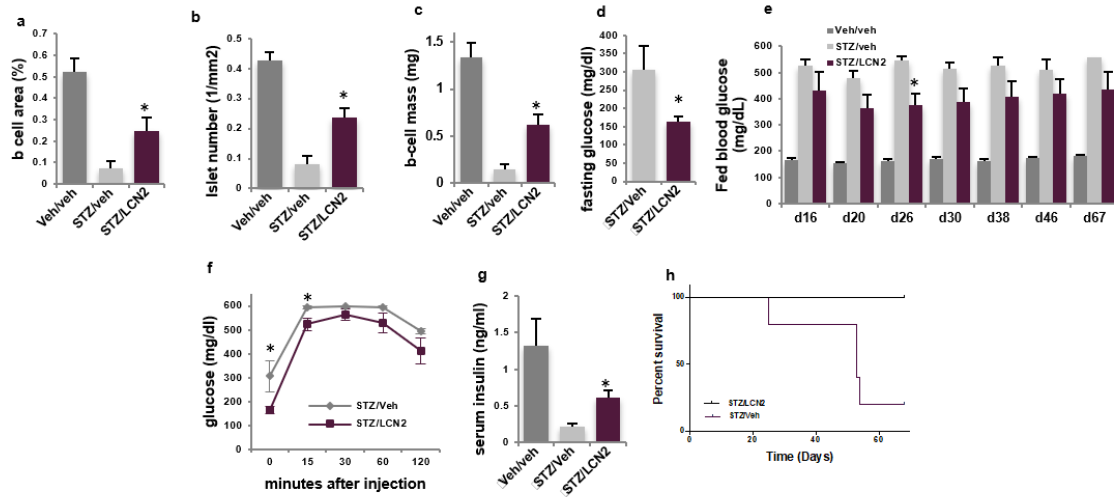
(a-h) analysis of β-cell function of 9-week old male WT mice given veh or STZ and treated with vehicle (n=8) or rLCN2 (n=8) **(a)** β-cell area **(b)** islet number **(c)** β-cell mass **(d)** fasting glucose **(e)** fed glucose **(f)** glucose tolerance test **(g)** serum insulin **(h)** Kaplan-Meier survival curve. Data are mean ± s.e.m. *$P < 0.05$ (Student's *t*-test).

Figure 7: LCN2 is necessary for compensatory insulin response after one week high-fat diet
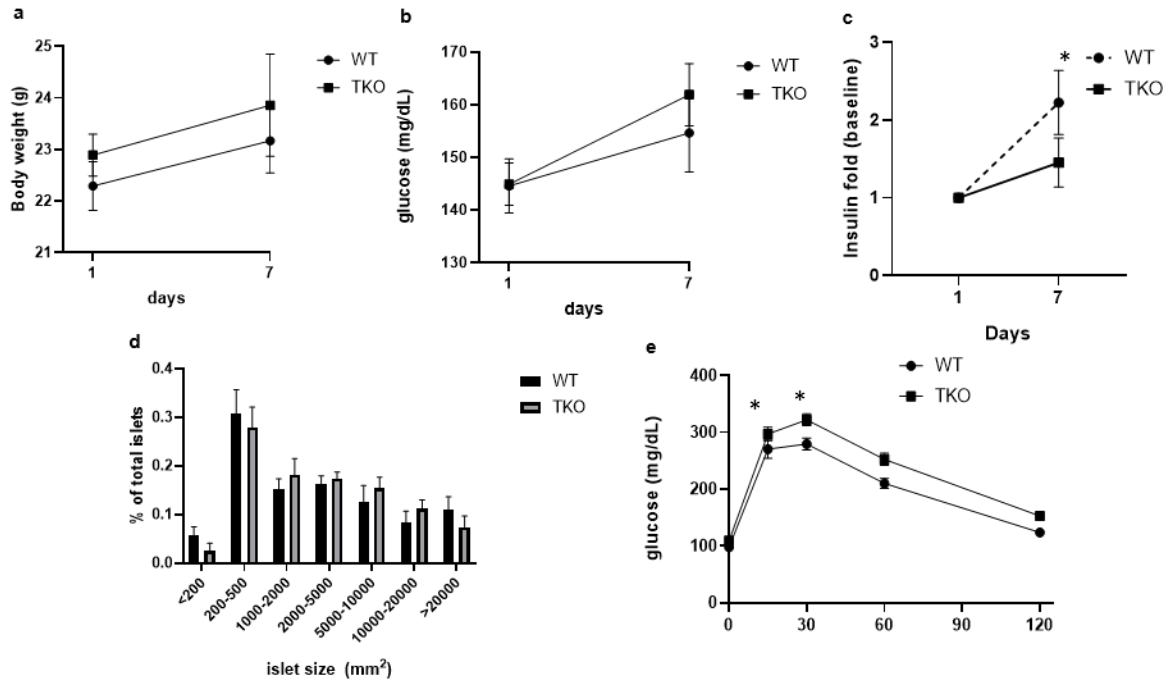
(a-e) analysis of insulin response following one-week HFD in 12-week female mice WT (n=5) and total-body Lcn2 knock-out mice (TKO) (n=5) **(a)** body weight **(b)** glucose **(c)** insulin **(d)** Islet size **(e)** glucose tolerance test**.** Data are mean ± s.e.m. *$P < 0.05$ (Student's t-test).

Tables

Table 1: Baseline characteristics of the prediabetic women population

Table 1: Baseline characteristics of the prediabetic women population	
Parameters	N=88
Age (yrs)	56.2 ± 10.8
BMI (Kg/m²)	32.2 ± 8.3
FINRISK score	15.8 ± 4.3
Waist circumference (cm)	97.4 ± 18.8
Blood glucose (mmol/L)	6.32 ± 0,54
HbA1C (%)	6.0 ± 0.4
Insulin (XX)	15.6 ± 9.3
Lipocalin 2 (ng/mL)	81.9 ± 29.4
Adiponectin (XX)	4.85 ± 2.88
HOMA-R	4.43 ± 2.86
HOMA-B	111.7 ± 63.4

Table 2: Pearson correlation coefficients between Lipocalin 2 and insulin resistance parameters

Table 2: Pearson correlation coefficients between Lipocalin 2 and insulin resistance parameters	
Parameters	r (p)
BMI (kg/ m^2)	0.30*
Waist circumference (cm)	0.29*
Insulin	0.39*
HOMA-B	0.39*
HOMA-IR	0.37*
Adiponectin	-0.29*
Blood glucose (mmol/L)	0.03

All variables were log-transformed

* p<0.01

Table 3 : Strengthenning of the correlation coefficients between Lipocalin 2 and BMI, waist circumference and HOMA-IR according to BMI cut-off

Table 3 : Strengthenning of the correlation coefficients between Lipocalin 2 and BMI, waist circumference and HOMA-IR according to BMI cut-off			
	BMI	Waist circumference	HOMA-IR
Whole population (n=88)	0.30**	0.29*	0.37**
BMI > 30 Kg/m² (n=39)	0.49**	0.47**	0.41*
BMI > 35 Kg/m² (n=25)	0.61**	0.52*	0.51*

All variables were log-transformed

*p≤0.01   **p<0.005

Odd-ratio risk of high lipocalin group = 2.81 [1.46-5.40] ; p=0.002
Odd-ratio risk of high lipocalin group = 2.85 [1.32-6.16] ; p=0.008 - adjusted on BMI
Odd-ratio risk of high lipocalin group = 2.44 [1.16-5.14] ; p=0.02 - adjusted on waist circumference
Odd-ratio risk of high lipocalin group = 2.62 [1.20-5.73] ; p=0.02 - adjusted on BMI and waist circumference (= overadjusted)

Table 4: Diabetes during the 5-year follow-up

Table 4: Diabetes during the 5-year follow-up				
	n	Mean (SD)	Median [Q1-Q3]	p (Wilcoxon)
CJP +	33	82.7 (27.9)	76.4[62.6-94.4]	
CJP -	55	81.5 (30.5)	76.0[62.4-100.6]	0.9
CJP1 +	30	83.4 (29.1)	76.7[62.4-101.2]	
CJP1 -	58	81.2 (29.8)	76.2[64.0-100.4]	0.87
CJP3 +	20	75.3 (22.6)	69.9[62.2-84.8]	
CJP3 -	68	83.9 (31.0)	77.6[63.3-101.6]	0.25

CJP =1 Fast blood glucose ≥ 1.26 g/l OR 1 HGPO (blood glucose 2h00 ≥2g/l) OR initiation of an oral antidiabetic treatment, and end of follow-up if bariatric surgery

CJP1 = 1 Fast blood glucose ≥ 1.26 g/l,

Table 5. Characteristics of the T2D and non-T2D study population

Table 5. Characteristics of the T2D and non-T2D study population					
	Non-T2D (n=43)			T2D (n=54)		
Parameters	Lean (n=11)	Overweight (n=14)	Obese (n=18)	Lean (n=10)	Overweight (n=11)	Obese (n=33)
Age (yrs)	61.63±2.42	58.64±1.80	61.38±1.54	68.00±2.77	65.36±1.82	54.81±
BW (Kg)	59.18±1.90	69.48±1.86	86.88±2.26	52.90±1.72	68.03±1.93	92.41±
BMI (Kg/m^2)	22.87±0.64	27.07±0.33	35.53±0.79	21.55±0.59	27.23±0.38	36.30±
HgbA1c (%)	5.68±0.07	5.65±0.08	5.90±0.08	7.35±0.26	8.31±0.64	7.90±0
Glucose (mg/dl)	87.54±2.12	88.85±1.84	91.72±2.46	118.90±13.20	167±23.79	160.81
Lcn2 (ng/ml)	58.58±7.61	85.84±7.09	79.88±3.83	82.88±8.84	89.21±12.09	87.97±

Chapter IV: General Discussion

Conclusion

Bone can act as an endocrine organ to regulate whole-body energy metabolism through the osteoblast-specific protein, osteocalcin. The question of whether additional osteoblast-derived hormones exist was addressed through genetic manipulation of osteoblast number. Mice with half of their osteoblasts ablated have a host of metabolic abnormalities including increased appetite. Fifty percent fewer osteoblasts led to a significant decrease in osteocalcin levels. Normalizing osteocalcin levels restored certain aspects of their metabolism, but the effect on food intake persisted. These series of experiments revealed osteocalcin-independent hormones might exist and identified appetite as another metabolic function regulated by osteoblasts[49].

The identification of the hormone responsible for this novel function was achieved by performing a microarray on primary osteoblasts from the osteoblast-specific FOXO1 knockout mouse[51]. FOXO1 is a transcription factor regulating osteoblast function. Its effects on energy metabolism are only in part due to its ability to monitor OCN activity; raising the possibility that additional hormones involved in energy metabolism may be targets of FoxO1. A microarray was performed comparing the gene expression profiles of wild-type and Foxo1 deficient primary osteoblasts. The experiment revealed the gene encoding Lipocalin-2 (LCN2) to be increased in primary osteoblasts of *FoxO1-/-* mice. Furthermore, the expression in bone and serum level was confirmed to be raised in the *FoxO1$_{osb}$-/-* mouse[54].

LCN2 is a secreted glycoprotein recognized for its role in innate immunity[66] and its involvement in metabolism as an adipokine[82]. However, expression profiling in wild-type mice revealed bone to be the predominant source of LCN2 under non-pathological conditions. *Lcn2* is expressed at least 10-fold higher in bone than in fat or any other tissue. This observation led to the generation of mice lacking Lcn2 specifically in osteoblasts (*Lcn2$_{osb}$-/-* mice). Analysis of these mutant mice showed that inactivation of *Lcn2*

in osteoblasts caused a 67% reduction in serum levels of LCN2 and increased food intake by 16% creating an increase in adiposity and body weight.

Furthermore, circulating insulin levels, glucose tolerance, and insulin sensitivity are all lower in mutant mice. Islet number and size, β-cell mass and proliferation, and insulin secretion were all decreased in $Lcn2_{osb}$-/- mice. Analysis of the time course of changes in food intake, glucose, and body weight revealed that changes in food intake preceded changes in glucose or body weight. Interestingly, pair-feeding to normalize food intake in the $Lcn2_{osb}$-/- mice restored body weight, fat mass, and insulin sensitivity but did not rescue the decrease in serum insulin levels or insulin secretion following a glucose load. As a result, glucose intolerance persisted indicating LCN2 might have a direct effect on insulin production and secretion. Treating primary b-cells in culture with LCN2 revealed an ability to favor β-cell proliferation and insulin secretion.

The canonical role of LCN2 as an acute phase protein, its ability to regulate food intake chronically and directly affect insulin secretion prompted the study of LCN2 in an acute feeding setting. One to three hours following refeeding, circulating LCN2 increase threefold corresponding to suppression of food intake at this time. The increase seems to contribute to postprandial satiety. $Lcn2$-null mice eat more than wild-type mice after refeeding and restoration of LCN2 via a single intraperitoneal injection of rLCN2 suppresses postprandial hyperphagia to wild-type levels in $Lcn2$-/-.

LCN2 crosses the blood-brain-barrier, accumulates in the hypothalamus, activates neurons in the paraventricular nucleus of the hypothalamus and binds to the melanocortin-4-receptor (MC4R) in the paraventricular nucleus and ventromedial neurons of the hypothalamus. To confirm that LCN2 acts centrally, an intracerebroventricular pump was implanted to release LCN2 which resulted in reduced food intake and body weight.

A series of molecular and biochemical studies showed the LCN2 activates the MC4R pathway. LCN2 treatment to hypothalamic cells induced cAMP production and induced MC4R target genes through direct binding to MC4R with an affinity similar to that of its known ligand, alpha-melanocyte stimulating hormone (aMSH). Accordingly, LCN2 cannot accumulate or activate the PVN neurons in the hypothalamus of MC4R-depleted mice. In addition, MC4R-knockout mice do not benefit from the anorexigenic effects of LCN2 treatment. These observations establish a central role for MC4R in mediating the anorexigenic response of LCN2.

The two previously reported receptors, 24p3R, and megalin do not seem to play a role in this response. Silencing 24p3R in hypothalamic cells showed no effect on the anorexia-promoting pathway of LCN2 and megalin is not expressed centrally. 24p3R is expressed in the pancreas, in the liver, but not in adipose tissue. By acting peripherally on these tissues LCN2 can affect aspects of energy metabolism, especially because LCN2 plays a primary role in insulin secretion. In the future, it would be interesting to evaluate how known mutant forms of endogenous LCN2 would affect food intake and glucose metabolism [112,113].

 Previous studies using different mouse models of germline deletion of Lcn2 have shown differential roles of LCN2 on metabolic health. Studies have reported a beneficial role for LCN2. It is protective in diet-induced obesity, fatty liver disease, atherogenic dyslipidemia, and insulin resistance, can suppress hepatic gluconeogenesis and promotes adaptive thermogenesis through activation of brown adipose tissues and FA oxidation[106,114–116]. In contrast, one study has reported a minimal effect of Lcn2 deficiency in glucose homeostasis with no impact on body weight[85] , whereas another showed protection from aging and obesity-induced insulin resistance[86]. Differences in targeting strategy and mainly the retention of a PGK-neo cassette in the latter studies, which shown to disrupt the expression of other genes located near the intended target, may account for differences in the phenotypes development.

Nevertheless, chronic administration of exogenous LCN2 in lean and obese mice decrease food intake, fat mass, and body weight gain, and improve glucose homeostasis and energy expenditure; providing further evidence that LCN2 plays a beneficial role in regulating energy metabolism[54]. Indeed, it would be helpful for the future study of LCN2 to conduct side-by-side experiments of available mouse models. A majority of studies using total-knock-out LCN2 mice have used mice initially generated by Flo et al., 2004 or Berger et al., 2006. In addition, both the Kousteni lab and Barasch lab have made floxed LCN2 mice for conditional cell ablation experiment which can be crossed with constitutive active CRE drivers like EIIa to create global knock-out mice. Conducting a battery of experiments in a controlled environment would clear up controversy and educate us on LCN2 genetics.

In agreement with Mosialou et al., a recent study showed that LCN2 deficient mice display hyperphagia, increased body weight and fat mass, hyperinsulinemia, polyuria, glycosuria, and fasted hypoglycemia compared to wild-type mice[111]. Moreover, increased LCN2 levels upon transgenic reconstitution of the estrogen-deactivating enzyme in adipose tissues of obese leptin-deficient mice, ob/ob mice contribute to reduced local and systemic inflammation, enhanced insulin sensitivity in peripheral tissues and improved overall diabetic phenotype[117].

Feeding experiments in mouse and human subjects have also observed the postprandial increase of LCN2[106,118]. Using a multiplexed screening approach to investigate metabolism-related changes in cytokines found LCN2 to be elevated after feeding compared to fasted mice[118]. Interestingly, LCN2 has also been reported to be increased in the fasted state[119]. The use of a fed-control group would have benefited the Peterson group. In humans, postprandial serum levels of LCN2 were significantly increased after various high-fat-meals. The largest increase was observed after a 40% saturated fat meal. This increase was accompanied by enhanced total energy expenditure, but only in normal-weight individuals. In obese subjects, a decrease in postprandial LCN2 concentrations occurred rather than an increase[106].

Yet to be uncovered is the critical component in feeding involved in LCN2 upregulation and secretion. Induction of Lcn2 expression has been observed by a variety of stimuli such as glucose, insulin, fatty-acids like palmitate and oleate, micronutrients like vitamin-D, and both pro- and anti-inflammatory cytokines[120]. In 3T3-L1 adipocytes, glucose and insulin synergistically act in LCN2 upregulation and secretion. The secretion of LCN2 can be induced by both glucose and a non-hydrolyzable form of glucose, methyl-O-glucose, but to a lesser degree, indicating a change in metabolic state is not entirely necessary[119]. In the kidney, ER stress drives proteinuria induced LCN2 production which is modulated through ATF4[121]. The mechanism by which LCN2 is secreted from various cell types may differ. How osteoblasts secrete LCN2 remains to be elucidated.

Furthermore, hyperinsulinemic induction by flowing glucose and insulin to maintain an increased level of insulin increases circulating LCN2 levels in humans[107]. Interestingly, the role of cytokines production and postprandial inflammation in humans have garnered attention[122–127]. The pathophysiology by which low-grade-chronic-inflammation develops in the metabolic syndrome may be due to prolonged ineffective resolution of postprandial inflammation[128–130].

The role of LCN2 in acute and chronic stress paradigms remains to be resolved. This debate seems to be dependent on cell type and context. In the gut, LCN2 protects from inflammation associated with microbiota alterations[131]. Changes in intestinal inflammation, via interaction with bacteria, precede and correlate with obesity and insulin resistance[132–134]. How proteins like heme which can be found in our diet, especially in animal protein, cause bacterial changes and modulate LCN2 is another potential avenue of investigation.

Another early site of metabolic inflammation is the brain[83,135–139]. There are diverse functional roles of LCN2 in the central nervous system (Jha et al., 2014). A recent publication found LCN2 to protect the brain during inflammatory conditions. An unbiased proteomic approach found LCN2 to be the most

124

substantially elevated cytokine in the CNS after peripheral LPS injection. The *Lcn2-/-* mice had exacerbated levels of pro-inflammatory cytokines and exhibited worse behavioral phenotypes indicating LCN2 serves as a protective factor. We have also seen that LCN2 accumulates in the hypothalamus following refeeding and would be interesting to investigate the role LCN2 has on resolving inflammation postprandially centrally.

Further supporting a beneficial over a detrimental homeostatic response of LCN2, its circulating levels increase in obesity and insulin resistance associated with hyperglycemia in humans, decreased in long-term diabetes, and are inversely correlated with body weight and glycated hemoglobin in diabetic patients[54,82,91,95,140,141]. Up-regulation of *Lcn2* in diabetics has also been reported but may be reflective of associated comorbidities such as kidney and cardiovascular disease[142]. Given that LCN2 is up-regulated in pro-inflammatory conditions to resolve inflammation in adipocytes and macrophages[109,133], its upregulation during obesity may be a protective mechanism against inflammation-induced insulin resistance at the early stages of the disease.

Therefore, while the increased LCN2 levels are indicative of metabolic deregulation during the onset of insulin resistance in the pre-diabetic state, they are indicative of better metabolic regulation in the presence of insulin resistance in T2D. This biphasic, opposite association of serum LCN2 levels with disease severity in the two stages of the disease possible reflects its inability to predict diabetes onset and its unlikely involvement as a causative factor in disease progression. On the contrary, and in light of our previous observations the increase in LCN2 levels with the onset of insulin resistance reflects a compensatory protective response for LCN2. As glucose increases and metabolism deteriorates, LCN2 works to improve b cell function and decrease hyperglycemia.

By examining different models of obesity in mice, *Lepr*[db/db] , *Lepr*[ob/ob] , *Mc4R-/-* and DIO we were able to observe the kinetics of the increase in LCN2. The increase of LCN2 levels coincides with the differential

onset of insulin resistance in each mouse model recapitulating our findings in prediabetic subjects. Congenital elevation of *Lcn2* in transgenic mice led to a decrease in food intake and improved metabolism but to a less profound degree as compared to LCN2 treatment in adult mice, possibly due to developmental adjustments. The improvement in metabolic parameters in the transgenic mice remained until at least six months of age, the latest time point these mice were monitored suggesting that sustained elevated LCN2 levels, do not lead to obesity and insulin resistance.

To further examine what the effect of increased production of LCN2 in mouse models of obesity, we silenced *Lcn2* in *Lepr$^{db/db}$* mice, reducing LCN2 levels by 50% and returning them to levels observed in wild-type mice. Lowering LCN2 had detrimental effects on metabolism. The silenced mice become more hyperphagic and had a greater increase in fat mass compared to *Lepr$^{db/db}$* controls. This effect is in opposition to a study which concluded a detrimental role of LCN2 in the pathogenesis of obesity, previously described. The group generated *Lepr$^{db/db}$* ;*Lcn2-/-* (DKO) mice which showed improvement in insulin tolerance compared to *Lepr$^{db/db}$* controls[86]. The specific effect of leptin and leptin receptor inactivation on LCN2 levels need further characterization. We did not see any changes in leptin in the *Lcn2$_{osb}$-/-* mice despite an increase in fat mass. Treatment with rLCN2 decreased leptin levels significantly and possibly to a disproportionate degree than would be observed due to decreases in fat mass. Previously, it has been shown that activating leptin receptor in RINm5F insulinoma cell line upregulated LCN2[143].

Indeed, our previous observations showed that LCN2 acts directly on mouse pancreatic islets to increase insulin secretion, and promote b-cell proliferation[54]. In addition to limiting appetite, LCN2 may also improve glucose handling in obesity by improving b-cell mass and function. This observation was shown to be true in two mouse models. A pharmacological model wherein β-cells are destroyed and treatment with LCN2 restored function of beta cells and a diet-induced-model where given HFD for one week produced proliferation of islets in wild-type mice but not in *Lcn2-/-* mice.

126

Whether LCN2 resistance occurs in obesity, whether LCN2 is induced by underlying inflammation to combat the deleterious effects of obesity, or whether there is even a change in the function of LCN2 under various pathophysiological conditions remains open and requires further research, as studies in humans are cross-sectional and causality is difficult to conclude [10].

References

1. Samuel, V. T. & Shulman, G. I. Mechanisms for Insulin Resistance: Common Threads and Missing Links. *Cell* **148,** 852–871 (2012).

2. DeBerardinis, R. J. & Thompson, C. B. Cellular Metabolism and Disease: What Do Metabolic Outliers Teach Us? *Cell* **148,** 1132–1144 (2012).

3. Samuel, V. T. & Shulman, G. I. The pathogenesis of insulin resistance: integrating signaling pathways and substrate flux. *Journal of Clinical Investigation* **126,** 12–22 (2016).

4. Schwartz, M. W. *et al.* Obesity Pathogenesis: An Endocrine Society Scientific Statement. *Endocrine reviews* **38,** 267–296 (2017).

5. Lumeng, C. N. & Saltiel, A. R. Inflammatory links between obesity and metabolic disease. *Journal of Clinical Investigation* **121,** 2111–2117 (2011).

6. Mozaffarian, D., Angell, S. Y., Lang, T. & Rivera, J. A. Role of government policy in nutrition—barriers to and opportunities for healthier eating. *BMJ* **361,** k2426 (2018).

7. Schwartz, G. J. & Zeltser, L. M. Functional Organization of Neuronal and Humoral Signals Regulating Feeding Behavior. *Annual review of nutrition* **33,** 1–21 (2013).

8. Chaudhri, O., Salem, V. & Physiol …, M. K. Gastrointestinal satiety signals. (2008).

9. Peruzzo, B., Pastor, F., Blázquez, J. & brain …, S. K. A second look at the barriers of the medial basal hypothalamus. (2000).

10. Liu, D.-M. M., Mosialou, I. & Liu, J.-M. M. Bone: another potential target to treat, prevent and predict diabetes. *Diabetes, obesity & metabolism* (2018). doi:10.1111/dom.13330

11. Elias, C., Lee, C., Kelly, J., Aschkenasi, C. & Neuron, A. R. Leptin activates hypothalamic CART neurons projecting to the spinal cord. (1998).

12. Schwartz, M. W., Tschöp, M. & Zeltser, L. M. A mother's influence on metabolic disorders. *Nature medicine* **20,** 244–5 (2014).

13. Hahn, T., Breininger, J. & neuroscience, B. D. Coexpression of Agrp and NPY in fasting-activated hypothalamic neurons. (1998).

14. Broberger, C. & of the …, J. J. The neuropeptide Y/agouti gene-related protein (AGRP) brain circuitry in normal, anorectic, and monosodium glutamate-treated mice. (1998).

15. Bewick, G., Gardiner, J., Dhillo, W. & FASEB …, K. A. Post-embryonic ablation of AgRP neurons in mice leads to a lean, hypophagic phenotype. (2005).

16. Evans, D., Calton, M., Kim, M., Kwok, P. & one, M. I. Genetic association study of adiposity and melanocortin-4 receptor (MC4R) common variants: replication and functional characterization of non-coding …. (2014).

17. reviews, C. R. Studies on the physiological functions of the melanocortin system. (2006).

18. Morrison, S. J. & Scadden, D. T. The bone marrow niche for haematopoietic stem cells. *Nature* **505,** 327–334 (2014).

19. Copp, D., Surgery, S. S., Medicine, O. & Pathology, O. The homeostatic function of bone as a mineral reservoir. (1963).

20. Ashley-Ross, M. A., Perlman, B. M., Gibb, A. C. & Long, J. H. Jumping sans legs: does elastic energy storage by the vertebral column power terrestrial jumps in bony fishes? *Zoology* **117,** 7–18 (2014).

21. Doherty, A. H., Ghalambor, C. K. & Donahue, S. W. Evolutionary Physiology of Bone: Bone Metabolism in Changing Environments. *Physiology* **30,** 17–29 (2015).

22. Botella, H., Blom, H., Dorka, M., Ahlberg, P. & Janvier, P. Jaws and teeth of the earliest bony fishes. *Nature* **448,** 583 (2007).

23. Ducy, P. *et al.* Leptin inhibits bone formation through a hypothalamic relay: a central control of bone mass. *Cell* **100,** 197–207 (2000).

24. Bar-Shavit, Z. The osteoclast: A multinucleated, hematopoietic-origin, bone-resorbing osteoimmune cell. *Journal of Cellular Biochemistry* **102,** 1130–1139 (2007).

25. Takeda, S., Elefteriou, F. & Karsenty, G. COMMON ENDOCRINE CONTROL OF BODY WEIGHT, REPRODUCTION, AND BONE MASS. *Annual Review of Nutrition* **23,** 403–411 (2003).

26. Wei, J. & Ducy, P. Co-dependence of bone and energy metabolisms. *Archives of Biochemistry and Biophysics* **503,** 35–40 (2010).

27. Razzaque, M. Osteo-renal regulation of systemic phosphate metabolism. *IUBMB Life* **63,** 240–247 (2011).

28. Karsenty, G. & Oury, F. Biology Without Walls: The Novel Endocrinology of Bone. *Physiology* **74,** 87–105 (2012).

29. Karner, C. M. & Long, F. Glucose metabolism in bone. *Bone* **115,** (2018).

30. Wei, J. & Karsenty, G. An overview of the metabolic functions of osteocalcin. *Reviews in Endocrine and Metabolic Disorders* **16,** 93–98 (2015).

31. de Araújo, I. M. *et al.* Marrow adipose tissue spectrum in obesity and type 2 diabetes mellitus. *European Journal of Endocrinology* **176,** 21–30 (2017).

32. Compston, J. E. *et al.* Obesity Is Not Protective against Fracture in Postmenopausal Women: GLOW. *The American Journal of Medicine* **124,** 1043–1050 (2011).

33. Khosla, S., Oursler, M. & Monroe, D. G. Estrogen and the skeleton. *Trends in Endocrinology & Metabolism* **23,** 576–581 (2012).

34. Nakamura, T. *et al.* Estrogen Prevents Bone Loss via Estrogen Receptor α and Induction of Fas Ligand in Osteoclasts. *Cell* **130,** 811–823 (2007).

35. Cifuentes, M., Advis, J. & of nutrition, S. S. Estrogen prevents the reduction in fractional calcium absorption due to energy restriction in mature rats. (2004). doi:10.1093/jn/134.8.1929

36. karsenty 2006.pdf.

37. Oury, F. *et al.* CREB mediates brain serotonin regulation of bone mass through its expression in ventromedial hypothalamic neurons. *Genes & development* **24,** 2330–2342 (2010).

38. Lee, N. *et al.* Endocrine Regulation of Energy Metabolism by the Skeleton. *Cell* **130,** 456–469 (2007).

39. Hauschka, P. V. & Wians, F. H. Osteocalcin-hydroxyapatite interaction in the extracellular organic matrix of bone. *The Anatomical Record* **224,** 180–188 (1989).

40. Ferron, M., Wei, J., Yoshizawa, T. & Cell, D. A. Insulin signaling in osteoblasts integrates bone remodeling and energy metabolism. (2010).

41. Oury, F. *et al.* Endocrine Regulation of Male Fertility by the Skeleton. *Cell* **144,** 796–809 (2011).

42. Oury, F., Ferron, M. & of …, H. W. Osteocalcin regulates murine and human fertility through a pancreas-bone-testis axis. (2013). doi:10.1172/JCI65952

43. Ferron, M. *et al.* Insulin Signaling in Osteoblasts Integrates Bone Remodeling and Energy Metabolism. *Cell* **142,** 296–308 (2010).

44. Schlessinger, J. Cell Signaling by Receptor Tyrosine Kinases. *Cell* **103,** 211–225 (2000).

45. Oury, F. *et al.* Osteocalcin regulates murine and human fertility through a pancreas-bone-testis axis. *Journal of Clinical Investigation* **123,** 2421–2433 (2013).

46. Wei, J. *et al.* Bone-specific insulin resistance disrupts whole-body glucose homeostasis via decreased osteocalcin activation. *The Journal of clinical investigation* **124,** 1–13 (2014).

47. Wei, J. *et al.* Glucose Uptake and Runx2 Synergize to Orchestrate Osteoblast Differentiation and Bone Formation. *Cell* **161,** 1576–1591 (2015).

48. Shimazu, J., Wei, J. & Karsenty, G. Smurf1 Inhibits Osteoblast Differentiation, Bone Formation, and Glucose Homeostasis through Serine 148. *Cell Reports* **15,** 27–35 (2016).

49. Yoshikawa, Y. *et al.* Genetic evidence points to an osteocalcin-independent influence of osteoblasts on energy metabolism. *Journal of Bone and Mineral Research* **26,** 2012–2025 (2011).

50. gross 2008.pdf.

51. Rached, M.-T. *et al.* FoxO1 expression in osteoblasts regulates glucose homeostasis through regulation of osteocalcin in mice. *Journal of Clinical Investigation* **120,** 357–368 (2010).

52. Rached, M.-T. T. *et al.* FoxO1 is a positive regulator of bone formation by favoring protein synthesis and resistance to oxidative stress in osteoblasts. *Cell metabolism* **11,** 147–60 (2010).

53. Kousteni, S. FoxO1, the transcriptional chief of staff of energy metabolism. *Bone* **50,** 437–443 (2012).

54. Mosialou, I. *et al.* Corrigendum: MC4R-dependent suppression of appetite by bone-derived lipocalin 2. *Nature* **546,** 440–440 (2017).

55. Grzyb, J., Latowski, D. & Strzałka, K. Lipocalins - a family portrait. *Journal of plant physiology* **163,** 895–915 (2006).

56. Flower, D. R., North, A. & Sansom, C. E. The lipocalin protein family: structural and sequence overview. *Biochimica et Biophysica Acta (BBA) - Protein Structure and Molecular Enzymology* **1482,** 9–24 (2000).

57. Chu, S. -T., Lin, H. -J., Huang, H. -L. & Chen, Y. -H. The hydrophobic pocket of 24p3 protein from mouse uterine luminal fluid: Fatty acid and retinol binding activity and predicted structural similarity to lipocalins. *The Journal of Peptide Research* **52,** 390–397 (1998).

58. Kjeldsen, L., Cowland, J. B. & Borregaard, N. Human neutrophil gelatinase-associated lipocalin and homologous proteins in rat and mouse. *Biochimica et Biophysica Acta (BBA) - Protein Structure and Molecular Enzymology* **1482,** 272–283 (2000).

59. Bundgaard, J., Sengelov, H. & and …, B. N. Molecular cloning and expression of a cDNA encoding NGAL: a lipocalin expressed in human neutrophils. (1994).

60. Goetz, D. *et al.* Ligand preference inferred from the structure of neutrophil gelatinase associated

lipocalin. *Biochemistry* **39,** 1935–41 (2000).

61. Bao, G.-H., Ho, C.-T. & Barasch, J. The ligands of neutrophil gelatinase-associated lipocalin. *RSC Advances* **5,** 104363–104374 (2015).

62. Goetz, D. H. *et al.* The Neutrophil Lipocalin NGAL Is a Bacteriostatic Agent that Interferes with Siderophore-Mediated Iron Acquisition. *Molecular Cell* **10,** 1033–1043 (2002).

63. Yang, J. *et al.* An Iron Delivery Pathway Mediated by a Lipocalin. *Molecular Cell* **10,** 1045–1056 (2002).

64. Yang, J., Mori, K., Li, J. & Barasch, J. Iron, lipocalin, and kidney epithelia. *American Journal of Physiology-Renal Physiology* **285,** F9–F18 (2003).

65. Saha, P. *et al.* Ectopic Expression of Innate Immune Protein, Lipocalin-2, in Lactococcus lactis Protects Against Gut and Environmental Stressors. *Inflammatory Bowel Diseases* **23,** 1120–1132 (2017).

66. Flo, T. H. *et al.* Lipocalin 2 mediates an innate immune response to bacterial infection by sequestrating iron. *Nature* **432,** 917 (2004).

67. Holmes, M. A., Paulsene, W., Jide, X., Ratledge, C. & Strong, R. K. Siderocalin (Lcn 2) Also Binds Carboxymycobactins, Potentially Defending against Mycobacterial Infections through Iron Sequestration. *Structure* **13,** 29–41 (2005).

68. Berger, T. *et al.* Lipocalin 2-deficient mice exhibit increased sensitivity to Escherichia coli infection but not to ischemia-reperfusion injury. *Proceedings of the National Academy of Sciences of the United States of America* **103,** 1834–9 (2006).

69. Friedl, A., Stoesz, S. P., Buckley, P. & Gould, M. N. Neutrophil Gelatinase-associated Lipocalin in Normal and Neoplastic Human Tissues. Cell Type-specific Pattern of Expression. *The Histochemical Journal* **31,** 433–441 (1999).

70. Chan, Y. R. *et al.* Lipocalin 2 Is Required for Pulmonary Host Defense against Klebsiella Infection. *The Journal of Immunology* **182,** 4947–4956 (2009).

71. Xu, M. *et al.* Liver is the major source of elevated serum lipocalin-2 levels after bacterial infection or partial hepatectomy: A critical role for IL-6/STAT3. *Hepatology* **61,** 692–702 (2015).

72. hmidt-Ott, K. *et al.* Neutrophil gelatinase-associated lipocalin-mediated iron traffic in kidney epithelia. *Current Opinion in Nephrology and Hypertension* **15,** 442–449 (2006).

73. Schmidt-Ott, K. M. *et al.* Dual Action of Neutrophil Gelatinase–Associated Lipocalin. *Journal of the American Society of Nephrology* **18,** 407–413 (2007).

74. Bu, D. *et al.* Induction of Neutrophil Gelatinase-Associated Lipocalin in Vascular Injury via Activation of Nuclear Factor-кB. *The American Journal of Pathology* **169,** 2245–2253 (2006).

75. Larsen 2014.pdf.

76. Devireddy, L. R., Gazin, C., Zhu, X. & Green, M. R. A Cell-Surface Receptor for Lipocalin 24p3 Selectively Mediates Apoptosis and Iron Uptake. *Cell* **123,** 1293–1305 (2005).

77. Richardson, D. R. 24p3 and Its Receptor: Dawn of a New Iron Age? *Cell* **123,** 1175–1177 (2005).

78. Hvidberg, V. *et al.* The endocytic receptor megalin binds the iron transporting neutrophil-gelatinase-associated lipocalin with high affinity and mediates its cellular uptake. *FEBS Letters* **579,** 773–777 (2005).

79. Devireddy, L. R., Teodoro, J. G., Richard, F. A. & Green, M. R. Induction of Apoptosis by a Secreted Lipocalin That is Transcriptionally Regulated by IL-3 Deprivation. *Science* **293,** 829–834 (2001).

80. Jha, M. K. *et al.* Diverse functional roles of lipocalin-2 in the central nervous system. *Neuroscience and biobehavioral reviews* **49,** 135–56 (2015).

81. Asimakopoulou, A., Weiskirchen, S. & Weiskirchen, R. Lipocalin 2 (LCN2) Expression in Hepatic Malfunction and Therapy. *Frontiers in Physiology* **7,** 430 (2016).

82. Yan, Q.-W. *et al.* The Adipokine Lipocalin 2 Is Regulated by Obesity and Promotes Insulin Resistance. *Diabetes* **56,** 2533–2540 (2007).

83. Zhang, X. *et al.* Hypothalamic IKKbeta/NF-kappaB and ER stress link overnutrition to energy imbalance and obesity. *Cell* **135,** 61–73 (2008).

84. Vijay_kumar 2010.pdf.

85. Jun, L. S., Siddall, C. & Rosen, E. D. A minor role for lipocalin 2 in high-fat diet-induced glucose intolerance. *American journal of physiology. Endocrinology and metabolism* **301,** E825-35 (2011).

86. Law, I. *et al.* Lipocalin-2 Deficiency Attenuates Insulin Resistance Associated With Aging and Obesity. *Diabetes* **59,** 872–882 (2010).

87. Jin, D. *et al.* Lipocalin 2 is a selective modulator of peroxisome proliferator-activated receptor-gamma activation and function in lipid homeostasis and energy expenditure. *FASEB journal : official publication of the Federation of American Societies for Experimental Biology* **25,** 754–64 (2011).

88. Alwahsh, S. *et al.* Diet high in fructose leads to an overexpression of lipocalin-2 in rat fatty liver. *World Journal of Gastroenterology* **20,** 1807–1821 (2014).

89. Asimakopoulou, A. *et al.* Lipocalin-2 (LCN2) regulates PLIN5 expression and intracellular lipid droplet

formation in the liver. *Biochimica et biophysica acta* **1842,** 1513–24 (2014).

90. Semba, T. *et al.* The FLS (Fatty liver Shionogi) mouse reveals local expressions of lipocalin-2, CXCL1 and CXCL9 in the liver with non-alcoholic steatohepatitis. *BMC Gastroenterology* **13,** 120 (2013).

91. Wang, Y. *et al.* Lipocalin-2 Is an Inflammatory Marker Closely Associated with Obesity, Insulin Resistance, and Hyperglycemia in Humans. *Clinical Chemistry* **53,** 34–41 (2007).

92. Xiang, Y. *et al.* Heterogeneity of Altered Cytokine Levels Across the Clinical Spectrum of Diabetes in China. *Diabetes Care* **34,** 1639–1641 (2011).

93. Lou, Y., Wu, C., Wu, M., Xie, C. & research and clinical practice, R. L. The changes of neutrophil gelatinase-associated lipocalin in plasma and its expression in adipose tissue in pregnant women with gestational diabetes. (2014).

94. Wu, C. *et al.* The changes of serum sKlotho and NGAL levels and their correlation in type 2 diabetes mellitus patients with different stages of urinary albumin. (2014).

95. la Chesnaye, E. *et al.* Lipocalin-2 plasmatic levels are reduced in patients with long-term type 2 diabetes mellitus. *International journal of clinical and experimental medicine* **8,** 2853–9 (2015).

96. Rashad, N. M., El-Shal, A. S., Etewa, R. L. & Wadea, F. M. Lipocalin-2 expression and serum levels as early predictors of type 2 diabetes mellitus in obese women. *IUBMB life* **69,** 88–97 (2017).

97. Ye, Z. *et al.* Serum lipocalin-2, cathepsin S and chemerin levels and nonalcoholic fatty liver disease. (2014).

98. Auguet, T. *et al.* Liver Lipocalin 2 Expression in Severely Obese Women With Non Alcoholic Fatty Liver Disease. *Experimental and Clinical Endocrinology & Diabetes* **121,** 119–124 (2013).

99. Borkham-Kamphorst_et_al-2011-Liver_International.pdf.

100. Tekkeşin, N. Urinary NGAL in Prediction of Acute Kidney Injury. *Journal of Nephrology & Therapeutics* **02,** (2012).

101. Ni, J. *et al.* Serum lipocalin-2 levels positively correlate with coronary artery disease and metabolic syndrome. *Cardiovascular Diabetology* **12,** 176 (2013).

102. Catalán, V. *et al.* Increased adipose tissue expression of lipocalin-2 in obesity is related to inflammation and matrix metalloproteinase-2 and metalloproteinase-9 activities in humans. *Journal of Molecular Medicine* **87,** 803 (2009).

103. Liu, X. *et al.* Circulating lipocalin 2 is associated with body fat distribution at baseline but is not an independent predictor of insulin resistance: the prospective Cyprus Metabolism Study. *European Journal*

of Endocrinology **165,** 805–812 (2011).

104. Zhao 2014.pdf.

105. Moreno-Navarrete, J. *et al.* Metabolic endotoxemia and saturated fat contribute to circulating NGAL concentrations in subjects with insulin resistance. *International journal of obesity (2005)* **34,** 240–9 (2010).

106. Paton, C. M. *et al.* Lipocalin-2 increases fat oxidation in vitro and is correlated with energy expenditure in normal weight but not obese women. *Obesity* **21,** E640–E648 (2013).

107. Tan, B. K. *et al.* Ex Vivo and In Vivo Regulation of Lipocalin-2, a Novel Adipokine, by Insulin. *Diabetes Care* **32,** 129–131 (2009).

108. Bläser, J., Triebel, S. & Tschesche, H. A sandwich enzyme immunoassay for the determination of neutrophil lipocalin in body fluids. *Clinica Chimica Acta* **235,** 137–145 (1995).

109. Costa, D., Lazzarini, E. & of cellular …, C. B. Altered bone development and turnover in transgenic mice over-expressing lipocalin-2 in bone. (2013).

110. Rucci, N. *et al.* Lipocalin 2: A New Mechanoresponding Gene Regulating Bone Homeostasis. *Journal of Bone and Mineral Research* **30,** 357–368 (2015).

111. Capulli, M. *et al.* A Complex Role for Lipocalin 2 in Bone Metabolism: Global Ablation in Mice Induces Osteopenia Caused by an Altered Energy Metabolism. *Journal of Bone and Mineral Research* **33,** 1141–1153 (2018).

112. Playford, R. J. *et al.* Effects of Mouse and Human Lipocalin Homologues 24p3/lcn2 and Neutrophil Gelatinase–Associated Lipocalin on Gastrointestinal Mucosal Integrity and Repair. *Gastroenterology* **131,** 809–817 (2006).

113. Barasch, J. *et al.* Disposal of iron by a mutant form of lipocalin 2. *Nature Communications* **7,** 12973 (2016).

114. Guo, H. *et al.* Lipocalin-2 Deficiency Impairs Thermogenesis and Potentiates Diet-Induced Insulin Resistance in Mice. *Diabetes* **59,** 1376–1385 (2010).

115. Guo, H. *et al.* Lipocalin 2, a Regulator of Retinoid Homeostasis and Retinoid-mediated Thermogenic Activation in Adipose Tissue. *The Journal of biological chemistry* **291,** 11216–29 (2016).

116. Zhang, Y. *et al.* Lipocalin 2 regulates brown fat activation via a nonadrenergic activation mechanism. *The Journal of biological chemistry* **289,** 22063–77 (2014).

117. Garbacz, W. G. *et al.* Sex- and Tissue-Specific Role of Estrogen Sulfotransferase in Energy

Homeostasis and Insulin Sensitivity. *Endocrinology* (2017). doi:10.1210/en.2017-00571

118. Petersen, P. S. *et al.* Dynamic and extensive metabolic state-dependent regulation of cytokine expression and circulating levels. *American Journal of Physiology-Regulatory, Integrative and Comparative Physiology* **307,** R1458–R1470 (2014).

119. Zhang, Y. *et al.* Lipocalin 2 expression and secretion is highly regulated by metabolic stress, cytokines, and nutrients in adipocytes. *PloS one* **9,** e96997 (2014).

120. Li, C. & Cytokine, C. Y. Lipocalin 2 regulation and its complex role in inflammation and cancer. (2011).

121. Karoui, K. *et al.* Endoplasmic reticulum stress drives proteinuria-induced kidney lesions via Lipocalin 2. *Nature Communications* **7,** 10330 (2016).

122. Poppitt, S. D. *et al.* Postprandial response of adiponectin, interleukin-6, tumor necrosis factor-α, and C-reactive protein to a high-fat dietary load. *Nutrition* **24,** 322–329 (2008).

123. Payette, C. *et al.* Sex differences in postprandial plasma tumor necrosis factor–α, interleukin-6, and C-reactive protein concentrations. *Metabolism* **58,** 1593–1601 (2009).

124. Myhrstad, M. C. *et al.* Effect of marine n-3 fatty acids on circulating inflammatory markers in healthy subjects and subjects with cardiovascular risk factors. *Inflammation Research* **60,** 309–319 (2011).

125. Miglio, C. *et al.* Antioxidant and inflammatory response following high-fat meal consumption in overweight subjects. *European Journal of Nutrition* **52,** 1107–1114 (2013).

126. Raz, O. *et al.* The effect of two iso-caloric meals containing equal amounts of fats with a different fat composition on the inflammatory and metabolic markers in apparently healthy volunteers. *Journal of Inflammation* **10,** 3 (2013).

127. Teeman, C. S. *et al.* Postprandial lipemic and inflammatory responses to high-fat meals: a review of the roles of acute and chronic exercise. *Nutrition & Metabolism* **13,** 80 (2016).

128. Lawrence, T. & Gilroy, D. W. Chronic inflammation: a failure of resolution? *International Journal of Experimental Pathology* **88,** 85–94 (2007).

129. Thaler, J. P. & Schwartz, M. W. Minireview: Inflammation and Obesity Pathogenesis: The Hypothalamus Heats Up. *Endocrinology* **151,** 4109–4115 (2010).

130. Serhan, C. N., Chiang, N. & Dalli, J. The resolution code of acute inflammation: Novel pro-resolving lipid mediators in resolution. *Seminars in immunology* **27,** 200–15 (2015).

131. Moschen, A. R. *et al.* Lipocalin 2 Protects from Inflammation and Tumorigenesis Associated with Gut Microbiota Alterations. *Cell Host & Microbe* **19,** 455–469 (2016).

132. Ding, S. *et al.* High-Fat Diet: Bacteria Interactions Promote Intestinal Inflammation Which Precedes and Correlates with Obesity and Insulin Resistance in Mouse. *PLoS ONE* **5,** e12191 (2010).

133. Ding, S. & Lund, P. K. Role of intestinal inflammation as an early event in obesity and insulin resistance. *Current Opinion in Clinical Nutrition and Metabolic Care* **14,** 328–333 (2011).

134. Beyaz, S. *et al.* High-fat diet enhances stemness and tumorigenicity of intestinal progenitors. *Nature* **531,** 53 (2016).

135. Thaler, J. P., Guyenet, S. J., Dorfman, M. D., Wisse, B. E. & Schwartz, M. W. Hypothalamic Inflammation: Marker or Mechanism of Obesity Pathogenesis? *Diabetes* **62,** 2629–2634 (2013).

136. Waise, Z. T. *et al.* One-day high-fat diet induces inflammation in the nodose ganglion and hypothalamus of mice. *Biochemical and Biophysical Research Communications* **464,** 1157–1162 (2015).

137. Dalvi, P. *et al.* High fat induces acute and chronic inflammation in the hypothalamus: effect of high-fat diet, palmitate and TNF-α on appetite-regulating NPY neurons. *International Journal of Obesity* **41,** 149 (2017).

138. Zhang, Y., Reichel, J. M., Han, C., Zuniga-Hertz, J. P. & Cai, D. Astrocytic Process Plasticity and IKKβ/NF-κB in Central Control of Blood Glucose, Blood Pressure, and Body Weight. *Cell metabolism* **25,** 1091-1102.e4 (2017).

139. Chowen, J. A., Horvath, T. L. & Argente, J. Microglial Proliferation in Obesity: When, Where, Why, and What Does It Mean? *Diabetes* **66,** 804–805 (2017).

140. Zhang, J. *et al.* The Role of Lipocalin 2 in the Regulation of Inflammation in Adipocytes and Macrophages. *Molecular Endocrinology* **22,** 1416–1426 (2008).

141. Alkharfy, K. M., Al-Daghri, N. M., Vanhoutte, P. M., Krishnaswamy, S. & Xu, A. Serum Retinol-Binding Protein 4 as a Marker for Cardiovascular Disease in Women. *PLoS ONE* **7,** e48612 (2012).

142. Fadel, F., Rahman, A. & of medical …, M. M. Plasma neutrophil gelatinase-associated lipocalin as an early biomarker for prediction of acute kidney injury after cardio-pulmonary bypass in pediatric …. (2012).

143. Hekerman, P. *et al.* Leptin induces inflammation-related genes in RINm5F insulinoma cells. *BMC Molecular Biology* **8,** 41 (2007).